Università degli Studi di Ferrara

UCA Universidad de Cádiz

INTERNATIONAL DOCTORAL COURSE IN

"EARTH AND MARINE SCIENCES (EMAS)"

CYCLE XXXIV°

COORDINATOR Prof. Coltorti Massimo

Natural zeolitites in combination with struvite precipitation technology for the recovery of nutrients from agricultural wastewaters

Scientific/Disciplinary Sector (SDS) GEO/08

Candidate

Dott. Galamini Giulio

Supervisor

Prof. Coltorti Massimo

Co-supervisor

Dott. Ferretti Giacomo

Years 2019/2022

INDEX

List of abbreviations:

exp. A: NH_4^+-N adsorption characterization from swine liquid manure (experiment A);

exp. B: Combination of cha-zeolitite adsorption and struvite precipitation for the treatment of an anaerobically digested wastewater (experiment B);

NUE: Nutrient Use Efficiency.

CEC: Cation Exchange Capacity (meq g^{-1});

N_{ZT}: Natural micronized cha-zeolitite;

gN_{ZT}: Natural granular cha-zeolitite;

K_{ZT}: K^+-enriched cha-zeolitite;

NZT-S: Treatment that foresees the use of cha-zeolitite + struvite precipitation;

KZT-S: Treatment that foresees the use of K^+-enriched cha-zeolitite + struvite precipitation;

CNTR: Treatment that foresees the use of struvite precipitation, without the use of any cha-zeolitite;

MR1: Molar ratio 1 ($Mg:NH_4:PO_4$ = 1:1.5:1);

MR2: Molar ratio 2 ($Mg:NH_4:PO_4$ = 2:1:1);

phase 1: 1st phase of the treatment: zeolitic tuff adsorption;

phase 2: 2nd phase of the treatment: struvite precipitation;

$C_{e.tg}$: NH_4^+-N target concentration at equilibrium condition (concentration desired to reach by a single cha-zeolitite adsorption batch);

$q_{e.tg}$: NH_4^+-N target adsorption capacity (expected adsorption capacity at the $C_{e.tg}$);

Tr: theoretical NH_4^+-N recovery;

Ar, actual NH_4^+-N recovery;

$R_{\%}$, NH_4^+-N recovery % (used as an indicator for struvite precipitation efficiency);

q_{max}: maximum adsorption capacity (Langmuir model, mg g^{-1});

K_L: Langmuir isotherm constant (L mg^{-1});

C_e: Equilibrium concentration (mg L^{-1});

q_e: Equilibrium adsorption capacity (mg g^{-1});

α_H: Harkins-Jura isotherm constant (g mg^{-1});

β_H: Harkins-Jura isotherm coefficient;

S: Specific surface area (m^2 g^{-1});

R: Universal gas constant (8.314 J mol^{-1} K^{-1});

T: Temperature (K);

N_A: Avogadro constant (6.022×10^{23} mol^{-1});

K_F: Freundlich isotherm constant (L g^{-1});

A_T: Temkin isotherm equilibrium binding constant;

b_T: Temkin isotherm constant (J mol^{-1});

K_d: Distribution coefficient (L g^{-1})

V: Batch volume (L);

m: sorbent mass (g);

C_0: initial concentration (mg L^{-1});

F(t): Fractional uptake;

q_t: Adsorption capacity at time t=t (mg g^{-1});

k_1: Pseudo first order rate constant;

k_2: Pseudo second order rate constant;

h: Initial adsorption rate (mg g^{-1} min^{-1});

k_{ID}: Intraparticle diffusion rate constant;

C: Intraparticle diffusion intercept;

α_E: Elovich isotherm constant;

R_E: Elovich approaching equilibrium coefficient;

t_{ref}: reference time (min);

q_{ref}: adsorption capacity at time $t=t_{ref}$ (mg g^{-1});

ΔG: Gibbs free energy change (J mol^{-1});

ΔH: Standard enthalpy change (J mol^{-1});

ΔS: Standard entropy change (J K^{-1} mol^{-1});

K_e: Thermodynamic equilibrium constant.

ABSTRACT

In a scenario where both the global population and the demand for meat consumption are increasing, the World Health Organization emphasize the importance to start turning the perception of "nutrient-rich wastewaters", from "wastes" to dispose of, to "resources", useful for plant nutrition (WHO, 2006). Despite this, 80% of municipal wastewaters globally produced are still discarded in the environment, without having been subjected to any treatment for the recovery of nutrients and the reduction of their environmental impact (https://www.unwater.org/water-facts/quality-and-wastewater/, accessed the 15/01/2022). On the other hand, also the thoughtless use of excreta and derived materials for fertilization practices threatens the environmental systems, leading to pollution, soil degradation, and water contamination.

The question on "how to efficiently dispose of nutrient-rich wastewaters" or, in other words, "how to improve the recycling of nutrients in agro-ecosystems", remains a crucial topic for the sustainability of human activities.

Wastewater treatments often focus on the "reduction" of nutrients, but more emphasis should be dedicated to the "recovery" of nutrients, as the reduction of nutrient loads does not always coincide with a circularity perspective. A careful application of wastewater treatment technologies may thus represent a solution for the management of excreta and derived materials and the reduction of the environmental impacts of agricultural activities.

A promising technology consists in the recovery of both nitrogen (N) and phosphorous (P) by struvite precipitation ($MgNH_4PO_4 \cdot 6H_2O$). These treatment processes are starting to scale up at industrial levels, as the European Commission recently introduced the "phosphate-based precipitates" in the registry of fertilizers (EU Regulation 2019/1009). However, the unbalance between the struvite components in wastewaters, and in particular, the significative higher amounts of ammonium ions (NH_4^+), respect both phosphate (PO_4^{3-}) and magnesium (Mg^{2+}), is one of the main issues for its implementation.

The possibility to recover the excess of NH_4^+ before struvite precipitation may thus increase the nutrient removal efficiency of struvite technology.

Within this thesis work, it was investigated a wastewater treatment process that uses natural zeolitites (rocks containing more than 50% in zeolite minerals) in combination with struvite precipitation, for the removal and recovery of N and P, in the form of struvite crystals and NH_4^+-N-enriched zeolitites. Scientific literature often investigates the adsorption of NH_4^+-N by zeolites in synthetic solutions, considering them as equivalent of real nutrient-rich wastewaters, but as pointed out by many authors, these materials can not represent with sufficient approximations the conditions of real wastewaters, where many competing species are present.

Thus, before the wastewater treatment experiment, the NH_4^+-N adsorption properties of the applied zeolitite were characterized (experiment A) in terms of isotherms, kinetic models, and thermodynamic parameters, from real livestock wastewater (pig manure). Two different grain sizes have been investigated, a granular zeolitite and a micronized one.

Even if both showed interesting features, the micronized zeolitite demonstrated to reach higher adsorption capacities, with better temperature stability. This material was thus chosen for experiment B, where different treatment strategies have been investigated for the recovery of N and P from a anaerobically digested wastewater.

The investigated treatment strategies were composed of two distinct phases: the 1st phase (zeolitite adsorption batch) tested the natural micronized zeolitite and a modified one (K^+-enriched) for the reduction of NH_4^+-N loads. In the 2nd phase (struvite precipitation), 2 different Mg:NH_4:PO_4 molar ratios were tested, in particular, a condition of NH_4^+ excess (MR1) and another with Mg^{2+} in excess (MR2) for the struvite precipitation. Both were considered in literature as the best conditions for struvite precipitation.

The outcomes of experiment B suggested that the most feasible practice consists in the use of the natural zeolitites, in combination with the MR1 condition. This treatment showed the highest nutrient removal efficiency, highest efficiency in struvite precipitation, and less alteration of the treated wastewater. The precipitate obtained was 89.9 mass % composed of struvite, poor in hazardous heavy metals, with 3.5% nitrogen.

The materials obtained, as the N-charged zeolitites, the struvite precipitates and the nutrient depleted wastewater may potentially be usable in agriculture, for crop nutrition and/or as soil amendment.

Even if the treatment described within this thesis work used livestock wastewaters and a derivate one, the methodology proposed may be appliable to any other nutrient-rich wastewater, as municipal ones.

1. INTRODUCTION

1.1 Challenges for agricultural wastewater management and N-P fertilization.

Technological progress and industrial revolutions have led to economic growth and agricultural expansion during the past centuries. The land area dedicated to agriculture increased during the last 4 decades of the 20th century by about 9.2% (from about 4.47 to 4.88 billion hectares) (FAOSTAT database, http://www.fao.org/faostat/en/#data/RL/visualize, accessed the 3.20.21) and this trend is bound to rise, as the world population will reach 10 billion people in about thirty/forty years (Worldometers.info, 2022).

Closely following the agricultural growth, fertilizers demand are increasing, with peak values estimated as about 112 million tons for nitrogen (N) and 10.7 for phosphorous (P) (FAO, 2019) for the year 2022. Furthermore, this trend will further increase if developing regions (e.g. North Africa), will increase their use of fertilizers, possibly affecting also their prices.

Most of the N-based fertilizers applied are produced by the Haber-Bosch process: an energy-consuming chemical process that converts the atmospheric dinitrogen (N_2) to ammonia (NH_3). P is

instead obtained by phosphate rock deposits, which are doomed to decrease for quantity and quality (Science Communication Unit, 2013).

Both nutrient-supply pathways are not sustainable. Contrary to these practices, the careful use of organic fertilizers, as animal manures, is a suitable alternative in areas where livestock activities are well established. Indeed, these materials represent a highly rich source of nutrients for crops, as more than 70% of feeds consumed by animals are excreted (Barnett, 1994). Zootechnical waste materials and derivates are thus commonly applied in many countries for fertilization, and their use will further increase, following the demand for meat consumption, which is raised three times higher than in the middle 1970s (Roser and Ortiz-Ospina, 2019).

However, both chemical and organic fertilizers, often inefficiently contribute to plant nutrition, as only a fraction of the nutrients added is effectively used by crops. It is estimated that only an average of 10-20% of the added P (Holford, 1997) is used by plants, while the remaining 80-90% is lost, contributing to the eutrophication of surface and ground waters, or precipitate as insoluble salts that remain in the soil for long times (Hata et al., 2010). On the other way, the introduced N may be quickly transformed into more mobile forms, like nitrate (NO_3^-), which is repelled by clay minerals, and easily leached (Ongley, 1996).

Leaching of both N and P are energy-wasting processes that consume enormous economic and environmental resources. Moreover, Nolan and Weber (2015) have correlated the increase of NO_3^- levels with uranium in two major aquifers in the United States, as NO_3^- may indeed dissolve naturally occurring uranium minerals, leading to potentially harmful levels.

Along with water pollution, N gaseous emissions as nitrogen oxides (NO_x), nitrous oxide (N_2O), and ammonia (NH_3), constitute one of the main classes of pollutants emitted by modern farming. In particular, the powerful greenhouse gas (GHG) N_2O arises from animal production in large quantities, depending on the N input and the management of zootechnical wastes and derivates (Aneja et al., 2008).

To improve crop nutrient use efficiency (NUE) and promote agricultural sustainability, actions need to be taken directly on the agri-food system and in agricultural practices.

The treatment of nutrient-rich wastes may be a great strategy but only in a view of nutrient recycling and reuse, trying to minimize their losses. In this optic, the implementation of practical solutions for the recovery of nutrients, and not only for their removal, may transform these materials in the perception and economic framework, from wastes to resources.

The World Health Organization (WHO) emphasizes the importance to start perceiving excreta (not only from animals but also humans) as resources instead of wastes, because their potential reuse in agriculture may significantly reduce the demand for synthetic fertilizers (World Health Organization, 2006).

However, 80% of the municipal wastewaters produced in the globe, are discarded in water bodies without having been subjected to any treatment (UN-Water, accessed the 15/01/2022), and even where excreta materials are applied in agriculture, their thoughtless use may contribute to environmental pollution.

Even though regulations like the Nitrates Directive (Council Directive 91/676/EEC, 1991) poses serious limitations on the nutrient inputs, livestock farming continues to produce large volumes of effluent, often difficult to dispose of, and illegal spills continue to occur (Capolupo et al., 2014).

By introducing in the industrial framework, treatment systems that allow the recovery of nutrients from wastes, thus the production of new types of fertilizers, the wastewater is effectively transformed into a resource, capable to gain economic relevance.

Furthermore, the transportation of nutrients from producing areas (where livestock farming is well established) to demanding ones is often not easily feasible; thus, concentrating nutrients in new forms may lead to positive effects on their disposal.

Among the processes that allow the recovery of nutrients for agricultural applications, one of the most promising and cutting-edge is represented by struvite precipitation technologies (Le Corre et al., 2009a; Sena and Hicks, 2018; Siciliano et al., 2020).

1.2 Nutrient recovery by struvite precipitation

One of the most promising techniques for the recovery of nutrients from wastewaters is the precipitation of struvite crystals ($MgNH_4PO_4\ 6H_2O$), as these techniques may allow the simultaneous recovery of both N and P.

Once separated, struvite may be used for plant nutrition and, because of its relatively low solubility, it is often referred to as a "slow-release fertilizer" because in general (if applied to non-acidic soils), it may release nutrients gradually, making it a promising strategy for improving crops NUE and fertilizer use efficiency (FUE) (Degryse et al., 2017; Robles-Aguilar et al., 2020; Talboys et al., 2016).

During the '70s, struvite was a problem for treatment plants, as it spontaneously precipitated, sometimes completely clogging the pipes. This led to the idea of intentionally producing struvite upstream to avoid any damage to the hydraulic system (Stratful et al., 2004). Since then, several studies and patents have been realized.

The European Union (EU) recently approved the commercialization of struvite and other "P-based fertilizers", produced from wastewater treatment plants. The recently revised "Fertilising Products Regulation" (EU Regulation EU 2019/1009) will soon represent the legal baseline for the implementation of struvite technologies, and the introduction of struvite fertilizers in the European market.

In the review of the regulation (Annexes to Regulation EU 2019/1009, 2021) are highlighted the minimum requirements to be met by these materials to cease to be considered "wastes" and to fall under the category of "fertilizers", as well as the production methods. Struvite and other P-based

fertilizers may thus actually be produced from ì) municipal wastewaters, ìì) sewage sludges, ìèì) food production wastes, ìv) waste separation wastes, v) bioethanol and biodiesel production wastes, vì) living or dead organisms, vìì) mixtures of these materials and vèìì) processed derived products. Unfortunately, even though the EU commission has expressed positive intentions about the possibility to add also liquid digestates (wastewaters derived from biogas plants), these materials are not allowed for struvite production because it is first necessary to define their "end-point" in the Animal by-products Regulation (ABPR) (EC regulation 1069/1009) (FAQs related to Regulation EU 2019/1009 (2021)).

Today, it is thus not possible to produce P-based fertilizers neither from raw zootechnical manure nor digestates, but this regulation is likely going to change.

The Chemical pathways for struvite precipitation in the presence of Mg^{2+}, NH_4^+ and orthophosphate ions may be summarized, in a simple way, by the following reactions (equation 1 and 2) (Le Corre et al., 2009b; Mohan et al., 2011):

$$Mg^{2+} + NH_4^+ + H_nPO_4^{3-n} + 6H_2O \rightarrow MgNH_4PO_4 \cdot 6H_2O_{(s)} + nH^+ \quad (1)$$

$$Mg^{2+} + NH_3 + H_nPO_4^{3-n} + 6H_2O \rightarrow MgNH_4PO_4 \cdot 6H_2O_{(s)} + (n\text{-}1)H^+ \quad (2)$$

(n = 0, 1, 2 depending on pH).

The crystallization process and the crystal composition depend on Mg^{2+}, NH_4^+, orthophosphate concentrations, pH, ionic strength, and N/P ratio (Desmidt et al., 2013; Gunay et al., 2008; Kozik et al., 2013; Stratful et al., 2001).

Struvite crystallizes in the orthorhombic system, space group $Pmn2_1$. The crystal structure contains PO_4^{3-} anions, hexaaqua magnesium cations ($Mg(H_2O)_6^{2+}$) that form octahedral units, and NH_4^+ cations connected within an extended three-dimensional hydrogen-bonded network (Prywer et

al., 2019). Hydrogen bonds are formed between both the H_2O and polyatomic ions (O-H···O) and between NH_4^+ and PO_4^{3-} (N-H···O) (figure 1).

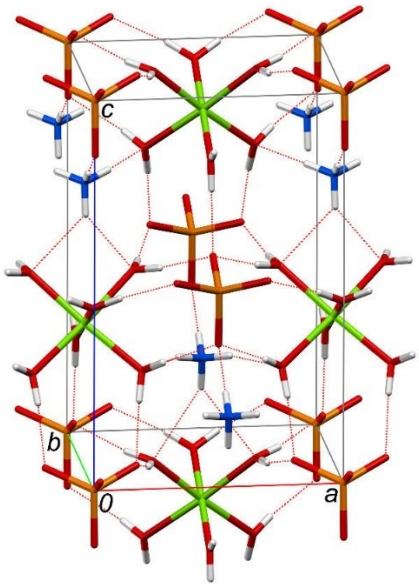

Figure 1. Struvite three-dimensional molecular structure with the unit cell. Blue-white structures are NH_4^+ tetrahedra ions; orange-red structures are PO_4^- tetrahedra and green structures represent Mg^{2+} ions, surrounded by 6 H_2O molecules in octahedral structures. The hydrogen-bond network is marked with dotted lines.

Nutrient-rich wastewaters commonly do nnaturalot match the chemical characteristics required for the synthesis of struvite. A high purity crystal should have a 1:1:1 ratio of Mg^{2+}, NH_4^+ and PO_4^{3-}, but biogenic wastewaters have average compositions in the range of 1:30-70:0.6-4.2 as Mg^{2+}:NH_4^+:PO_4^{3-} (values extrapolated from Tuszynska et al., 2021), thus highly different from the stoichiometric ratio. Being from 15 to 35 times higher than PO_4^{3-} and from 60 to 70 times higher than Mg^{2+}, NH_4^+ molecule is the most abundant one, thus, to overcome its high excess and obtain sufficient amounts of struvite, it is usually needed to highly increase both Mg^{2+} and PO_4^{3-} or, alternatively, to reduce NH_4^+.

The traditional way to obtain struvite involve the use of Mg^{2+} and PO_4^{3-} chemical reagents as $MgCl_2 \cdot 6H_2O$, $MgSO_4 \cdot 7H_2O$, MgO, $MgOH_2$, H_3PO_4, Na_2HPO_4 and KH_2PO_4, (Siciliano et al., 2020) but, to obtain effective production yields, generally high amounts of reagents are required, thus inevitably altering the wastewater itself and possibly introducing high amounts of unwanted species as Na^+, K^+, Cl^- and SO_4^{2-}, with consequent deterioration of the treated wastewater quality (Kabdaşlı and Tünay, 2018; Kataki et al., 2016). Furthermore, the required dosages of Mg^{2+} reagents is undoubtedly the most expensive component that contributes to about the overall 75% of the total costs for struvite production (Dockhorn, 2009).

The unbalance between the struvite components and the cost of reagents represents the main obstacles to the implementation of struvite technologies at an industrial scale (Kumar and Pal, 2015; Wang et al., 2018).

New advanced technologies and integrated management practices may significantly reduce the demand for reagents, as membrane separation technologies, or bioelectrochemical systems (as microbial fuel cells and microbial electrolysis cells), that may convert microbial metabolic energy into electrical energy, producing biofuels as well as struvite (Kumar and Pal, 2015; Siciliano et al., 2020). However, most of these methods are difficult to be applied due to the high investment costs and highly specialized labor required. For these reasons, struvite production from zootechnical and derivate wastewaters is currently perceived more for the recovery of P than N, because most of N seems to be doomed to remain in the liquid as NH_4^+ ions.

A feasible way to improve struvite NH_4^+ removal efficiency may be its upstream recovery, before struvite precipitation. In this way, the molar concentration of struvite components will be better-balanced and fewer amounts of reagents would be needed.

An energy-safe and easy-to-manage method to store NH_4^+ and reduce its concentration in the wastewater before struvite precipitation may be the use of cationic exchangers, as zeolites.

1.3. Natural zeolites, contextualization, and applications for N recovery

The so-called "Integrated Zeolitite Cycle" is a strategy that promotes the use of natural zeolites for agricultural wastewater treatment and NH_4^+ recovery and reuse (Faccini et al., 2018, 2015; Ferretti et al., 2017a; Malferrari et al., 2013a).

The zeolites are a mineral family characterized by an open 3D framework formed by linked tetrahedra of $[SiO_4]^{4-}$ and $[AlO_4]^{5-}$ that delimits open cavities as channel and cages, usually occupied by H_2O molecules and exchangeable extra-framework ions (Coombs, 2001). The general formula used for describing natural zeolites is shown below:

$$M_xM'_yN_z\,[T_mT'_n \ldots O2_{(m+n)-\varepsilon}(OH)_{2z}]\,(OH)_{br}\,(aq)_p \cdot qQ \qquad (3)$$

where M and M' are exchangeable and non-exchangeable cations, respectively; N are non-metallic cations (generally removable on heating); (aq) represents chemically bonded water (or other strongly held ligands of T-atoms); Q represents sorbate molecules; T, T' are Si^{4+} and Al^{3+} (Rehákova et al., 2004).

Due to the partial substitution of Si^{4+} with Al^{3+} ions in the oxygen-tetrahedra structures, zeolite minerals have an active framework negative charge which is balanced by alkali and alkaline earth cations. These ions do not occupy fixed positions and have relative free mobility through the extra-framework channels.

Being able to be replaced by other ions present in the surrounding environment, they act as counterions, and the substitution process is referred to as "cation exchange".

The Si/Al ratio is one of the main parameters that determine the cation exchange capacity (CEC) of the mineral. Common CEC values (meq g^{-1}) referred to some of the most common zeolites are as follows: chabazite and phillipsite (3.0-3.5), clinoptilolite (2.0-2.3), mordenite (1.8-2.0).

The structure and chemistry of zeolites determine their peculiar characteristics as ì) low density and large extra-framework interconnected spaces, ìì) high degree of reversible hydration, ìèì) high crystallinity, èv) possibility of adsorption of ions and molecules, v) high CEC, and vì) catalytic properties (Coombs, 2001; Król, 2020; Moshoeshoe et al., 2017).

In natural systems, zeolitized deposits are associated with volcanic ones, resulted from explosive activities, and then subjected to diagenesis. Thus, along with the CEC of pure zeolite minerals, it is more important from an applicational point of view, the "bulk" CEC of the total zeolite-rich rock, that may be referred to also as zeolitic-tuff, or zeolitite.

The main factors that affect zeolite crystallization in nature are ì) temperature (geothermal gradient), ìì) pressure (geobaric gradient), ìèì) the presence of circulating water (chemical gradient) and èv) the chemical and mineralogical nature of the parent material.

Normally zeolites are secondary phases, but they occur also in some igneous rocks as primary minerals (e.g. authigenic analcime). At high temperatures, they may develop by hydrothermal alteration or by metamorphism processes (contact or burial). Near the surface, thus at low temperatures, they may crystallize under specific chemical gradients of the interstitial waters (Lijima, 1980).

It has been estimated that the larger zeolite deposits are in the deep-sea floor, where about 1.5 and 2% of the sediments are composed of phillipsite and clinoptilolite respectively, derived from low P–T alteration of volcanic glass (Petzing and Chester, 1979), but these deposits are not exploitable. Extractable zeolites are commonly found in volcanoclastic deposits (Gottardi and Galli, 1985), as secondary phases due to hydrothermal alteration of tuffaceous rocks (Delkash et al., 2015).

Nowadays, more than sixty different natural zeolite minerals have been discovered (http://www.iza-online.org/natural/default.htm accessed date 9 June 2021), differing in terms of structure and properties. However, only a few of them occurs in sufficient quantity and purity to be

exploitable (Kesraoui-Ouki et al., 1994). Among them, clinoptilolite is the most studied and applied natural zeolites in the world, followed in order by mordenite, chabazite, phillipsite and erionite (Galli and Passaglia, 2011).

Although less abundant than clinoptilolite, chabazite zeolite (CHA), is particularly attractive for agricultural and industrial applications because of its high CEC and easiness in sorption and subsequent release of NH_4^+ ions (Gualtieri and Passaglia, 2006; Mumpton, 1999).

Chabazite has randomly arranged domains with perfect (Si, Al) ordering (Mazzi and Galli, 1983). It is characterized by a framework of a stacked sequence of 6-rings, in the order AABBCC..., forming double 6-rings at each apex of the rhombic unit cell (figure 2). Each of the largest hexagonal channels, perpendicular to [001], is confined by eight-membered rings. The framework topology of the CHA structure is rhombohedral, R3m. Chabazite has four channel cation sites (figure 2).

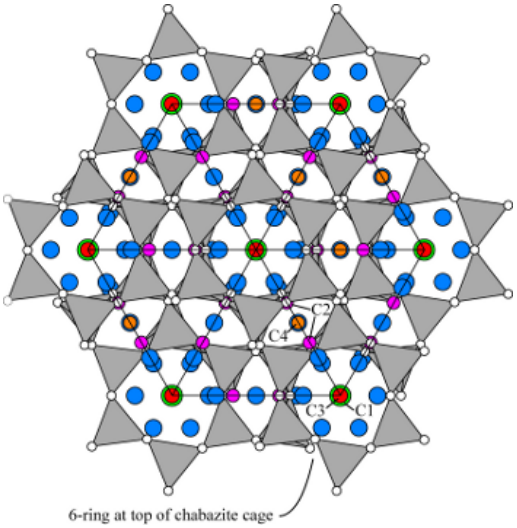

Figure 2. Crystal structure of chabazite and cation sites represented by circles. C1 (green) is located outside the double 6-ring and bonded with 3 oxygen atoms of the ring; C2 (magenta) is near the 8-ring port of the chabazite cage and bonded to three framework oxygen atoms; C3 (red) is near the center of the cage, not bonded to the framework and C4 (orange) is at the center of the 8-ring. C1 and C3 generally contain most of the extra-framework exchangeable cations. Blue circles represent H_2O molecules (International Zeolite Association, chabazite, accessed the 13/01/2022.)

In central Italy, volcanic tuff deposits have been zeolitized, reaching up to 80% zeolite content, mostly chabazite and phillipsite, characterized by high amounts of exchangeable Ca^{2+} and K^{+}.

Because of these properties and their high availability, natural zeolites are being studied for decades for their potential use in agricultural applications (Ahmed et al., 2010; Dwairi, 1998; Ferretti et al., 2018; Ming and Allen, 2001; Mumpton, 1999; Passaglia, 2008; Söderström et al., 2014). One of their main application is for the amendment of agricultural soils, where they may improve the water and nutrient retention, and the soil CEC, resulting in increasing water reserve for plants and reducing N losses (Colombani et al., 2016; Ferretti et al., 2017b; Omar et al., 2015; Vilcek et al., 2013).

It is important to highlight an aspect that often leads to misunderstandings in the literature. In particular, if it is intended to refer to the zeolitic deposit; if the zeolite content exceeds 50% of the mass, the recommended terminology should be "zeolitite" or "zeolite-rich tuff", instead of using the general term "zeolite" which instead indicate the mineral and not the rock (Galli and Passaglia, 2011).

Both zeolites and zeolitites are particularly interesting for the recovery of NH_4^{+} from nutrient-rich wastewaters. If these materials are put into contact for a certain amount of time with the liquid phase, it will be obtained ì) N-depleted wastewater, with less potential environmental impacts, and

ìì) NH_4^{+}-charged zeolitite, potentially useful for plant nutrition and soil amendation.

In the following section, a brief description of adsorption processes (not strictly related to zeolite minerals) is provided.

1.4. Introduction to adsorption studies

Adsorption and desorption take place in a zone called interface, where they involve processes with different nature and physical meanings. The chemical species that is retained by surface interactions is called adsorbate, while the material (solid in general) within its surface the adsorption processes occur, is called adsorbent.

Even if different adsorption mechanisms exist in natural materials, with not always strictly defined boundaries, a general subdivision is referred to the nature of the interactions between the adsorbent and the adsorbate. In general, if chemical reactions are involved it is referred to as "chemisorption", while if physical interactions occur, the term "physisorption" is used. A third category is reserved for the "ion-exchange reactions".

Chemisorption provides the monolayer condition, for whom the adsorbed species is located in specific sites, disposed in a single layer within the interface, and without the possibility of "overlappings". Activation energy, which is the energy required for adsorption to occur, is often needed, and it is represented by the reaction energy with functional groups present along the surface (Saha and Chowdhury, 2011). Binding energies are strongly higher than other adsorption mechanisms and, for this reason, chemisorption is an irreversible process (https://old.iupac.org/reports/2001/colloid_2001/manual_of_s_and_t/node16.html, accessed the 05/01/2022).

Physisorption involves weaker dipolar interactions (van der Waals forces), thus no activation energy is needed, and the process is reversible. Being that physisorption does not involve chemical reactions, the adsorbates may be arranged into consecutive layers by bridging bonds, thickening the interface, and forming adsorption multilayers.

In the case of ion exchange, dissolved cations or anions replace other (or the same ions) already present along the surface of the adsorbent. The ion exchangers contain permanently bound functional groups of opposite charge-type (LeVan and Carta, 2008). In the case of zeolite minerals,

the aluminate groups $[AlO_4]^{5-}$ that partially substitute the $[SiO_4]^{4-}$ cause the presence of surface negative charges, balanced by weakly bonded cations, exchangeable with other cations in solution by specific selectivity pathways. The binding energies are weak, thus ion exchange is considered a reversible process.

In adsorption studies, the adsorption of a chemical species from a solution (liquid or gaseous phase) is usually defined under thermodynamic conditions of equilibrium, or non-equilibrium.
In the first case, it is often important to define models useful to control and manage the adsorption process. These mathematical equations are represented by equilibrium isotherms. On the other hand, the investigation on how the relationship between the adsorbate and the adsorbent change over time, in a condition where equilibrium is not reached, is referred to as the study of kinetic models.
While some of these models are purely empirical formulations, others provide a physical basis for adsorption processes, therefore usually imposing precise assumptions.

For a given adsorption/desorption system, an isotherm is a mathematical model representing the equilibrium balance of the system. It describes the condition between adsorption and desorption when thermodynamic equilibrium is reached (Foo and Hameed, 2010). If the temperature does not change, equilibrium is established after a certain amount of time, depending on thermodynamic parameters and the kinetic of the processes involved (Limousin et al., 2007).

Adsorption kinetics investigates instead how the adsorbate moves and is transferred to the adsorbent surface. In general, kinetic processes include ì) diffusion in the solution (bulk transport), ìì) diffusion through the interface (film transport), and ìiì) diffusion through the pore structure (intra-particle diffusion) (Halim et al., 2010; Ho et al., 2011).

From liquid-solid systems, both isotherms and kinetic models are in general experimentally derived, by measuring the adsorbate molar, or mass, concentrations (equilibrium concentration (C_e), or time-dependent concentration (C_t) for isotherm or kinetic investigations, respectively), and

calculating the corresponding adsorption capacity (at equilibrium (q_e) or time-dependent capacity (q_t)) by applying equation 4 (Wasielewski et al., 2018):

$$q_{e,t} = \frac{V}{m}(C_0 - C_{e,t}) \quad (4)$$

where C_0 is the initial adsorbate concentration, V is the volume of the liquid and m is the mass of adsorbent.

A brief discussion is reserved for thermodynamic parameters, because, particularly in the case of chemical adsorption, along with kinetic factors it highly determines the performance of adsorption processes.

Both the measurable thermodynamic properties as temperature (T) and the equilibrium constant (K_e), and the derived parameters as the activation energy, Gibb's free energy (ΔG), enthalpy (ΔH) and entropy (ΔS) change, are necessary for the evaluation of the adsorption efficiency and the process optimization (Saha and Chowdhury, 2011).

ΔG describes the adsorption spontaneity. If $\Delta G < 0$, the energy of the system decreases during the reaction to reach a more stable state, thus the process is spontaneous.

ΔH and ΔS are T independent. If $\Delta H < 0$, adsorption is exothermic while, if $\Delta H > 0$, adsorption is endothermic. In the first case, the energy absorbed is less than the total energy released, resulting in the release of extra energy in the form of heat, out the adsorption interface to the surrounding environment. The opposite applies in the case of endothermic energy exchange.

In physisorption and ion exchange processes, the heat involved is considerably low, the same magnitude order as condensation heat (e.g., 2.1–20.9 kJ mol^{-1}), while chemisorption energy exchanges are generally higher (80–200 kJ mol^{-1}). ΔH value may thus be an indicator of the underlying process involved (Saha and Chowdhury, 2011).

ΔS represents the state of disorder (or homogeneity) of the system. If $\Delta S > 0$, the homogeneity increases, thus favoring adsorption, as adsorption tends to minimize the concentration gradient. If ΔS

< 0, the homogeneity decreases, and the adsorbate is released to the environment. Thus, adsorption capacity decreases when ΔS lowers (Raghav and Kumar, 2018).

2. AIM

The unbalance between the struvite-forming "bricks" in nutrient-rich wastewaters (NH_4^+>>PO_4^{3-}>Mg^{2+}) is a major issue for struvite precipitation technologies. A possible strategy to balance their stoichiometry may rely on the use of adsorbent materials, like zeolitites, as zeolite minerals may remove the NH_4^+ in excess, storing it along their inner surfaces.

The possibility to recover part of the NH_4^+ before struvite precipitation and the simultaneously controlled raise of the Mg^{2+}/NH_4^+ and PO_4^{3-}/NH_4^+ ratios will better balance the wastewater stoichiometry for struvite precipitation, without the need to add excessive amounts of chemical reagents, possibly permitting to reassess the efficiency of struvite precipitation by cutting down the need of reagents and the potential side effects related to the presence of unwanted chemical residues in the treated wastewater.

Thus, improving the stoichiometric ratios may contribute to making the recovery of N as important as the recovery of P in struvite separation, which currently remains a difficult goal because it can only be prosecuted if the alteration of the effluent is not excessive to preclude any further uses.

Therefore, the aims of the present work were:

- To investigate whether the use of natural and modified zeolites may be a viable strategy to improve the N and P recovery efficiency by struvite chemical precipitation, from agricultural wastewater.
- To define which, between different treatment strategies, could be the best option from an applicational point of view, in terms of ì) nutrient recovery, ìì) reagent use efficiency, ìì) less alteration of the treated wastewater.

- To characterize the materials obtained by the treatment (N-charged zeolitites and struvite precipitates), the treated wastewater; and to access their possible uses in agriculture.

To these purposes, the investigation has been divided into three subsequent steps:

1. **Pre-test:** A preliminary test was carried out on a solution of NH_4Cl and KCl, to study the NH_4^+-N adsorption of a chabazite-rich zeolitite (cha-zeolitite) in the presence of competing ions (K^+); a common condition for agricultural wastewaters. The desorption isotherms of Ca^{2+}, Mg^{2+} and Na^+ were also determined.

2. **Experiment A (exp. A):** A series of tests were carried out to characterize the NH_4^+-N adsorption isotherms, kinetics and thermodynamics of the cha-zeolitite, from zootechnical wastewater (liquid manure). Two different particle sizes had been tested, a micronized cha-zeolitite and a granular one (0.7-2 mm) at three different temperatures (13, 20 and 37 °C).
   The best performing conditions have been selected for experiment B.

3. **Experiment B (exp. B)**: A treatment system has been described at the laboratory scale, that foresees, on one hand, the use of natural zeolites (phase 1) and, on the other hand, the precipitation of struvite (phase 2) for improving the nutrient removal efficiency from an anaerobically digested wastewater (digestate).
   Two different treatment strategies (use of cha-zeolitite and K^+-enriched cha-zeolitite) have been tested and compared with a third treatment (control), in which struvite was obtained in a traditional way, without any use of zeolites.

It is also intended to highlight the following two points:

1) while NH_4^+ adsorption has been largely investigated in synthetic solutions (commonly prepared by using $(NH_4)_2CO_3$ or NH_4Cl) (H.-F. Chen et al., 2018; Gunay, 2007; Huang et al.,

2010; Jha and Hayashi, 2009; Moussavi et al., 2011; Nguyen and Tanner, 2010; Saltali et al., 2007; Wasielewski et al., 2018), only a few studies provided detailed characterizations in real agricultural wastewaters (e.g. Cheng et al., 2017). For this reason, real wastewater (liquid pig slurry) was used in exp. A, thus the adsorption of NH_4^+-N was investigated in a real condition, instead of a simulated one.

2) Struvite precipitation research often uses synthetic wastewaters, defining them as "equivalent" of real wastewaters, but, as stated by many authors, solutions prepared with limited ionic compositions are not representative of real wastewaters (Bonmatí and Flotats, 2003; Huang et al., 2011; Ichihashi and Hirooka, 2012; Nelson et al., 2003; Rahman et al., 2011). The quality of struvite produced from real wastes and its possible contamination (heavy metals, harmful microorganisms etc.) represent indeed a big challenge for its possible use for plant nutrition (Forrest et al., 2008). For these reasons, exp. B was carried out in real wastewater, commonly used as organic fertilizer (liquid digestate from a biogas production plant).

3. MATERIALS

3.1. The adsorbent: cha-zeolitite

The cha-zeolitite was quarried near Sorano village (Italy, 42◦41J26.53" N; 11◦44J35.07" E. Grosseto, Italy), supplied by Verdi S.p.a. company. Its mineralogical composition and CEC are shown in table 1. The material was characterized by the presence of chabazite zeolite (68.5%), naturally enriched in exchangeable potassium (K^+) and calcium ions (Ca^{2+}), a specific feature characteristic of Italian zeolitic deposits. The total CEC of the cha-zeolitite is 2.17 meq g^{-1}. Along with Ca^{2+} and K^+, small amounts of sodium (Na^+) and Mg^{2+} are present as exchangeable cations.

QPA		**CEC**	
Mineral	*[%]*	Cation	*[meq g^{-1}]*
chabazite	68.5 ± 0.9	Ca^{2+}	1.46
phillipsite	1.8 ± 0.4	K^{+}	0.60
Analcime	0.6 ± 0.3	Na^{+}	0.07
k-feldspar	9.7 ± 0.7	Mg^{2+}	0.04
Mica	5.3 ± 0.6		
Pyroxene	2.9 ± 0.4		
volcanic glass	11.2 ± 1.0		
TZC	70.9 ± 1.6	Total CEC	2.17

Table 1. Quantitative Phase Analysis (QPA) by X-ray diffraction (XRD) and Rietveld RIR refinement (at the left of the table), and cation exchange capacity (CEC) (at the right). TZC refers to the total zeolitic content. Data from Malferrari et al., (2013b).

The NH_4^+-N adsorption properties (exp. A) were characterized for two different particle sizes. A granular one (gN_{ZT}) and a micro-sized one (N_{ZT}). The gN_{ZT} particle size distribution (PSD), measured by sequential sieving was as follows: ≤ 5 and > 2 mm (12.5%), ≤ 2 and > 0.8 mm (60.4%), ≤ 0.8 and > 0.425 mm (24.1%), and ≤ 0.425 mm (3%).

PSD of N_{ZT} was measured by X-ray sedimentation technique (Micromeritics SediGraph 5100, USA), imposing a standard particle density at 2.7 g cm^{-3}. Samples were treated with 0.5% Sodium hexametaphosphate ($Na_6[(PO_3)_6]$) in a 1:5 ratio (w:v) before the analyses, to obtain a complete dispersion of the particles. The results, as expressed by the Wentworth classification were: ≤ 250 and > 125 μm - fine sand (0.4%), ≤ 125 and > 62.5 μm - very fine sand (2.8%), ≤ 62.5 and > 3.9 μm – silt (75.6%), and ≤ 3.9 μm – clay (21.2%).

Both gN_{ZT} and N_{ZT} were washed with Milli-Q water and oven-dried at 105° C for 48 h to eliminate any extra-framework water.

To obtain the K^+-enriched cha-zeolitite (K_{ZT}) used in exp. B, an adsorption batch with 1 M KCl was performed with some of the previously washed-and-dry micronized cha-zeolitite (N_{ZT}). 150 g of the adsorbent were added to 500 ml of solution (30% w:v dosage) and mixed at 400 rpm for 24 hours with a drill stirrer. Then, the mixture was washed multiple times with Milli-Q water, until Electrical Conductivity (EC) ≤ 500 μS cm^{-1}. K_{ZT} was separated by decantation and oven-dried at 105°C for 48 hours.

3.2. The wastewaters

Two different nutrient-rich wastewaters were used between exp. A and B. In the first case it was used liquid manure while, in the second, it was employed an anaerobically digested wastewater. Due to their high nutrient loads, both these materials are commonly used as agricultural fertilizers. Two different materials were used for the experiments because of logistical reasons.

3.2.1. Liquid manure (exp. A)

The liquid manure was sampled from a livestock farm located in the Rovigo province (Italy). A rough solid-liquid separation has been applied on the liquid manure by centrifugation (4000 rpm for 10 minutes). The supernatant was collected and used for the exp. A, while the coarser fractions were eliminated.

The pH and NH_4^+-N were measured in 3 replicates as 8.07 ± 0.03 and 2438 ± 35 mg L^{-1}, respectively.

3.2.2. Digestate (exp. B)

The wastewater was sampled in a biogas production plant located near Ferrara city (San Biagio village, Italy 44°58'47″ N; 11°85'86″). It resulted by anaerobic digestion of dairy manure and triticale, and in the following, it will be referred to as "digestate". Suspended solids as vegetable residues and the heavier granular fractions were separated by centrifugation (4000 rpm for 10 minutes) and

discarded. The collected liquid part was stored in closed PVC canisters at 4 °C and soon used in exp. B. The main physical-chemical properties of the digestate are reported in table 2.

pH	7.94 ± 0.02	**NH_4^+-N**	2555 ± 26	**Na^+**	178 ± 5
EC	37.1 ± 1.7	**NO_3^--N**	1.14 ± 0.57	**Mg^{2+}**	85.4 ± 0.4
TN	3132 ± 13	**PO_4^{3-}-P**	59.7 ± 22.2	**K^+**	4159 ± 93
N_{org}	576 ± 7	**Cl^-**	1756 ± 190	**Ca^{2+}**	59.3 ± 2.8

Table 2. Physico-chemical properties of the liquid digestate used in the experiment. The electrical conductivity (EC) is expressed as mS cm^{-1}, The total nitrogen (TN), organic nitrogen (N_{org}), and the other inorganic ions dissolved are expressed as mg L^{-1}. Considering that nitrite amount was below the detection limit (b.d.l.), N_{org} has been derived as:

$$N_{org} = TN - (NH_4^+\text{-}N + NO^{3-}\text{-}N)).$$

4.METHODS

4.1. Pre-test: NZT adsorption and desorption isotherms in the presence of K+ competing ions.

Often, livestock wastewaters have high potassium loads (K^+) which may cause competition with NH_4^+ in exchange processes with cha-zeolitite (Ferretti et al., 2020). Therefore, to develop an efficient treatment process, it is necessary to know how the adsorbent material affects the chemistry of the wastewater during adsorption, and how the cha-zeolitite interacts with K^+ ions and other exchangeable cations in solution.

Therefore, a test was designed to evaluate the adsorption isotherms of NH_4^+ and K^+, and the desorption isotherms of Na^+, Mg^{2+} and Ca^{2+}, in a condition that simulated the NH_4:K molar ratio commonly found in real wastewaters. For the pre-test, only the micronized cha-zeolitite (N_{ZT}) was used. Instead of a real effluent, it was used an NH_4Cl and KCl solution in a 1.0:0.5 molar ratio. This condition perfectly reflected the digestate used in exp. B, which had an NH_4:K molar ratio of 1.00:0.58, or more specifically 182.5 ± 2 and 106 ± 2 mM of NH_4^+ and K^+, respectively.

To define adsorption isotherms in liquid-solid systems, it is necessary to study the variation of the adsorption capacity (q_e) when one of the following parameters changes: ì) the initial adsorbate concentration, ìi) the batch volume, or ììì) the sorbent mass (see equation 4, section 1.4). For this test the first methodology was chosen, therefore 5 solutions were prepared with the following NH_4:K molar concentrations (28:14, 55:28, 83:42, 122:61, 166:83 mM). Each solution was prepared in 3 replicates in 100 mL plastic flasks (closed), thus a total of 15 samples were prepared.

A mass of 3 g of N_{ZT} was added to each flask (6% w:v dosage) and stirred with an orbital shaker at 200 rpm for 20 h.

The NH_4^+-N in solution was measured with an Ion-Selective Electrode (ISE) Orion 95-12 (Thermo-Fisher), while Na^+, K^+, Mg^{2+} and Ca^{2+} were measured by spectroscopic techniques, with an inductively coupled plasma mass spectrometer (ICP-MS) iCAPTQ model (Thermo Scientific, Germany).

4.2. Experiment A: NH4+-N adsorption characterization from liquid manure

The exp. A aimed at the characterization of the adsorption properties of the cha-zeolitite in real zootechnical wastewater and also at the identification of the best performing particle size to use in the exp. B. The NH_4^+-N adsorption of N_{ZT} and gN_{ZT} were evaluated in a nutrient-rich swine liquid manure.

4.2.1. Isotherms

For the evaluation of N_{ZT} and gN_{ZT} isotherms, carried out at 13, 20 and 37 °C, different masses of cha-zeolitite (0.5, 1, 1.5, 3, 5, 8, and 12 g) were mixed with 50 mL of liquid manure inside closed pp bottles (50 mL) in three replicates and stirred with an orbital shaker at 200 rpm for 20 h. Many studies have reported that NH_4^+-N sorption by zeolites is not affected by pH in the range 2–8 while it is negatively affected at pH > 9 (Guo et al., 2008; Li et al., 2011). Since pH barely varied between 8.07

and 8.48 from the beginning of the experiment to the equilibrium conditions, we decided to not investigate the pH effect and thus to avoid buffering the liquid manure. The possible air stripping effects and/or adsorption onto plastic parts of the bottles were considered by including blanks, without any addition of cha-zeolitite. After equilibrium was reached, samples were centrifuged at 4000 rpm for 10 minutes to separate the solid phase from the liquid. NH_4^+-N equilibrium adsorption capacity (q_e, mg g^{-1}) was determined in the supernatant by equation 4 (see section 1.4).

In the following paragraph, only the isotherms that showed the most significant correlations with the experimental data will be discussed.

The Langmuir isotherm (Langmuir, 1918) is a function used for chemisorption that assumes that the energetic properties of the adsorption sites are equivalent, it is thus commonly used for energetically homogeneous systems. Due to the formation of one single adsorption layer (monolayer condition), the Langmuir model assumes the existence of a maximum adsorption capacity q_{max} (the most correct way to express adsorption capacity should be as the amount of adsorbate per surface area (mol m^2), but for practical reasons, it is preferred to referred to as mass of adsorbate per unit mass of adsorbent (mg g^{-1})). q_{max} represents a saturation condition that is practically impossible to reach. Langmuir isotherm is expressed by equation 5:

$$q_e = \frac{q_{max} K_L C_e}{1 + K_L C_e} \tag{5}$$

where q_e is the equilibrium adsorption capacity (mg g^{-1}), K_L is the Langmuir constant and C_e is the equilibrium concentration of the adsorbate (mg L^{-1}). The linearization is given by equation 6 (Wang and Guo, 2020):

$$\frac{1}{q_e} = \frac{1}{q_{max} K_L} \frac{1}{C_e} + \frac{1}{q_{max}} \tag{6}$$

Harkins-Jura isotherm has been originally proposed for explaining the physical adsorption of gas molecules, but it has been extended also to liquid-solid systems (Iyer and Kunju, 1992). It assumes

the possibility of multilayer adsorption in adsorbents with a heterogeneous pore distribution (Harkins and Jura, 1944). Rawajfih et al., 2010 have applied the Harkins-Jura model to a cha-zeolitite to describe the adsorption of α, β, and γ-picoline from an aqueous solution. The linear form of the Harkins-Jura model is expressed by equation 7 (Shanavas et al., 2011):

$$\frac{1}{q_e} = \beta_H \, In(C_e) + \alpha_H \tag{7}$$

where q_e is the equilibrium adsorption capacity (mg g^{-1}), C_e is the equilibrium concentration of the sorbate in the liquid phase (mg L^{-1}), α_H and β_H are constants, in particular, for the plot $1/q_e$ against $In(C_e)$, α_H represent the intercept (at C_e=0), while β_H is the slope, which is linked to the specific surface area (S) by equation 8 (Iyer and Kunju, 1992):

$$\beta_H = -\frac{q \, S^2}{4.606 \, R \, T \, N_A} \tag{8}$$

where q is a constant dependent on the nature of the adsorbate, R is the universal gas constant (8.314 J K^{-1} mol^{-1}), T is the temperature (K) and N_A is the Avogadro constant (6.022×10^{23} mol^{-1}).

The Freundlich isotherm is an empirical model that can be used to explain the equilibrium relation in the case of multilayer adsorption with heterogeneous materials (Ho and McKay, 2002). It has been widely used in gas adsorption and environmental soil chemistry (Sparks, 2002). The isotherm model is expressed by equation 9:

$$q_e = K_F \, C_e^{1/n} \tag{9}$$

where K_F is the Freundlich constant, C_e is the equilibrium concentration (mg L^{-1}) and n is a constant dependent on the nature of the adsorbate, the adsorbent and temperature. A linear form of Freundlich isotherm is given by equation 10 (Subramanyam and Das, 2014):

$$In(q_e) = n^{-1} \, In(C_e) + In(K_F) \tag{10}$$

Temkin isotherm is an empirical model that presumes multilayer adsorption. It is expressed by equation 11 (Temkin and Pyzhev, 1940):

$$q_e = \frac{R\,T}{b_T} In(A_T\,C_e) \quad (11)$$

where A_T is the Temkin isotherm equilibrium binding constant and b_T is the Temkin isotherm constant (J mol^{-1}) (Dada et al., 2012).

4.2.2. Kinetics

For the study of NH_4^+-N adsorption kinetic, 123 g of N_{ZT} or gN_{ZT} (0.2 g per mg NH_4^+-N L^{-1} (Wasielewski et al., 2018)) was added to 0.5 L of liquid manure and mixed at 400 rpm, 20° C for 420 minutes. An aliquot of 10 mL was sampled at periodic intervals (5, 10, 20, 30, 45, 60, 120, 180, 270, 360, and 420 min), immediately centrifuged at 4000 rpm for 4 minutes to separate the solid from the liquid fraction and the NH_4^+-N concentration was measured by using an Ion-Selective Electrode (ISE) (Orion 95–12). Because of the sampling, the volume of the batch was continuously reduced, but it can be assumed that no changes in the solid/liquid ratio occurred because of the homogeneity of the suspension.

Experiments were carried out in three replicates and a batch without zeolitite (blank) was also included to evaluate the possible air stripping effect. NH_4^+-N at every time point were measured (C_t, mg L^{-1}) as well as the pH. The time-dependent NH_4^+-N adsorption capacity (q_t, mg g^{-1}) was calculated by equation (4) (see section 1.4).

To test the validity of kinetic models, it is important to compare not only the r^2 of the model but also the calculated q_e with the measured one (Simonin, 2016). A "near-equilibrium" condition was reached at 180 minutes; it was therefore assumed that $q_{t,180} \approx q_e$.

As pointed out by Simonin (2016), for kinetic investigations it should be taken into account only data sufficiently far from equilibrium condition, and for this reason only data with a fractional uptake F(t) < 85% have been considered (equation 12), corresponding to the data collected between 0 and 120 minutes.

$$F(t) = q_t/q_e \tag{12}$$

where q_e is the equilibrium adsorption capacity (mg g^{-1}) and q_t is the time-dependent adsorption capacity (mg g^{-1}).

The pseudo-first-order model (PFO), proposed by Lagergren and Sven (1898), can be described by equation 13:

$$\frac{dq_t}{dt} = k_1(q_e - q_t) \tag{13}$$

where q_e and q_t are the equilibrium adsorption capacity and the adsorption capacity at time t=t respectively (mg g^{-1}). The expression (q_e−q_t) is the driving-force; it governs the adsorption kinetic and it is proportional to the available numbers of active sites (Ho, 2006); t is the contact time (min) and k_1 is the PFO rate constant (Ho and McKay, 1998).

Its linearization is given, by equation 14 (Qiu et al., 2009):

$$In(q_e - q_t) = -\frac{k_1}{2.303}\ t + In(q_e) \tag{14}$$

If sorption kinetic is a second order mechanism, the pseudo-second-order (PSO) model should be considered as expressed by equation 15 (Ho and McKay, 1998):

$$\frac{dq_t}{dt} = k_2(q_e - q_t)^2 \tag{15}$$

where q_t is the time-dependent adsorption capacity (mg g^{-1}), t is the contact time (min), k_2 is the PSO rate constant and q_e is the equilibrium adsorption capacity (mg g^{-1}).

The linear form may be expressed by equation 16 (Ho and McKay, 1999):

$$\frac{t}{q_t} = \frac{1}{q_e}t + \frac{1}{h} \tag{16}$$

where h is the initial adsorption rate (mg g^{-1} min^{-1}). k_2 may be derived from this expression by equation 17:

$$k_2 = \frac{h}{{q_e}^2} \quad (17)$$

All the PSO parameters are thus determinable from the plot t/q_t against t (Dursun et al., 2005; Mall et al., 2006; Widiastuti et al., 2011).

The intra-particle diffusion (ID), proposed by Weber and Morris (1962), is a diffusion-controlled process that assumes that the adsorption mechanism occurs through the diffusion of the adsorbates into the pores of the adsorbent material (Simonin and Bouté, 2016; Weber and Morris, 1962). In ID models, the adsorption onto the active sites, and/or the diffusion of the adsorbate in the liquid film around the adsorbent are instantaneous. ID, as expressed by Weber and Morris, (1962), is given by equation 18:

$$q_t = k_{ID}\, t^{1/2} + C \quad (18)$$

where q_t is the adsorption capacity at time t=t (mg g^{-1}), k_{ID} is the ID rate constant (mg g^{-1} min^{-1}) and C is the intercept of the plot q_t against $t^{1/2}$ (mg g^{-1}) and it is proportional to the thickness of the boundary layer (Widiastuti et al., 2011).

If $C \approx 0$, it can be assumed that kinetic is governed by ID (Wasielewski et al., 2018), while if two or more regression lines are present, multiple diffusion processes occurred and adsorption was not governed only by ID (Martins et al., 2015). In general, the first line represents the external surface adsorption and/or macropore diffusion (Ø > 50 nm), while the others, if present, are representing the diffusion through mesopores ($2 \leq Ø \leq 50$ nm) and micropores (Ø < 2 nm) (Widiastuti et al., 2011).

The Elovich kinetic model was historically applied to determine the kinetics in the chemisorption of gases onto heterogeneous solids (Ho and McKay, 1998; Rudzinski and Panczyk, 2000) where the rate of adsorption decreases with time due to the increase in the surface coverage. Starting from twenty years ago, the Elovich kinetic model has been applied to describe adsorption processes of different pollutants from aqueous solutions (Cheung et al., 2001; Sağ and Aktay, 2002). In 2004, it has been applied to natural zeolites, to describe the sorption kinetics of cadmium(II) from a solution (Cortés-Martínez et al., 2004).

The Elovich equation is in general expressed as follows:

$$\frac{dq_t}{dt} = \alpha_E \exp(-\beta_E q_t) \tag{19}$$

where q_t is the adsorption capacity (mg g^{-1}), t is time, α_E and β_E are constants and, in particular, α_E is related to the initial adsorption rate.

The Elovich model can be expressed in linear form by equation 20 (Ho and McKay, 1998):

$$q_t = \left(\frac{2.303}{\alpha_E}\right) In\,(t + t_0) - \left(\frac{2.303}{\alpha_E}\right) In(t_0) \tag{20}$$

The dimensionless Elovich model (equation 21), introduces R_E which is an "approaching-equilibrium parameter" that represent the velocity, or tendency of the system to approach equilibrium (Wu et al., 2009):

$$\frac{q_t}{q_{ref}} = R_E\, In\left(\frac{t}{t_{ref}}\right) + 1 \tag{21}$$

where q_t is the adsorption capacity (mg g^{-1}), t_{ref} (reference) is the longest operating time in the adsorption experiment (min) and q_{ref} is the adsorption capacity at time $t=t_{ref}$ (mg g^{-1}). In kinetic tests of the exp. A, the last sampling was at 420 minutes, thus that time corresponded to t_{ref}. For estimating the q_e, it was assumed that $t_{ref} = t_e$, thus $q_{ref} = q_e$.

4.2.3. Thermodynamics

ΔG was calculated by equation (22):

$$\Delta G = -RT\, In(K_e) \tag{22}$$

where R is the universal gas constant (8.314 J K^{-1} mol^{-1}), T is the temperature (K) and K_e is the thermodynamic equilibrium constant. K_e has been derived by equation 23, extrapolating its value from the plot q_e/C_e against C_e at the intercept $C_e = 0$ (Khan and Singh, 1987).

$$K_e = \lim_{C_e \to 0} \frac{q_e}{C_e} \tag{23}$$

The standard enthalpy change (ΔH, J mol^{-1}) and the standard entropy change (ΔS, J K^{-1} mol^{-1}) have been calculated by the van 't Hoff isochore (plot of ln(K_e) against 1/T) from which the regression line has a slope equal to -ΔH/R and intercept equal to ΔS/R (equation 24) (Gunay, 2007).

$$In(K_e) = -\frac{\Delta H}{R}\frac{1}{T} + \frac{\Delta S}{R} \quad (24)$$

4.2.4. Analytical techniques and data analysis

For the exp. A, the NH_4^+-N concentration in liquid manure was measured in a 1:20 dilution with Milli-Q water, by using an Ion-Selective Electrode (ISE) Orion 95–12. pH was measured using an Orion 9102BNWP pH-meter. Both ISE and the pH-meter were connected to an Orion 4star pH–ISE benchtop (Thermo Fisher Scientific, Waltham, MA, USA).

Thermodynamic parameters were calculated at three different temperatures (286, 293, and 310 K, equal to 13, 20, and 37 °C respectively).

Isothermal and kinetic models were tested by using R Studio software (R Core Team, 2019) with the packages PUPAIM (Saroyda et al., 2001) and SorptionAnalysis (Chattopadhyay, 2017).

4.3. Experiment B: Combination of cha-zeolitite adsorption and struvite precipitation for the treatment of an anaerobically digested wastewater

Within exp. B, cha-zeolitite has been applied in combination with struvite precipitation. The outcomes of exp. A (section 5.2) led to the choice of using the micronized zeolitite (N_{ZT}) in the exp. B, instead of the granular one (gN_{ZT}). This decision was driven by the ì) higher adsorption capacities achieved by N_{ZT}, ìì) more stability respect temperature changes, and ìiì) higher velocities to reach equilibrium conditions. All these aspects are significant for the possible future scaling up of the system.

In general, the treatment was composed of two distinct phases, in order ì) phase 1: cha-zeolitite adsorption batch; ìì) phase 2: struvite precipitation. Both the cha-zeolitite and the struvite were separated from the digestate after each phase.

Three different treatment strategies were tested: ì) NZT-S: N_{ZT} adsorption batch (phase 1) + struvite precipitation (phase 2); ìì) KZT-S: K_{ZT} batch (phase 1) + struvite (phase 2); ìiì) CNTR: struvite precipitation (phase 2) directly from the digestate, without any cha-zeolitite adsorption phase. The CNTR represented a traditional chemical struvite treatment, thus it was included for the comparison with the proposed strategies of NZT-S and KZT-S.

After phase 1, PO_4^{3-} and Mg^{2+} reagents were used in different amounts, to test different conditions for struvite precipitation. Two $Mg:NH_4:PO_4$ molar ratios were tested, in particular: ì) 1:1.5:1 (MR 1) and ìì) 2:1:1 (MR 2).

In MR 1, it was tested a condition of NH_4^+ excess, which better represents the natural state of many wastewaters, including the digestate used in this experimentation. Furthermore, an excess of NH_4^+ in solution has been described as the optimum way to obtain high purity crystals (Stratful et al., 2004). In MR 2 a strong excess of Mg^{2+} was tested, while NH_4^+ and PO_4^{3-} ions were the limiting factors for struvite precipitation. It was chosen to investigate MR 2 conditions because many authors reported

strong positive effects for P recovery by increasing the Mg^{2+}:PO_4^{3-} molar ratio (Kim et al., 2007; Martí et al., 2010; Quintana et al., 2005).

For each treatment, the N-enriched cha-zeolitites (post-treatment), the precipitates and the digestate chemical-physical characteristics were investigated.

In summary, in the exp. B the following conditions were tested:

Materials tested:

- N_{ZT}: micronized cha-zeolitite.
- K_{ZT}: K^+-enriched micronized cha-zeolitite.

Treatments tested:

- NZT-S: phase 1 (cha-zeolitite adsorption) + phase 2 (struvite precipitation, MR 1 and MR 2).
- KZT-S: phase 1 (K^+-enriched cha-zeolitite adsorption) + phase 2 (struvite precipitation, MR 1 and MR 2).
- CNTR: only phase 2 (struvite precipitation, MR 1 and MR 2), without any cha-zeolitite adsorption phase.

Molar ratios ($Mg:NH_4:PO_4$) tested:

- MR1: 1:1.5:1.
- MR2: 2:1:1.

Every treatment was tested in 4 replicates.

4.3.1. Preparation of the K+-enriched cha-zeolitite (KZT)

N_{ZT} has significant amounts of exchangeable Ca^{2+} that may greatly inhibit the formation of struvite crystals, leading to other unwanted species as analogues of struvite, insoluble phosphates, carbonates, or others (Acelas et al., 2015; Hao et al., 2008; Stefov et al., 2004; Yang et al., 2011; Yang and Sun, 2004; ZhangHan et al., 2019). For this reason, to counteract any possible Ca^{2+} interference it was

chosen to test a cha-zeolitite pre-exchanged with K^+ (K_{ZT}). The removal (or desorption) of most of the Ca^{2+} ions and the enrichment in K^+, which is a macronutrient for plants, could represent an interesting option, even if it is reported less NH_4^+ removal efficiencies obtained by a K^+-enriched cha-zeolitite (Leyva-Ramos et al., 2010).

The details about the K_{ZT} preparation are described in section 3.1.

4.3.2. Equilibrium concentration target

Cha-zeolitite adsorption (phase 1) is aimed at the mitigation of the strong excess of NH_4^+ ions, which is a constant feature of agricultural and zootechnical wastewaters in general. The aim was to better balance the concentration ratios of Mg^{2+}, NH_4^+ and PO_4^{3-} for the struvite precipitation purpose.

To normalize the process and better compare the results, it was chosen to obtain the same NH_4^+-N removals for both N_{ZT} and K_{ZT}. Phase 1 should have thus dropped the NH_4^+-N from the initial value of 2555 mg L^{-1} (C_0) (see section 3.2.2) to the equilibrium concentration wanted (here referred to as C_e target; $C_{e.tg}$), arbitrarily chosen at 1300 mg L^{-1}, corresponding to an abatement of about 50%.

To estimate the amount of N_{ZT} and K_{ZT} needed, the adsorption isotherms were evaluated as following described. Different amounts of N_{ZT} or K_{ZT} (1.5, 3, 4, 5, 7, 10 and 12 g) were mixed with 50 mL of digestate inside closed plastic bottles and stirred with an orbital shaker at 170 rpm, 20 °C. After 10 hours, it was assumed that a near-equilibrium condition was reached. The liquid fraction was separated from the cha-zeolitite by centrifugation (4000 rpm for 10 min). NH_4^+-N concentrations were immediately measured by Kjeldahl direct distillation (5 ml of samples diluted in 25 ml of Milli-Q water (v:v = 1:6). NH_4^+-N losses due to NH_3 stripping were negligible, as demonstrated by C_e measurements obtained from 3 blanks (composed only by digestate, without any cha-zeolitite). q_e (mg g^{-1}) were calculated by equation 4 (section 1.4).

4.3.3. Phase 1: NH4+-N recovery by NZT and KZT adsorption

To reach the $C_{e.tg}$ (1300 mg L^{-1} of NH_4^+-N) by a single adsorption batch, precise amounts of N_{ZT} or K_{ZT} were used, extrapolated from the respective isotherms. The mass balance for an adsorption system at equilibrium may be expressed by equation 25:

$$VC_0 = VC_e + m\, q_e \tag{25}$$

where m is the mass of the adsorbent (g), V is the batch volume (L), q_e is the equilibrium adsorption capacity (mg g^{-1}), C_0 is the initial NH_4^+-N concentration (mg L^{-1}) and C_e is the adsorbate concentration in solution at equilibrium condition (mg L^{-1}).

By imposing $C_e = C_{e.tg}$ (arbitrarily chosen at 1300 mg NH_4^+-N L^{-1}) and $q_e = q_{e.tg}$ (derived from the isotherms), it is possible to calculate the mass of adsorbent (equation 26):

$$m = \frac{V}{q_{e.tg}}(C_0 - C_{e.tg}) \tag{26}$$

The calculated dosages of N_{ZT} and K_{ZT} needed were 25.0 and 25.7% (w:v), respectively. Thus, 12.5 g of N_{ZT} or 12.93 g of K_{ZT} were added to 50 ml of liquid digestate in closed plastic tubes and stirred at the same conditions described in section 4.3.2 (10 hours at 170 rpm, 20 °C). The cha-zeolitites were then separated from the liquid fraction by centrifugation at 4000 rpm for 10 minutes. An aliquot of 5 ml was sampled from each replicate and pH, EC and NH_4^+-N were immediately measured. Another aliquot of 5 ml was sampled and stoked at -4 °C for further IC and ICP-MS analysis.

N_{ZT} and K_{ZT} were washed several times with Milli-Q water until the EC was ≤ 500 µS cm^{-1}. In this condition, it was assumed that most of the residues were eliminated.

It was chosen to dry at low temperatures (65 °C for 48 hours) to not lose any adsorbed N. Once dried, the materials were stored in closed plastic tubes, inside a desiccator, maintained at room temperature (20 °C) until further analysis.

The digestate post-phase 1, depleted in NH_4^+-N, was instead immediately used for the following struvite precipitation step (phase 2).

4.3.4. Phase 2: NH4+-N and PO43--P recovery by struvite precipitation

It was chosen to not use any NH_4^+-based reagent in the digestate, thus struvite has been produced only by the NH_4^+-N present in the wastewater. This amount corresponded to the initial NH_4^+-N load in the case of the CNTR treatment (C_0 = 2555 mg L^{-1}), or it corresponded to the equilibrium concentration for NZT-S and KZT-S treatments after phase 1 (C_e = 1388 ± 31 and 1334 ± 26 mg L^{-1} obtained by N_{ZT} and K_{ZT}, respectively; see section 5.3.2.).

To reach MR1 and MR2 conditions, Mg^{2+} and PO_4^{3-} reagents have been used in the forms of $MgSO_4 \cdot 7H_2O$ and K_2HPO_4, respectively.

It is important to remember that not all the treatments tested involved the zeolite adsorption phase, thus, to reach MR1 and MR2, more amounts of reagents have been used in the CNTR than NZT-S and KZT-S because these two treatments provided a preliminary adsorption phase which depleted the wastewater in NH_4^+-N, permitting to use fewer amounts of reagent to reach the molar ratios desired. In the CNTR, the reagents were added directly into the untreated digestate, thus more amounts of reagents were used in CNTR compared with NZT-S and KZT-S, while in these two treatments, reagents were added after phase 1. In table 3, the Mg^{2+}, NH_4^+ and PO_4^{3-} concentrations in the wastewater (mM) are displayed, before and after the addition of the reagents.

	CNTR		**NZT-S**		**KZT-S**	
	MR 1	MR 2	MR 1	MR 2	MR 1	MR 2
T_0 *[mM]*	3.5:182:3.4		6.1:99:1.6		6.1:95:0.52	
T_s *[mM]*	121:182:121	364:182:182	63:94:63	188:94:94	63:94:63	188:94:94

Table 3. Mg:NH_4:PO_4 molar concentrations (mM) in the digestate before struvite precipitation (T_0) and after the addition of the Mg^{2+} and PO_4^{3-} reagents (T_s). CNTR T_0 represents the untreated raw digestate, while NZT-S T_0 and KZT-S T_0 represent the conditions after phase 1 (cha-zeolitite adsorption by N_{ZT} and K_{ZT} respectively).

Reagents were dissolved in little amounts of Milli-Q water at a ratio of 1:0.4 (v:v; digestate/water) and quickly added together at the same time. pH was immediately adjusted to 9 by the use of KOH 30%. During this phase, digestate was constantly stirred at 150 rpm. It was chosen to dose the reagents before the adjustment of the pH because many authors reported that the best performances are expected (Kim et al., 2007; Siciliano and De Rosa, 2014). The optimal pH is reported to be between 8.9-9.2 (Muster et al., 2013) or 8.8-9.4 (Gunay et al., 2008) thus it was chosen to buffer at pH 9. Potassium hydroxide (KOH) 30% was used. During the addition of KOH, a light brownish powder precipitate quickly appeared.

Many studies in literature reported the use of sodium hydroxide (NaOH) for pH adjustment (Brown et al., 2018; Xavier et al., 2014; Zhang et al., 2014), but aiming to obtain treated wastewater usable for fertilization, it was avoided the use of NaOH to not enrich it in sodium (Na^+) ions which are known to be dangerous both for soil structure (particle dispersion) and plants (toxicity) (Ferretti et al., 2018).

To separate the precipitate from the liquid fraction, samples were centrifuged at 4000 rpm for 10 min. An aliquot of 5 ml was immediately taken from the top from which pH, EC and NH_4^+-N were suddenly measured. Another aliquot of 5 ml was stoked at -4 °C for further IC and ICP-MS analyses. The precipitates were washed multiple times with Milli-Q water until EC was < 500 µS cm^{-1}. Most of the precipitate was beige-colored, but some thin and dark-brown, muddy layers were deposited on top of it, especially in MR 2 conditions. The two materials were separated and the most significant one (beige-colored) was the most characterized. The amount of the dark matter collected by each sample was insufficient for characterization, so it was chosen to mix it before analysis.

Only in the CNTR_MR 2 (the treatment with the higher addition of Mg^{2+} and PO_4^{3-}), some secondary phases (spheric-shaped precipitates) developed after a few hours from the addition of the reagents. These phases were also collected and investigated.

Struvite is highly sensitive to temperature, and it easily decomposes by losing both water and NH_3-N at relatively low temperatures (Bayuseno and Schmahl, 2019; Bhuiyan et al., 2008; Frost et al., 2004). Pre-tests were made from 65 to 105 °C and significant amounts of N were lost, so it was chosen to dry at 35 °C for 48 hours. In this way, probably not all the extra-framework water was eliminated, and it was not possible to accurately estimate its residual amounts, but it was thought to be a good compromise between the dryness and the possibility to lose N. The dried precipitates were stored in a desiccator at 20° C, inside closed plastic tubes until analyses.

4.3.5. Analytical techniques

Different analytical techniques were applied for the liquid digestate (post phase 1 and post phase 2) and the solids obtained (N-enriched N_{ZT}, N-enriched K_{ZT} and the precipitates of phase 2). Regarding the digestate, the aim was to monitor its chemical differentiation among each treatment phase, while, for the solids, the aim was to characterize their N-content (cha-zeolitite and precipitates).

The following parameters were evaluated before and after each phase of the experiment.

pH was measured with an electrode connected to an 877 TitrinoPlus automatic titration unit (Methrom, Italy).

EC was measured in 1:100 (v:v) diluted samples (Milli-Q water) with a RS 180-7127 probe (Hannah instrument, Italy); the dilution aimed also at bypassing any possible bias due to turbidity.

Total Kjeldahl Nitrogen (TKN) was evaluated only in the initial digestate (used in exp. B) for its characterization but, being that the investigated processes (cha-zeolitite adsorption and struvite precipitation) mainly involve NH_4^+ ions, it was chosen to not characterize the TKN among each treatment tested. TKN was measured according to the classic Kjeldahl method. TKN requires sample digestion in concentrated H_2SO_4 before the analysis. In this way, N bonded to organic matter is converted to mineral NH_4^+. The acid digestion was performed with a SpeedDigester K-425 (Büchi,

Switzerland) by adding 10 ml of 98% H_2SO_4 and 1 tablet of catalyst (containing TiO_2, $CuSO_4$, K_2SO_4) to the sample and raising the temperature until complete digestion.

NH_4^+-N was immediately measured after each step by Kjeldahl direct distillation (without acid digestion). Both the digested and the undigested samples were distilled with a K-360 Distillation unit (Büchi, Switzerland) connected to a titration unit (TitrinoPlus). The addition of NaOH and the steam distillation converts the NH_4^+ into NH_3, which is conveyed into an H_3BO_3 4% acid trap buffered at pH 4.56 ± 0.01. N (both TKN and NH_4^+-N) was then accounted for, by end-point titration using certified 0.25 M H_2SO_4.

Fluoride (Fl^-), chloride (Cl^-), nitrite (NO_2^-), bromide (Br^-), nitrate (NO_3^-), phosphate (PO_4^{3-}) and sulfate (SO_4^{2-}) were measured in Milli-Q diluted (1:25; v:v) and filtered (with PTFE syringe filters, 20 µm) samples, by liquid ion chromatography (LIC) with an ICS 1000 Dionex isocratic dual pump system connected to an AS40 Autosampler. The LIC system was constituted by an AS9-HC 4x250 mm anion column, an AG9-HC 4x50 mm guard column and an ADRS600 suppressor.

Total phosphorous (TP), Alkali, alkaline earth elements and metals were measured by ICP-MS (iCAPTQ model, Thermo Scientific, Germany) in Milli-Q diluted samples (1:1000; v:v) acidified with 3% HNO_3 and filtered with PTFE syringe filters (20 µm).

The applied N_{ZT} and K_{ZT}, as well as the precipitates, were additionally characterized for their total N (TN) and total carbon (TC) by an Elementar Analyzer (EA) (Elementar, Vario Micro Cube, Germany) in line with an Isotopic Ratio Mass Spectrometer (IRMS) (Thermo Fischer Scientific, ISOPRIME 100, USA) operating in a continuous-flow mode.

The imaging of the precipitates was carried out by a ZEISS EVO MA 15 scanning electron microscope (SEM) coupled with an energy-dispersive X-ray spectroscopy (EDS) system (Aztec Oxford), equipped with a silicon drift detector (SDD). A LaB6 filament as electron source and cobalt as calibration standard were used for microstructural characterization and to determine the chemical

compositions of samples. The samples were studied at 20 kV and an 8.5 mm working distance under a high vacuum. Samples were precoated with graphite film.

Two selected precipitates obtained by NZT-S_MR 1 and KZT-S_MR1 were further characterized for their mineral composition by XRD technique, performed using a X'Pert Pro MPD (PANAlytical, Netherlands) diffractometer. The instrument implements long fine focus Cu anode working at 40 kV, 40 mA and goniometer (radius=240 mm) that operates in the θ/θ geometry. Incident beam optics include divergence slits of ½°, antiscatter slits of 1°, Soller slits of 0.04 rad, beam mask of 20mm side aperture. A beam knife, positioned above the sample centerline, has been used to reduce air scattering contribution at low 2θ angle.

Diffracted beam optics are composed of antiscatter slit of 9.1mm aperture, Soller slits of 0.04 rad, Ni-filter to suppress Kbeta and PIXCel Position Sensitive Detector with a 3.347° 2θ active length. Total scan time is approximatively 45 minutes.

Measures were carried out between 5° and 90° 2θ angle, using a 0.013° step size, counting 100s per virtual step on a spinning sample (1 rev. per second). The two precipitates were front-loaded over a zero-background silicon crystal sample holder. For the quantification of the amorphous phase, a 20% (w:w) dose of ZnO has been added to the zeolitic tuff sample. The fundamental parameters approach, as implemented in Profex-BGMN (v.5.0.1), was used in the Rietveld refinements and the associated quantitative phase analyses (QPA) (Rietveld, 1967; Bish and Howard, 1988; Gualtieri, 2000; Cheary et al., 2004; Doebelin and Kleeberg, 2015) Crystal structures were obtained from the BGMN database.

Heavy metals were measured only for the NZT-S MR1 precipitate (3 replicates), by ICP-MS technique, in hot-plate mineralized samples. Thus, a 2:1 (v:v) mixture of 65% HNO3 and 40% HF were added to 0.5 g of sample into a Teflon digestion vessel and heated at 180 °C until complete mineralization and drying. The dried residue was then resuspended in 100 mL of 1.3% HNO3 solution and measured by ICP-MS.

4.3.6. Estimation of the reagent use efficiency

To better visualize the struvite precipitation efficiency, and to better confront MR1 and MR2, it may be useful the concept of theoretical NH_4^+-N recovery (Tr, mg L^{-1}), where Tr represents the maximum amount of NH_4^+-N theoretically removable from 1 L of solution by struvite precipitation.

The Tr values were calculated by equation 27:

$$T_r = [NH_4^+ N]_{b.s} \times \frac{e_r}{100} \quad (27)$$

where $[NH_4^+\text{-N}]_{b.s}$ is the concentration in the digestate before struvite precipitation (mg L^{-1}) and e_r is the expected NH_4^+-N recovery.

$[NH_4^+\text{-N}]_{b.s}$ was equal to the initial concentration for the CNTR (2555 mg L^{-1}), or the residual concentration (after phase 1) for NZT-S (1389 mg L^{-1}) and KZT-S (1333 mg L^{-1}).

The e_r parameter account for the possible limitations in struvite precipitation reactions, due to the different molar ratios applied. In fact, not the same amount of NH_4^+-N could have been recovered in both MR1 and MR2 conditions, as the $Mg:NH_4:PO_4$ ratios testes (1:1.5:1 and 2:1:1 for MR1 and MR2, respectively) were highly different from the theoretical ratio of pure struvite (1:1:1). Therefore, in MR1, both Mg^{2+} and PO_4^{3-} limited the struvite precipitation, and NH_4^+ was in excess, while, NH_4^+ and PO_4^{3-} were the limiting agents, and Mg^{2+} was in excess in MR2. Following, e_r was equal to 100 for MR2, or $66.\overline{6}$ for MR1.

The NH_4^+-N recovery efficiencies by struvite precipitation may then be estimated by the ratio between the actual recovery (Ar, mg L^{-1}) and Tr, expressed as NH_4^+-N recovery % ($R_{\%}$) in equation 28:

$$R_{\%} = 100 \times \frac{A_r}{T_r} \quad (28)$$

Note: for a more precise evaluation of $R_{\%}$, Tr and Ar have been corrected for the dilution factor, due to the addition of water used for dissolving the reagents during phase 2 (see section 4.3.4).

Finally, it should be noted that $R_{\%}$ is not indicating the absolute NH_4^+-N recovery by struvite, or the amounts of struvite produced. It is instead related to the efficiency in the use of reagents, the higher $R_{\%}$, the most the NH_4^+-N recovered approached the expectations, thus fewer reagents were "wasted".

5. RESULTS AND DISCUSSION

5.1. Pre-test: adsorption and desorption isotherms

NH_4^+-N and K^+ q_e vs. C_e plots are represented in figure 3.

While equilibrium adsorption of NH_4^+-N well related with Harkins-Jura isotherm (equation 7, section 4.2.1), the behavior of K^+ was different and none of the models tested correlated with the experimental data, so it was decided to use a 3rd degree polynomial to illustrate the general trend.

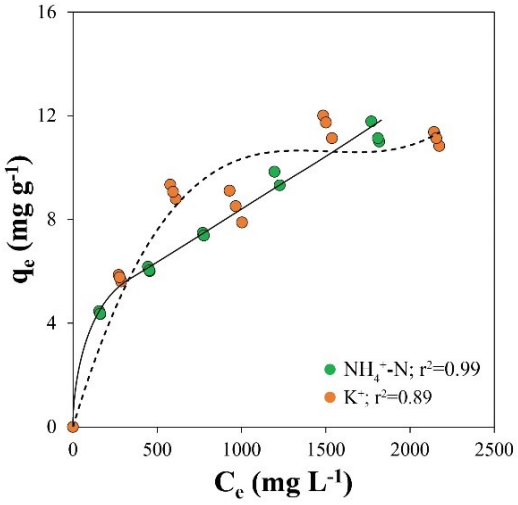

Figure 3. q_e vs. C_e plot for NH_4^+-N and K^+. The line represents the Harkins-Jura isotherm for NH_4^+-N adsorption, while the dashed line is a 3rd degree polynomial for K^+.

In ion exchangers, when the concentration of the studied ion is low compared to the concentration of other competing ions, the composition of the bulk solution can be considered constant and a single-species isotherm can be applied, whose characteristics remain strongly dependent on the composition

of the bulk solution. However, when the concentration of the studied ion reaches the same order of magnitude as other competing ions, the composition of the bulk solution can no longer be considered constant, and a multispecies isotherm may be needed (Limousin et al., 2007). In the pre-test, a molar concentration of 1.0:0.5 (NH_4^+:K^+) was used (section 4.1). The presence of competing ions (NH_4^+ for K^+ adsorption, and K^+ for NH_4^+ adsorption) may possibly explain the particular shape of the isotherms, and the presence of an inflection point (at least in Harkins-Jura isotherm) that represent a renewed availability of adsorption sites (at the right of the graph), and thus, changes in the dynamic equilibrium between adsorption and desorption.

Ca^{2+}, Na^+ and Mg^{2+} have described linear isotherms (C-type) with zero-point origin. C-type isotherms indicate that the ratio between the concentration of the ions in solution and the adsorbed ones are always constant (figure 4) (Limousin et al., 2007).

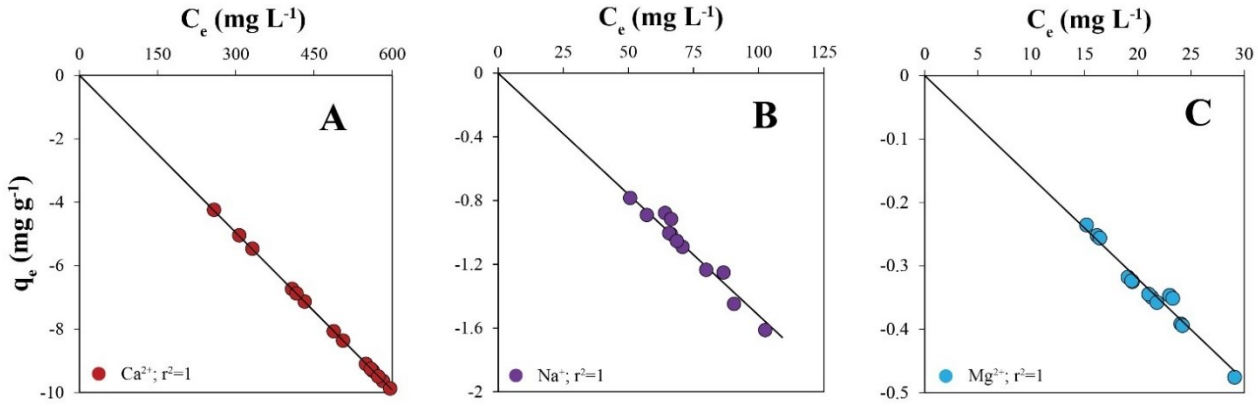

Figure 4. Desorption linear isotherms and relative r^2 for A: Ca^{2+}; B: Na^+ and C: Mg^{2+}.

C-type isotherms are mathematically expressed by equation 29:

$$q_e = K_d C_e \tag{29}$$

where the constant K_d (L g^{-1}) is the distribution coefficient.

These isotherms are approximations that, in real applications, are applicable only if the chemical species is present in small amounts, compared with other competing species (e.g. for the study of trace pollutants). An estimate was calculated for the desorption of Ca^{2+}, Na^+ and Mg^{2+} expected in

the exp. B, based on the isotherms of figure 4, but the calculated values were strongly overestimated, compared to the real enrichments measured in the digestate (see section 5.3.3).

As expected, the desorption followed the CEC of the N_{ZT}, being Ca^{2+}>Na^{+}>Mg^{2+} (see section 3.1). The K_d was not significantly different, being 0.0165, 0.0152 and 0.0160 L g^{-1} for Ca^{2+}, Na^{+} and Mg^{2+}, respectively.

5.2. Experiment A

5.2.1. Isotherms

The plots of q_e against C_e are reported in figure 5, while the best representative isotherm model parameters (Harkins-Jura, Freundlich, and Langmuir isotherms) between the tested models, are reported in table 4.

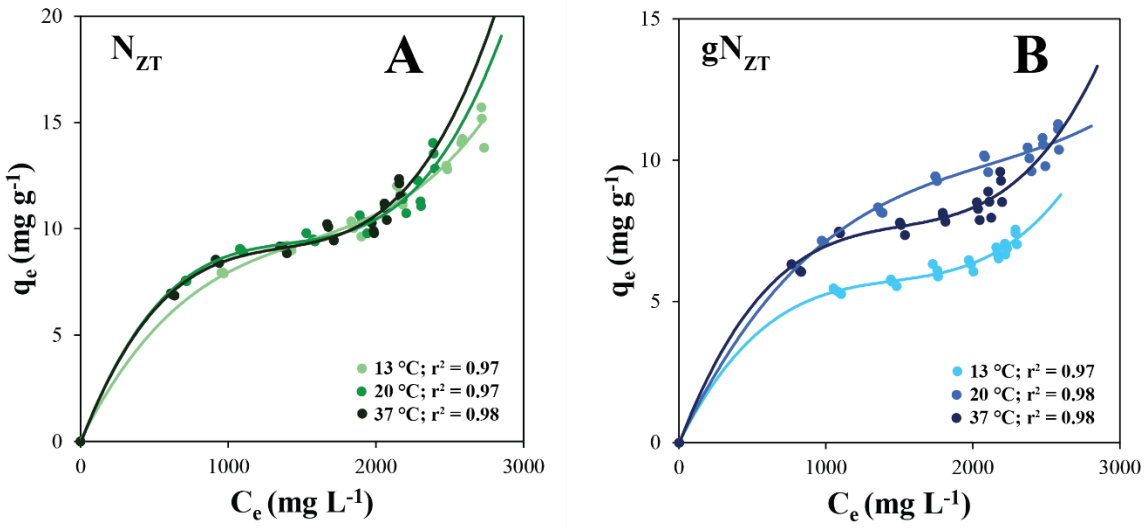

Figure 5. NH_4^+-N equilibrium adsorption capacity q_e (mg g^{-1}) vs equilibrium concentration C_e (mg L^{-1}) after 20 hours of contact with the liquid manure at 13, 20 and 37 °C, and relative r^2 values.

Curves are 3rd degree polynomials. A: N_{ZT} curves; B: gN_{ZT} curves. Both N_{ZT} and gN_{ZT} have shown L3-type isotherms (following the classification proposed by Giles et al., 1960).

Sorbent	Temp.	Harkins-Jura			Freundlich			Langmuir		
	T	r^2	α_H	β_H	r^2	K_F	n	r^2	K_L	q_{max}
	[K]	*[-]*	*[g mg^{-1}]*	*[-]*	*[-]*	*[L g^{-1}]*	*[-]*	*[-]*	*[L mg^{-1}]*	*[mg g^{-1}]*
N_{ZT}	286	0.97	0.092	-0.025	0.90	0.14	1.67	0.88	$3.98 \cdot 10^{-4}$	22.9
	293	0.94	0.073	-0.020	0.85	0.66	2.55	0.86	$10.27 \cdot 10^{-4}$	15.2
	310	0.92	0.081	-0.022	0.90	0.77	2.71	0.91	$12.03 \cdot 10^{-4}$	14.1
gN_{ZT}	286	0.88	0.175	-0.046	0.83	0.45	2.68	0.80	$9.12 \cdot 10^{-4}$	9.3
	293	0.93	0.092	-0.024	0.94	0.56	2.55	0.95	$7.40 \cdot 10^{-4}$	14.7
	310	0.84	0.101	-0.026	0.83	0.95	3.23	0.84	$13.03 \cdot 10^{-4}$	10.9

Table 4. Harkins-Jura, Freundlich, and Langmuir isotherm parameters (equations 7, 9 and 5 respectively) at 286, 293, and 307 K (13, 20 and 37 °C respectively).

The shape of the curves in the first region of the graphs (left side) indicates that, as more exchange sites are occupied by NH_4^+, the sorption of other NH_4^+ ions in solution becomes increasingly difficult. The presence of a semi-flat region, in the middle of the graphs, means that a saturation condition is beginning to occur for NH_4^+-N, but, since the end of the curve rises again, it was demonstrated a renewed availability for NH_4^+ adsorption (Giles et al., 1960). This behavior was observed for both N_{ZT} and gN_{ZT} and it started approximately with a dosage < 6% (w:v).

L3-type isotherms are not in agreement with the Langmuir monolayer assumption, which determines an L2-type isotherm, because the Langmuir model assumes the existence of a horizontal asymptote, which determines the maximum adsorption capacity (q_{max}, see equation 5 in section 4.2.1). Normally, the L3-type isotherms are in general not in agreement also with the pure ion-exchange theory (Shanavas et al., 2011), because ion exchange processes should determine a monolayer condition.

It is however important to consider that the material used was a zeolite-rich tuff, thus an heterogeneous material, with the presence of also other mineral phases along with zeolites.

To explain the L3-type isotherms, which were observed also in the pre-test (section 5.1), the following two different scenarios are thus plausible:

1) In addition to the ion-exchange of the zeolite minerals, other processes were simultaneously involved, (physisorption), which involved other phases constituting the adsorbent material. As pointed out by Chen et al. (2018), the adsorption of NH_4^+ ions in zeolitites is strongly dependent on their degree of heterogenicity and, on this behalf, it may involve both ion exchange (due to the presence of zeolites) and physisorption.
2) In the case of competing ions, ion exchange equilibrium isotherms may show an inflection point that represents a change in the affinity of the adsorbent towards different competing adsorbates, which occur only when a certain amount of sites are occupied by one chemical species (Limousin et al., 2007).

The presence of other phases in the cha-zeolitite, as well as the heterogeneity of the adsorption sites, indicated by the "n" parameter of the Freundlich model (n > 0) (Dada et al., 2012), supported hypothesis 1. On the other hand, the presence of competing species for ion exchange in the liquid manure supported the hypothesis 2.

Unfortunately, it is not possible to confirm one of the two conditions, and it is also not excluded that both could have coexisted. In any case, the L3 shape of the curves in figure 5 suggested that the adsorption of NH_4^+ was particularly favored by the use of small amounts of cha-zeolitite, < 6 %.

Between the isotherms tested, Harkins-Jura showed, in general, the best correlations (figure 6), in particular for N_{ZT}. Two distinct lines can be obtained in this model, whose intersection has been described, in the case of multilayering, as the equilibrium condition at which the first layer is complete, ad a new layer starts to develop (Iyer and Kunju, 1992).

In this study, two distinct lines could be observed only for some conditions (at 37 and 20 °C for N_{ZT}; or 37 and 13 °C for gN_{ZT}. Represented by dotted lines in figure 6), at C_e between 2020 and 2170 mg L^{-1} (NH_4^+-N), which corresponded to the application of 6% (w:v) of cha-zeolitite.

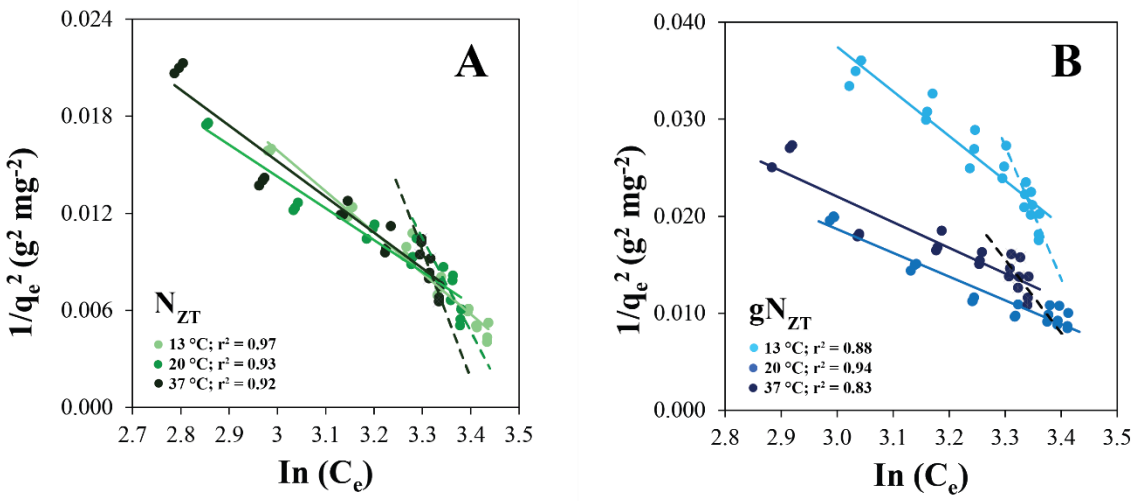

Figure 6. Linear Harkins-Jura isotherms; (equation 7) at 13, 20 and 37 °C. A: N_{ZT} isotherms; B: gN_{ZT} isotherms. The intersections between dotted and continuous lines represent the inflection point. Dotted lines have been noticed for both N_{ZT} (at 37 and 20 °C), and gN_{ZT} (at 37 and 13 °C).

Regarding the effect of temperature on NH_4^+-N adsorption, N_{ZT} showed higher stability than gN_{ZT}, which instead demonstrated greater dependencies on temperature, as indicated by the clear separation of each isotherm. Therefore, from the experimental data, it seems that a correlation exists between particle size and the effect of temperature on NH_4^+ adsorption at equilibrium. An explanation of this phenomenon is particularly difficult to provide with the collected data, taking also into account that, to my knowledge, the scientific literature lacks information on the correlation between temperature and particle size, in NH_4^+ adsorption.

Alshameri et al., (2014) observed "ambiguous effects" of temperature in the adsorption of NH_4^+ by a clinoptilolite-rich zeolitite, where the NH_4^+ removal increased from 25 to 35 °C and decreased from 35 to 45 °C.

In the case of gN_{ZT}, the NH_4^+ removal efficiency was in general: 20 °C > 37 °C > 13 °C, thus, at 20 °C, gN_{ZT} performed better, whereas at 13 °C it showed the worst adsorption capacities.

5.2.2. Kinetics

The change in adsorption capacity (q_t) through time, and the adsorption rate variation, expressed as the amount of NH_4^+-N (mg) adsorbed by one gram of cha-zeolitite per minute, are shown in figure 7, A and B respectively.

N_{ZT} reached higher adsorption capacities than gN_{ZT}, and it was significantly faster in NH_4^+-N adsorption, particularly during the first 5 minutes of contact with liquid manure (figure 7.B). Between the first 10 minutes of contact, the adsorption rate of N_{ZT} suddenly dropped, while gN_{ZT} showed significantly higher adsorption rates until about 60 minutes.

The changes in adsorption rate and q_t through time are the results of the underlying kinetic processes, that govern the transfer of NH_4^+-N from the bulk solution, to the external surfaces, and through the pore structure.

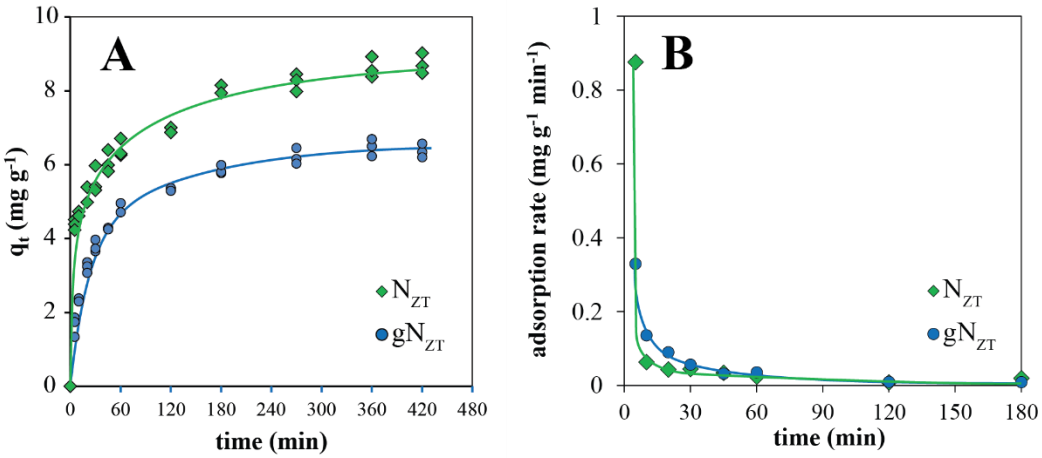

Figure 7. A: q_t against t plot; B: adsorption rate vs. t. N_{ZT} is represented by green squares, while gN_{ZT} by blue circles. The adsorption rates of figure B have been calculated from the means of the q_t values, measured in 3 replicates for each time point.

The fact that both the materials showed high initial adsorption rates represented a very rapid adsorption phase that ended in the first few minutes, followed by a slower process that lasted for the next hours.

The reason for the differences observed between N_{ZT} and gN_{ZT} is in the different particle sizes of the two materials. The study of the kinetic models may elucidate these aspects. Kinetic parameters of the PFO, PSO and Elovich models are reported in table 5, while PSO and Elovich graphs are reported in figure 8.A and B, respectively.

Sorbent	$q_{e,180}$	PFO			PSO				Elovich		
		r^2	k_1	$q_{e,1}$	r^2	k_2	h	$q_{e,2}$	r^2	α	R_E
		[-]	*[min^{-1}]*	*[mg g^{-1}]*	*[-]*	*[g mg^{-1}min^{-1}]*	*[mg g^{-1}min^{-1}]*	*[mg g^{-1}]*	*[-]*	*[mg g^{-1}min^{-1}]*	*[-]*
N_{ZT}	6.35	0.68	0.011	4.18	0.98	0.028	1.29	5.43	0.93	1.52	0.28
gN_{ZT}	4.55	0.89	0.015	3.77	0.99	0.018	0.44	4.35	0.98	1.06	0.52

Table 5. Pseudo-First-Order (PFO), Pseudo-Second-Order (PSO), and Elovich kinetic models for N_{ZT} and gN_{ZT}, with the relative r^2 values. $q_{e,180}$ is the measured equilibrium adsorption capacity (at t=180 min.); $q_{e,180}$ values are reported for comparison with the q_e calculated by the models ($q_{e,1}$ and $q_{e,2}$ for PFO and PSO respectively).

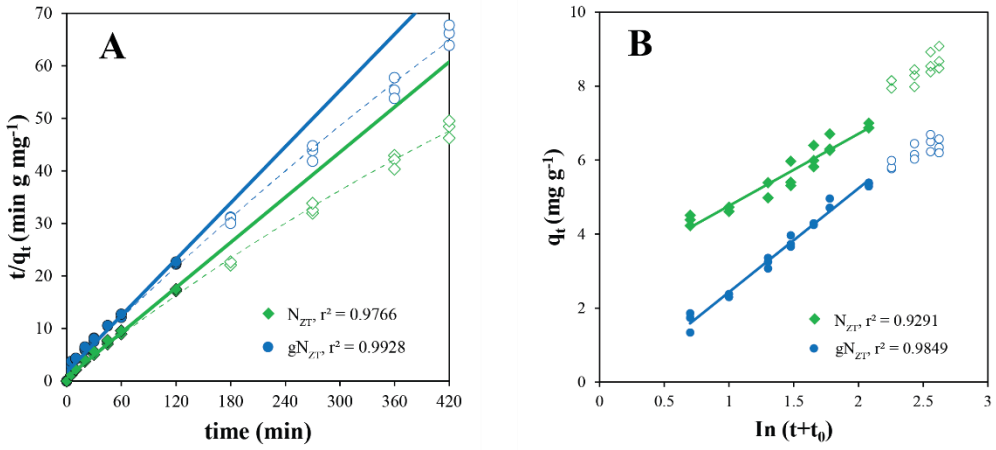

Figure 8. N_{ZT} and gN_{ZT} adsorption kinetic models, represented by green squares or blue circles, respectively. Full dots represent data with F(t) < 85%, thus, considered in kinetic modelling; empty dots represent data with F(t) > 85%, thus not considered because near equilibrium. A: t/q_t against t plot (PSO); dotted curves are representing the general trend, while the straight lines are the PSO model (equation 16); B: $\ln(t+t_0)$ against q_t plot (Elovich, equation 20).

For the comparison between PFO and PSO models in kinetic analyses, in addition to the evaluation of $r^{2,}$ it is also recommended to compare the measured equilibrium adsorption capacity (q_e) with the calculated ones ($q_{e.1}$ and $q_{e.2}$ for the PFO and PSO models, respectively).

A "close-to-equilibrium" condition was assumed at t = 180 minutes, where the adsorption rate was close to zero (figure 7.B), thus $q_{t,180} \approx q_e$ = 6.35 and 4.55 mg g^{-1} of NH_4^+-N, for N_{ZT} and gN_{ZT} respectively (see section 4.2.2).

PFO did not correlate well with the experimental data, while PSO showed good r^2 values, and a good correlation with the measured q_e, particularly with gN_{ZT}, being $q_{e,2}$ = 4.35 mg g^{-1}, really close to the measured one (4.55 mg g^{-1}).

The Elovich model showed a good correlation with gN_{ZT}. R_E parameter indicates that N_{ZT} approached equilibrium faster than gN_{ZT}.

The intraparticle diffusion model (ID) is represented in figure 9.A and B, for N_{ZT} and gN_{ZT} respectively. Differences have been observed between the two-particle sizes, as N_{ZT} showed only a straight line with an intercept C ~ 3, while gN_{ZT} clearly showed two lines, representing a change in diffusion process after about 60 minutes of contact with the liquid manure.

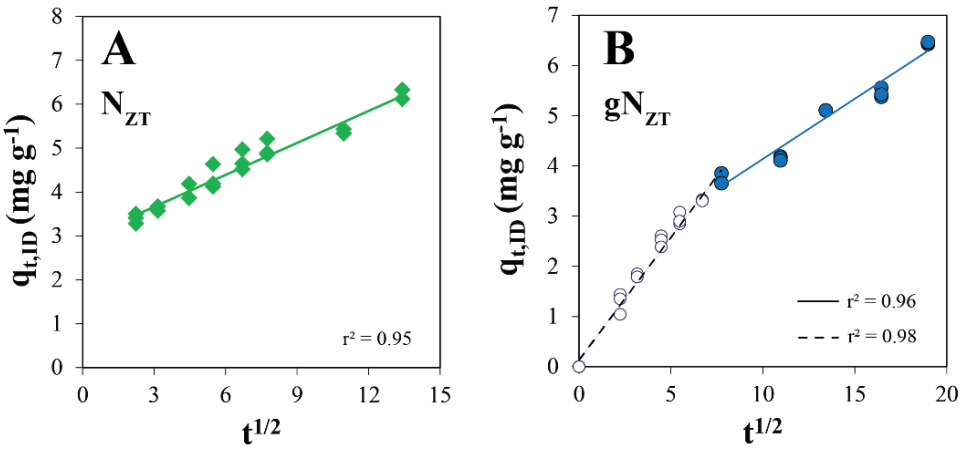

Figure 9. $t^{1/2}$ against $q_{t,ID}$ (ID plots) derived from equation 18 for N_{ZT} (A) and gN_{ZT} (B), and the relative r^2 values. In graph B, the dotted line represents the first hour of contact, while the other lone represent a change in diffusion processes.

ID parameters are reported in table 6. The intercept C has been described as proportional to the thickness of the boundary layer (Mall et al., 2006), thus, being C close to 0 for gN_{ZT} (C = 0.13; dotted line in figure 9.B), the internal diffusion governed the adsorption kinetic of NH_4^+ ions during the first hour of contact, with the development of one single adsorption layer.

The increase in C value (1.74) indicates that the diffusion slowed down after about 60 minutes; possibly due to the formation of multiple adsorption layers, not related to zeolite minerals, but on an underlying physisorption process, simultaneous to ion exchange but significantly less intense, that may have characterized the late adsorption kinetic.

N_{ZT} ID showed only one regression line with a higher C (2.93), indicating a really fast diffusion in the pore structure of the finer cha-zeolitite.

It is interesting to note the similarities between K_{ID} values for both $gN_{ZT,}$ (after about 1 hour of contact), and $N_{ZT,}$ probably indicating that the late adsorption kinetics had similar nature and same intensity for both the particle sizes.

		ID model				
Sorbent	**$q_{e,180}$**		**$q_{e,ID}$**	**r^2**	**K_{ID}**	**C**
	[mg g^{-1}]		*[mg g^{-1}]*	*[-]*	*[mg $g^{-1}min^{-1/2}$]*	*[mg g^{-1}]*
N_{ZT}	6.35		3.82	0.95	0.24	2.93
gN_{ZT}	4.55	before 60 min.	4.96	0.98	0.49	0.13
		after 60 min.		0.96	0.24	1.74

Table 6. ID parameters for N_{ZT} and gN_{ZT}; gN_{ZT} showed two different patterns, before and after 60 minutes of contact with the digestate.

The reason behind the differences observed between gN_{ZT} and N_{ZT} was plausible related to the structural differences derived from the grinding process and the different dimensions of the mineral particles. The micronization process, undergone by $N_{ZT,}$ undoubtedly increased its specific surface area (SSA), but the microporous structure of zeolite minerals was not destroyed (N_{ZT} particle dimensions are indeed about 95-105 times larger than the average diameter of the micropores of

chabazite mineral (http://www.iza-online.org/natural/Datasheets/Chabazite/Chabazite.html, accessed the 09/25/2021).

It is thus plausible that the grinding process has exposed to the environment a larger number of pores into which NH_4^+ was able to easily enter, thus explaining the higher NH_4^+-N adsorption rates observed in the first minutes of contact (figure 7.B). Furthermore, the increased SSA and the exposure of new fresh surfaces may also have enhanced physisorption processes.

5.2.3. Thermodynamics

Thermodynamic parameters are reported in table 7. For both N_{ZT} and gN_{ZT}, ΔG was always negative, indicating the spontaneity nature of NH_4^+ adsorption, which was in general, thermodynamically more favoured in the case of the finer material, as indicated by its lowest ΔG values. ΔG was tendentially inversely proportional to temperature.

Sorbent	**Temperature**	**K_e**	**ΔG**	**ΔH**	**ΔS**
	[K]	[-]	[kJ mol-1]	[J mol-1]	[J K-1 mol-1]
N_{ZT}	286	8.83	-1.80	2124	13.7
	293	11.80	-1.96	2091	13.8
	310	12.61	-2.06	2146	13.6
gN_{ZT}	286	6.25	-0.74	2654	11.9
	293	8.86	-1.46	2343	13.0
	310	9.60	-1.42	2479	12.6

Table 7. Thermodynamic parameters (K_e, ΔG, ΔH and ΔS), as calculated by equations 22, 23 and 24 for N_{ZT} and gN_{ZT}, at 286, 293 and 310 K (13, 20 and 37 ◦C, respectively).

The K_e had positive values for both the particle sizes with differences between N_{ZT} and gN_{ZT}, where it showed higher values for the first one and positive correlation with temperature, indicating a greater tendency to equilibrium for the finer material, directly proportional to the increase in temperature.

ΔS values were always positive, indicating that the randomness in the solid-liquid interface increased along with NH_4^+ adsorption, reflecting a good affinity between the sorbent and the sorbate, and a condition that favored the adsorption process (Ghosal and Gupta, 2017).

ΔH was positive for both N_{ZT} and gN_{ZT}, indicating an endothermic exchange, with significative higher values for gN_{ZT}. The endothermy is also supported by the increase of the Freundlich constant (K_F) with temperature (see section 5.2.1, table 4) (Xiang et al., 2019).

While many authors have observed exothermic adsorption of NH_4^+ by cha-zeolitites (Aydın Temel and Kuleyin, 2016; Gunay, 2007; Saltali et al., 2007), others have reported endothermic conditions (Wasielewski et al., 2018; Widiastuti et al., 2011). In all these studies, the nature of the employed materials (cha-zeolitite type and liquid phase) significantly varies, possibly resulting in differences in adsorption processes and justifying the observed variability in thermodynamic parameters.

5.3. Experiment B

5.3.1. N_{ZT} and K_{ZT} isotherm

Contrary to what was expected from the outcomes of the exp. A, in which the isotherm applied was Harkins-Jura, in exp. B, Langmuir regression best correlates with the experimental data ($r^2 = 0.93$ and 0.99; p-value = 4.4×10-4 and 6.2×10-7 for N_{ZT} and K_{ZT} respectively) (figure 10).

A possible explanation may lie in the different nature of the two wastewaters, as liquid manure was used in exp. A, while digestate was applied in exp. B. Indeed the isotherms in multicomponent systems with different competing ions strongly depends on the concentration of the ions and the composition of the bulk solution (Limousin et al., 2007). The physical and chemical differences between the two wastewaters may therefore have influenced the adsorption processes of NH_4^+-N.

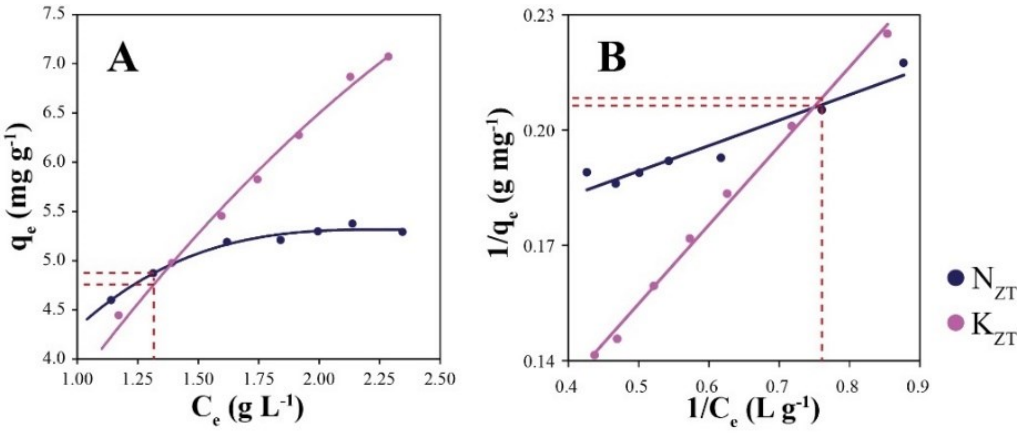

Figure 10. N_{ZT} and K_{ZT} adsorption isotherms related to NH_4^+-N from a liquid digestate.

A: C_e (g L^{-1}) against q_e (mg g^{-1}) plot; B: linear Langmuir isotherms (equation 6).

r^2 was equal to 0.93 and 0.99 for N_{ZT} and K_{ZT} respectively.

Red dotted lines represent the $C_{e.tg}$ and the corresponding $q_{e.tg}$ (see section 4.3.2).

The q_{max} of K_{ZT} was about 3 times higher than N_{ZT} (19.2 ± 1.5 against 6.4 ± 0.1 mg NH_4^+-N g^{-1}). The K_L was also highly different between the two materials (425 ± 65 and 3940 ± 430 for N_{ZT} and K_{ZT} respectively). The isotherms highly diverge in the right part of the graph (figure 10.A), where K_{ZT} reached higher adsorption capacities. In a view of multiple batch adsorption, or if it is intended to reach higher $C_{e.tg}$ (in this study, $C_{e.tg}$ was arbitrarily chosen at 1300 mg NH_4^+-N L^{-1}; see section 4.3.2), K_{ZT} may thus be a very performant option. However, at the considered $C_{e.tg}$, the two isotherms were close to each other, with no significant differences in adsorption capacities.

The amounts of N_{ZT} and K_{ZT} used for phase 1 of the treatment (NH_4^+-N adsorption) were calculated from the isothermal data, by imposing $C_{e.tg}$ = 1300 mg L^{-1} (equation 26 in section 4.3.2) and they corresponded to a dosage of about 25 and 25.7% (w:v) for N_{ZT} and K_{ZT}, respectively.

5.3.2. Process efficiencies

N and P removal efficiencies

The nutrient removal efficiencies of the different treatments tested in the exp. B are illustrated in figure 11, expressed as NH_4^+-N removal (figure 11.A) and total dissolved phosphorous (TDP) (figure 11.B).

Figure 11. Nutrient removal efficiencies of the three treatments tested (NZT-S, KZT-S and CNTR) with MR1 (purple) and MR2 (green). A: NH_4^+-N removal efficiency (%); B: TDP removal efficiency (%).

The $Mg:NH_4:PO_4$ molar ratios were 1:1.5:1 and 2:1:1 for MR1 and MR2, respectively; thus, while only PO_4^{3-} limited struvite precipitation in MR1, both PO_4^{3-} and NH_4^+ were limiting agents in MR2. The expectations were thus that, within every treatment (NZT-S, KZT-S, and CNTR), lower NH_4^+-N removal efficiencies would be observed in MR1, against MR2. At the same time, no differences were expected in the TDP removal efficiencies between the two molar ratios tested.

While the NH_4^+-N followed the expectations, particularly with KZT-S and CNTR; TDP revealed different behaviors, being generally the removal of P significantly lower for MR1 than MR2, at least for KZT-S and the CNTR.

NZT-S showed a different trend in comparison with the other treatments, as no significant differences have been observed between MR1 and MR2, for both the NH_4^+-N and the TDP removal efficiencies.

It is interesting to note that the CNTR revealed the lowest NH_4^+-N removal efficiencies compared with all the other treatments that have provided the use of cha-zeolitite. This was an excellent result that demonstrated that, in these experimental conditions, the partial recovery of NH_4^+-N by zeolitite adsorption (phase 1), not only allowed for a considerable decrease in the use of reagents (about 50% less in NZT-S and KZT-S, respect the CNTR, as discussed in the following sub-section "Materials required") but also showed higher nutrient removal efficiencies.

Contrary to the expectations, KZT-S, where most of the exchangeable Ca^{2+} ions were substituted by K^{+}, performed worse than NZT-S for the recovery of both NH_4^{+}-N and P, indicating that the possible interferences of Ca^{2+} did not strongly threaten the struvite precipitation.

Indeed, the NZT-S treatment proved to be the most efficient strategy for the recovery of both N and P, apparently with no significant effect between MR1 and MR2.

NH_4^{+}-N removal efficiencies by each component (zeolitite and struvite)

To better visualize the NH_4^{+}-N removal efficiency, it is important to evaluate the contribution of each component that had taken part in the treatment process, as the zeolitites adsorption (phase 1), the struvite precipitation (phase 2), and also the effect of dilution (phase 2), due to the addition of Milli-Q water used for solubilizing the Mg^{2+} and PO_4^{3-} reagents before their addition (see section 4.3.4).

Figure 12 shows how each component contributed to the total NH_4^{+}-N removal efficiency.

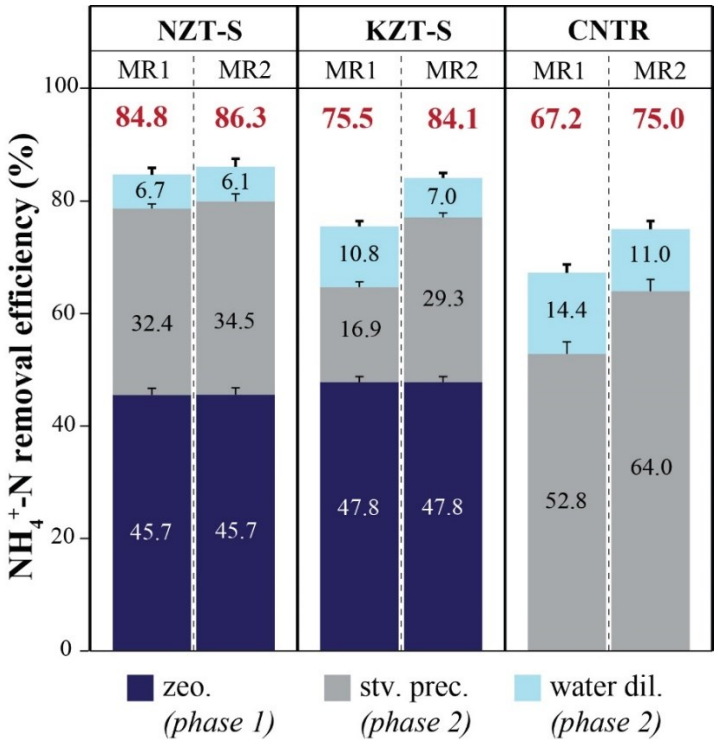

Figure 12. NH_4^{+}-N removal efficiencies by single components for NZT-S (left), KZT-S (center) and CNTR (right), divided by MR1 and MR2. "Zeo" indicates the zeolitite used in phase 1 (N_{ZT} at the left, K_{ZT} in the

center); “stv. prec.” Indicate the effect of struvite precipitation, during phase 2, while “water dil.” is the dilution effect during the addition of reagents in phase 2 (see section 4.3.4 for further details).

Red numbers on top represent the total NH_4^+-N removal efficiencies,

the same values are reported in figure 11.A.

As expected, about the same residual NH_4^+-N concentrations were obtained by both the N_{ZT} and K_{ZT} cha-zeolitite (C_e = 1388 ± 31 and 1334 ± 26 mg L^{-1}, for N_{ZT} and K_{ZT}, respectively), thus, excellent results were obtained considering that the target residual NH_4^+-N was set to 1300 mg L^{-1} ($C_{e.tg}$), confirming what obtained from the isotherm models (section 5.3.1)

The effect of struvite precipitation was highly different among the treatments. Even if it showed the worst total removal efficiencies, the CNTR had the highest struvite recoveries, significantly higher than the other treatments, as about 52.8% and 64.0% of the removed NH_4^+-N, was attributable to struvite precipitation in MR1 and MR2, respectively.

As expected, along with the CNTR, also the other treatments showed general better struvite recoveries with MR2 condition.

About 32.4 or 34.5% of the total NH_4^+-N removed from the digestate was recovered by struvite precipitation in NZT-S_MR1 and MR2 treatments, respectively, while fewer amounts were recovered by KZT-S, being only 16.9 and 29.3% for MR1 and MR2. This aspect confirmed that the interferences with Ca^{2+} were not stronger as expected. Thus NZT-S confirmed higher efficiency in struvite recovery than the KZT-S strategy.

As demonstrated by SEM-EDS analyses in section 5.3.4, this result was achieved because Ca^{2+} ions did not interfere with PO_4^{3-}, as expected, but with carbonate ions (CO_3^{2-}), to produce calcite precipitates, thus preserving the PO_4^{3-} for struvite precipitation.

Struvite recovery (reagent use efficiencies)

The $R_{\%}$ parameter (equation 28 in section 4.3.6), is related to the process efficiency. Even if it was estimated only by the NH_4^+-N in solution, it may be considered as a general indicator of the efficiency in the use of reagents during the struvite precipitation process.

In this work, it is considered as directly related to the "reagent-use-efficiency", because the higher $R_{\%}$, the most the NH_4^+-N recovered as struvite crystals approached the expectations, thus fewer reagents were "wasted", remaining in solution, or precipitating as other phases, without any involvement of NH_4^+ ions.

$R_{\%}$, Tr (equation 27) and Ar are expressed in table 8.

Treatment	Molar Ratio	Tr	Ar	$R_{\%}$
		[mg L^{-1}]	*[mg L^{-1}]*	*[%]*
NZT-S	**MR 1**	926	887	95.8
	MR 2	1389	883	63.6
KZT-S	**MR 1**	889	432	48.6
	MR 2	1333	748	56.1
CNTR	**MR 1**	1704	1339	78.6
	MR 2	2555	1622	63.5

Table 8. Reagent use efficiency in struvite precipitation expressed as $R_{\%}$ (equation 28). Tr is the theoretical recovery (equation 27) and Ar is the actual (or measured) recovery (mg NH_4^+-N L^{-1}). The higher the $R_{\%}$, the fewer reagents were wasted; see section 4.3.6 for further details.

$R_{\%}$ reached the highest values for NZT-S_MR1 treatment, thus in a condition of excess of NH_4^+, instead of Mg^{2+}. This feature is a positive aspect because commonly, the majority of nutrient-rich wastewaters are characterized by high amounts of NH_4^+-N.

As the costs of reagents are one of the main issues for the implementation of struvite technologies, the $R_{\%}$ parameter is a particularly important factor for the evaluation of the feasibility of the different treatment strategies proposed in the exp. B.

The lower values obtained, especially for KZT-S and for the CNTR, compared to NZT-S_MR1, may be explained by the competition of other salts for Mg^{2+} and PO_4^{3-}. Indeed, not only struvite, but many other precipitates may be stable, involving Mg^{2+} and PO_4^{3-} in alternative chemical pathways and leading to the nucleation and growth of phases as hydroxides, carbonates, or other phosphates, causing the loss of both Mg^{2+} and PO_4^{3-} in other phases (some examples are reported in table 9 and figure 13).

	Possible competing reactions	**Mineral phase**	**Disputed ions**
1)	$NH_4^+ + Mg^{2+} + PO_4^{3-} + 6H_2O \rightarrow MgNH_4PO_4 \cdot 6H_2O$	Struvite	-
2)	$K^+ + Mg^{2+} + PO_4^{3-} \rightarrow KMgPO_4 \cdot 6H_2O$	K-struvite	Mg^{2+}; PO_4^{3-}
3)	$Mg^{2+} + HPO_4^{2-} + 3H_2O \rightarrow MgHPO_4 \cdot 3H_2O$	Newberyite	Mg^{2+}; PO_4^{3-}
4)	$3Mg^{2+} + 2(PO_4)^{3-} + 8H_2O$	Bobierrite	Mg^{2+}; PO_4^{3-}
5)	$Mg^{2+} + 2OH^- \rightarrow Mg(OH)_2$	Brucite	Mg^{2+}
6)	$Mg^{2+} + CO_3^{2-} \rightarrow MgCO_3$	Magnesite	Mg^{2+}
7)	$Ca^{2+} + HPO_4^{2-} \rightarrow CaHPO_4 \cdot 2H_2O$	Brushite	PO_4^{3-}
8)	$5Ca^{2+} + 3PO_4^{3-} + H_2O \rightarrow Ca_5(PO_4)_3OH + H^+$	Hydroxiapatite	PO_4^{3-}
9)	$NH4^+ + HCO_3^- \rightarrow NH4HCO3$	Am. bicarbonate	NH_4^+
10)	$Mg^{2+} + 2HCO_3^- \rightarrow Mg(HCO_3)_2$	Mag. bicarbonate	Mg^{2+}

Table 9. Possible reaction pathways that may compete with struvite in the presence of competing ions as K^+, Ca^{2+}, CO_3^{2-} or OH^-. The name of the mineral is indicated, as well as the ions that may be subtracted from struvite (disputed ions) (modified from https://www.aqion.de/site/16#form, accessed the 04/12/2021 and Siciliano et al. (2020)).

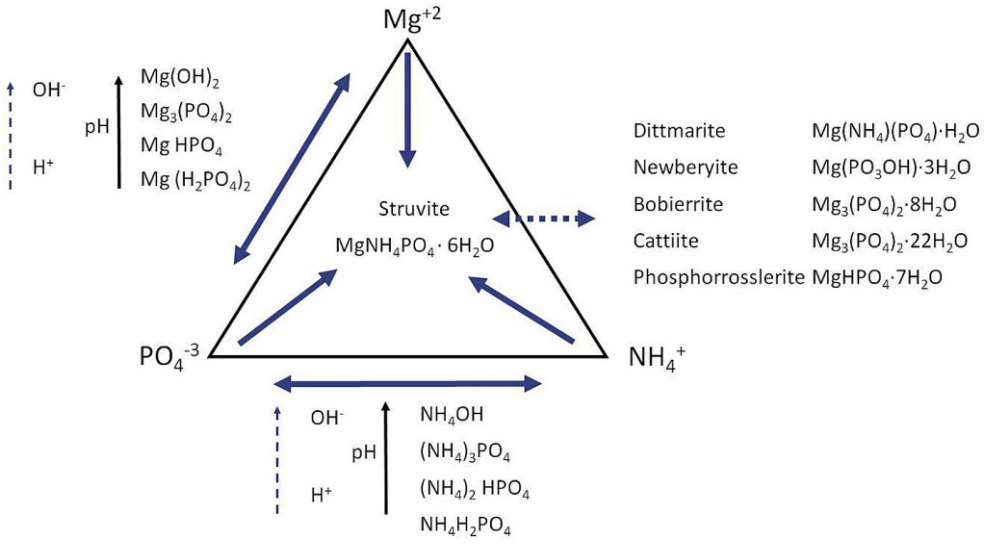

Figure 13. Possible pH-related interactions between NH_4^+, PO_4^{3-}, and Mg^{2+} ions for struvite precipitation and other phases. From Tansel et al. (2018).

Different sources of possible competing species were present. First of all, digestates are complex matrices, naturally rich in many possible competing ions. The N_{ZT} used in phase 1 was also rich in exchangeable Ca^{2+} and K^+ (see sections 3.1), while K_{ZT} was highly rich in exchangeable K^+. Finally, both KH_2PO_4 and, in a minor way, KOH, used for struvite precipitation added significant amounts of K^+ ions to the digestate.

Two hypotheses may thus explain the lower $R_{\%}$ values observed for the KZT-S treatment, as 1) the precipitation of other phases, which led to significant losses of Mg^{2+} and PO_4^{3-}, and 2) significant amounts of Mg^{2+} and/or PO_4^{3-} that remained in solution, without reacting with NH_4^+.

The strongly higher amounts of residual Mg^{2+} in the post-KZT-S treatment digestate, compared to the values observed in the digestate of NZT-S (see figure 15, below in this section) seemed to suggest the 2nd hypothesis. However, the SEM-EDS semiquantitative analyses (see table 12 in section 5.3.4) revealed higher K, Mg and P concentrations in the precipitates of the KZT-S treatment, thus suggesting the 1st hypothesis.

Being that one hypothesis does not preclude the other, the best explanation may be that KZT-S showed lower reagent use efficiencies because significant amounts of Mg^{2+} ions remained dissolved

in the digestate, and a part of it interfered, along with PO_4^{3-}, for the nucleation of other crystal phases than struvite.

Materials required

The amounts of reagents used in the CNTR for struvite precipitation doubled those used for NZT-S and KZT-S (figure 14). Thus, even if the CNTR has shown significative higher struvite productions (but lower NH_4^+-N removal efficiencies) than the other treatments (see figure 12), the materials required, the low reagent use efficiency (estimated in table 8), the higher potential costs, and the possible adverse effects on the wastewater due to the massive addition of reagents, may not justify this treatment strategy. Indeed, the CNTR treatment aimed at testing a traditional struvite production technology, via chemical precipitation, where it is known that the high amount of reagents required represents its main issue.

On the other hand, the application of the cha-zeolitite in both NZT-S and KZT-S, and therefore the removal of NH_4^+-N before struvite precipitation, allowed then, during phase 2, to achieve the desired molar ratios by using fewer amounts of reagents.

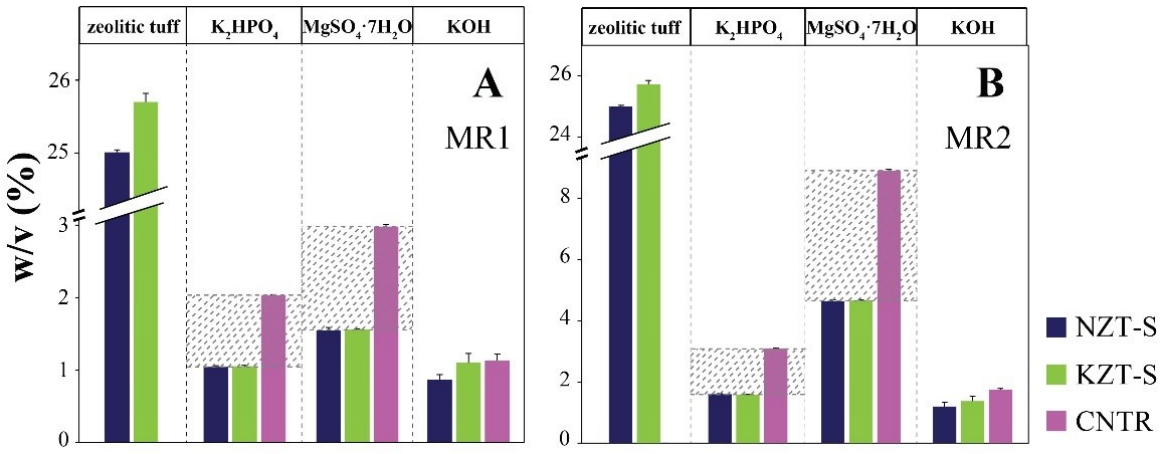

Figure 14. Zeolitic tuff (N_{ZT} and K_{ZT}), reagents (K_2HPO_4 and $MgSO_4 \cdot 7H_2O$) and pH buffer (KOH) required, expressed as w:v (%). A: MR1 condition; B: MR2. Dotted areas highlight the differences in the reagents required by the CNTR with the amounts required by NZT-S and KZT-S.

Higher amounts of reagents were used in MR2 than MR1, being that the dosage of K_2HPO_4 and $MgSO_4 \cdot 7H_2O$ was about 1.5 and 3 times higher, respectively. However, the NH_4^+-N removal efficiencies by struvite precipitation were just slightly higher for MR2 than MR1 (see figure 11, section 5.3.2), thus not justifying the significantly greater needs of reagents.

In this experiment, the MR1 condition (1.0:1.5:1.0 as $Mg:NH_4:PO_4$) proved to be the best feasible strategy for the recovery of struvite, than MR2 (2:1:1), better representing also the natural conditions of many nutrient-rich wastewaters, where the NH_4^+ greatly exceed both Mg^{2+} and PO_4^{3-}.

5.3.3. Digestate chemical differentiation

The chemical differentiation of the digestate strongly differed between each phase and treatment tested. In this section, it will be discussed the differences in the concentrations of the main inorganic ions dissolved, both released by the cha-zeolitites, and the ones added with the reagents, as well as the total dissolved phosphorous (TDP), the heavy metals in trace amounts, and the electrical conductivity (EC).

It will not be discussed the NH_4^+-N because it has already been treated in section 5.3.2.

Differences among the main inorganic ions dissolved

In this section, it will be described the main effects of each treatment phase on the chemical differentiation of the digestate, concerning the most important inorganic ions dissolved.

It is important to highlight that the comparison between different diagrams in figure 15 may be misleading because each slice does not represent absolute amounts, but they represent the relative abundances. To compare the different treatments and different phases, it is useful to refer to the concentration values, expressed as mg L^{-1}, reported on top of the slices, or inside them.

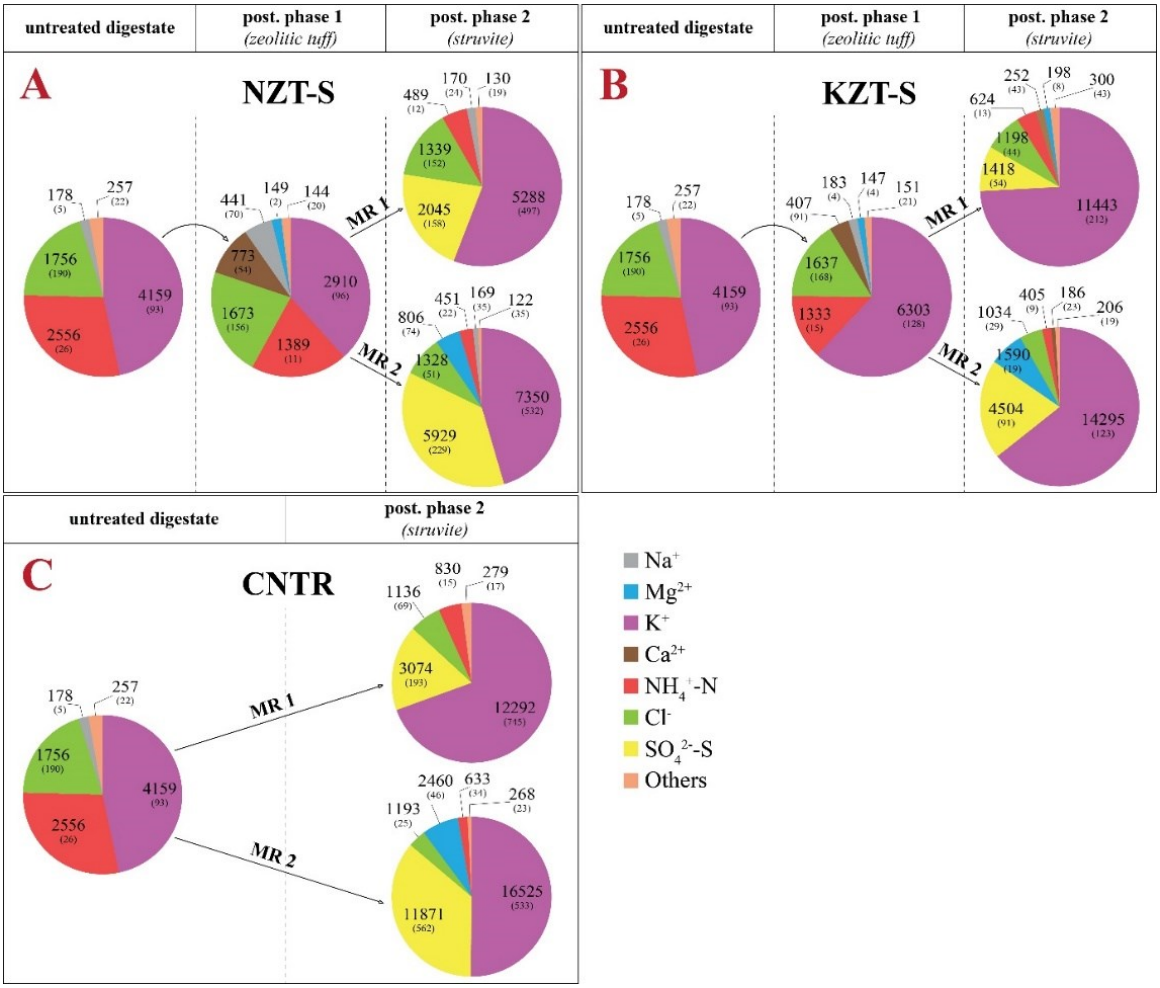

Figure 15. Relative abundances (cakes) and absolute abundances (numbers, mg L^{-1}) of the principal dissolved ions in the digestate among every treatment phase (untreated digestate → post zeolitic tuff → post struvite). Letters indicate different treatments as follows: A: NZT-S; B: KZT-S; C: CNTR. In the legend, the word "others" indicates the sum of TDP, Na^+, Ca^{2+}, Mg^{2+}, SO_4^{2-}-S and trace elements (Br^-, Fe^{2+}, Fe^{3+}, B^-, Al^{3+}, NO_3^--N, Sr, F^-). Note[1]: comparing segment areas between different cake graphs is misleading; refer to concentration values for these comparisons.

Within phase 1, the digestate was enriched in Ca^{2+}, which was desorbed in higher amounts by N_{ZT} than K_{ZT}. The use of N_{ZT} decreased the K^+ in solution, which was in part adsorbed by the cha-zeolitite (figure 15.A), while K_{ZT} desorbed significant amounts of K^+, enriching the digestate after phase 1 from about 4160 (initial value) to 6300 mg L^{-1} (figure 15.B).

As expected, both N_{ZT} and K_{ZT} led to NH_4^+-N reductions of about 50%, thus, the NH_4^+-N remained after the adsorption phase was close to the expected target concentration ($C_{e.tg}$) of 1300 mg L-1 (see section 5.3.1 for further details).

P was affected by the adsorption phase, as both N_{ZT} and K_{ZT} batches reduced the amount of TDP (accounted in figure 15 into the voice: "others") from the initial value of the digestate (105 ± 6 mg L^{-1}), to 70.4 ± 1.7 and 86.2 ± 3.5 mg L^{-1}, respectively. Therefore, the release of Ca^{2+} and, in a minor way, the release of K^+ by the cha-zeolitite, possibly led to the precipitation of unwanted phosphates during phase 1, such as $Ca_5(PO_4)_3OH$, $CaHPO_4 \cdot 2H_2O$ or $KMgPO_4 \cdot 6H_2O$. Unfortunately, these phases have not been observed by SEM-EDS because only the struvite precipitates have been analyzed, while no imaging has been carried out for the cha-zeolitites post-phase 1.

At the end of the process (post phase 2), the treatment that least modified the initial amounts of Na^+, K^+, Mg^{2+} and Ca^{2+} was NZT-S_MR1, where Na^+, Mg^{2+} and Ca^{2+} returned to levels close to the initial concentrations.

The final digestate was in general highly enriched in K^+, derived from the K_2HPO_4 reagent used for struvite precipitation, but with significant differences among the treatments. In particular, KZT-S and CNTR showed about 1.8 and 2.3 times higher levels of K^+ than NZT-S, independently of the molar ratio (figure 15).

From this point of view, the treatment that least modified the K^+ levels was NZT-S_MR1, with a concentration in the treated wastewater as about 5290 mg L^{-1}, thus 1130 mg L^{-1} higher than the untreated one (4160 mg L^{-1}).

Along with K^+, also SO_4^{2-}-S increased during phase 2 by the addition of $MgSO_4 \cdot 7H_2O$ reagent, with a maximum excursion from 1418 ± 54 to 11871 ± 562 mg L^{-1} (KZT-S_MR1 and CNTR_MR2 respectively). As expected, the CNTR, where the higher amounts of reagents were applied, showed the highest K^+ and SO_4^{2-}-S enrichments.

In the view of circular reuse of the wastewater, the accumulation of SO_4^{2-}-S and K^+ by using $MgSO_4 \cdot 7H_2O$ as the main Mg^{2+} source and K_2HPO_4 as PO_4^{3-} source, should be accounted for, before agricultural application. If the enrichments may be considered not excessive, as in example the case of NZT-S_MR1 condition (figure 19.A), the treated digestate may be an interesting option for fertilization, in particular in the case of S or K deficiencies of the soil.

Many alternatives exist to overcome the Mg^{2+} and PO_4^{3-} deficiencies of the wastewater, that may be used in combination with the reagents used in this work, or substitution of them, as MgO (Huang et al., 2014), $MgCl_2 \cdot 6H_2O$ (Escudero et al., 2015) or even better, the use of low expensive bone meal, magnesite and seawater bittern (Siciliano et al., 2020).

The possibility to use combinations of different sources could be also an interesting option, but further research is still needed.

As a final point, mention should also be made for Cl- ions, that significantly decreased after phase 2, but only because of the dilution applied during the addition of the reagents (see section 4.3.4), in fact, by correcting the data for the dilution factor, the amount of Cl^- at the end of the treatments not differed significantly from the initial concentrations.

Heavy metals

Minor and trace elements are reported in table 10.

Both the N_{ZT} and K_{ZT} batches increased the dissolved Mn, Zn and Ba, particularly in the case of K_{ZT}.

The struvite precipitation phase decreased the metallic elements illustrated in table 10, leading to the consideration that significant enrichment might have been possible in the precipitates. For this reason, heavy metals have been measured on the NZT-S_MR1 precipitate (see section 5.3.4).

treatment	phase	Mn	Ni	Cu	Zn	As	Ba	Pb
					[μg L^{-1}]			
	untreated dig.	**317 ± 17**	**213 ± 18**	**496 ± 29**	**545 ± 90**	**119 ± 10**	**205 ± 3**	**338 ± 19**
CNTR	**MR 1**	344 ± 2	168 ± 6	527 ± 12	2360 ± 41	b.d.l.	376 ± 24	b.d.l.
	MR 2	226 ± 4	141 ± 17	492 ± 85	581 ± 97	123 ± 10	250 ± 25	320 ± 12
NZT-S	**post phase 1**	781 ± 62	224 ± 7	553 ± 97	910 ± 269	137 ± 3	1807 ± 70	429 ± 53
	MR 1	68 ± 33	64 ± 24	467 ± 31	503 ± 211	105 ± 4	192 ± 46	343 ± 24
	MR 2	46 ± 25	57 ± 29	605 ± 43	442 ± 125	116 ± 6	94 ± 47	353 ± 3
KZT-S	**post phase 1**	1806 ± 174	271 ± 35	309 ± 34	3854 ± 564	b.d.l.	4291 ± 702	180 ± 4
	MR 1	1014 ± 40	158 ± 2	88 ± 26	2297 ± 824	b.d.l.	2525 ± 39	33 ± 42
	MR 2	490 ± 7	142 ± 6	66 ± 83	901 ± 74	b.d.l.	1138 ± 23	b.d.l.

Table 10. Minor and trace element concentrations in the untreated digestate, and the digestate through each phase of the treatments. "b.d.l." account for "below detection limit".

Electrical conductivity

The EC of the initial digestate was 37.1 ± 1.7 mS cm^{-1}. Both the N_{ZT} and K_{ZT} adsorption batches caused the EC to drop down (29.3 ± 1.2 and 28.8 ± 1.2 mS cm^{-1}, respectively).

It is interesting to note that, in the case of the NZT-S_MR1 treatment, the EC of the final digestate reached levels even below the initial conditions (24.5 ± 0.7 mS cm^{-1}), while with MR2 it turned back to values equal to the untreated digestate (36.8 ± 2.2 mS cm^{-1}).

Significantly higher results were obtained by KZT-S (39.8 ± 1.2 and 59.9 ± 2.5 for MR1 and MR2, respectively), and the highest EC values were reached by the CNTR (55.3 ± 1.7 and 87.7 ± 1.7 mS cm^{-1} for MR1 and MR2, respectively).

Also from the EC perspective, the NZT-S strategy proved to be the most interesting one, among the treatment studied, in a view of reuse of the wastewater for agricultural purposes.

5.3.4. The solids obtained: cha-zeolitite and precipitates characterization

In this section, it will be described the NH_4^+-N enrichment of the cha-zeolitite (both N_{ZT} and K_{ZT}), the exchangeable cations, their total nitrogen (TN) and carbon (TC) and the struvite precipitates; their morphology and the semiquantitative chemical composition.

The precipitates of the treatment that was considered as the most efficient and feasible strategy (NZT-S_MR1), were further characterized for their mineral composition, and heavy metal contents.

Exchangeable cations of the cha-zeolitites

The enrichment or depletion of the cha-zeolitite is described by its adsorption, or desorption equilibrium capacities (q_e). Table 11 shows the exchangeable cations present in N_{ZT} and K_{ZT}, after phase 1, as NH_4^+-N, K^+, Ca^{2+}, Na^+ and Mg^{2+}.

	q_e *[mg g^{-1}]*				
	NH_4^+-N	**K^+**	**Ca^{2+}**	**Na^+**	**Mg^{2+}**
N_{ZT}	4.67	5.00	-2.85	-1.06	-0.26
K_{ZT}	4.73	-8.29	-1.35	-0.02	-0.24

Table 11. equilibrium adsorption/desorption capacities (q_e) of N_{ZT} and K_{ZT} after phase 1 (mg g^{-1}). Positive values represent adsorption, while negative values represent desorption capacities.

N_{ZT} exchanged, in the following order of importance, $Ca^{2+} > Na^+ > Mg^{2+}$ with K^+ and NH_4^+-N. As expected, K_{ZT} desorbed significantly lower masses of Ca^{2+} and almost no Na^+, while its release of K^+ was significative high.

N and C contents of cha-zeolitites and struvite

The total N (TN) and carbon (TC) of the cha-zeolitite and the precipitates are shown in figure 16. Within phase 1, both N_{ZT} and K_{ZT} adsorbed NH_4^+-N, rising their TN contents from about zero to 0.43 and 0.46% (N_{ZT} and K_{ZT} respectively). Both the cha-zeolitites showed also an increase in TC as a result of digestate residues adhered to the particles.

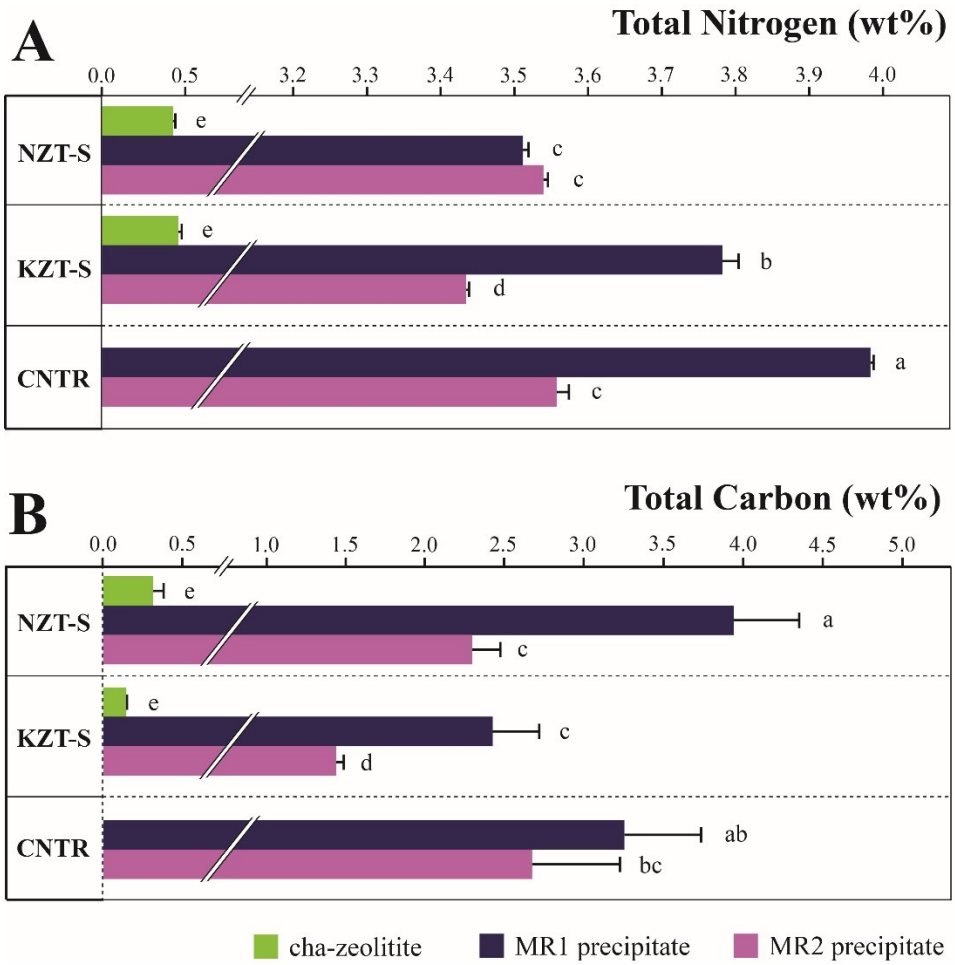

Figure 16. Total nitrogen (TN) and carbon (TC) of the cha-zeolitite (N_{ZT} and K_{ZT}) and the struvite precipitates (MR1 and MR2), obtained by the three treatments tested (NZT-S, KZT-S and CNTR). A: TN (wt%); B: TC (wt%). Different letters indicate significant differences, as resulted by ANOVA and Tukey (HSD) tests ($p < 0.05$).

TN and TC were in general higher in MR1 struvite precipitates rather than MR2, suggesting some differences in their mineral composition. The TN of the precipitates ranged between 3.51 ± 0.06% (NZT-S_MR1) and 3.98 ± 0.03% (CNTR_MR1) (figure 16.A).

In the case of pure struvite crystals, the N content is equal to 5.71% of the mass (http://webmineral.com/data/Struvite.shtml#.YdxXtP7MJPZ, accessed the 22/12/2021), but the measured N values in the precipitates were significantly lower. Even by considering that the precipitate was not entirely composed of struvite (at least for NZT-S_MR1, where the mineral accounted for 89.9, see XRD spectra, below in this section), the measured value of 3.51 still considerably lower than the expected N (5.13% instead of 5.71%, if 89.9% of struvite is considered). K_2HPO_4 introduced significant amounts of K^+. Thus, a possible explanation could have been the precipitation of also the isomorph struvite-(K) ($MgKPO_4 \cdot 6H_2O$) along with "NH_4^+-struvite (http://webmineral.com/data/Struvite-(K).shtml#.YdxbtP7MJPY, accessed the 22/12/2021). For this reason, XRD analyses has been carried out in NZT-S_MR1 and KZT-S_MR1 precipitates (see "Struvite purity of the NZT-S MR1 and KZT-S MR1 precipitates" at pag.73).

For phosphate precipitate fertilizers, the maximum EU limit for organic carbon (C_{org}) is 3% (Annexes to Regulation EU 2019/1009, 2021). In this case, C_{org} was not measured, but only the TC. However, in some cases, TC exceeds this threshold (CNTR_MR1 and NZT-S_MR1) (figure 16.B). By considering that: ì) C_{org} is by definition ≤ TC, and ìì) significative amount of C in the precipitate was part of calcite minerals as inorganic C (see figure 18), it is plausible that the obtained precipitate complied with the legal limit for the C_{org}.

After every phase of the treatment, the digestate tent to clarify and visibly loose suspended solids, while a dark, brown matter is deposited on top of the centrifuge tubes, especially after phase 2 (see section 4.3.4). This material was composed of C (17.7%) of which 97.7% was C_{org}, while N accounted for about 2.4%. Thus, the treatment processes also induced the recovery of significant amounts of organic matter, facilitating its separation from the liquid.

Crystal morphologies of struvite precipitates and semiquantitative chemical composition

The precipitates were composed of polyhedral morphologies (significative examples are shown in figure 17. A, B and C). Crystals were well separated, without aggregates. The struvite tendency to aggregation highly depends on supersaturation conditions, thus, if it is intended to separate the liquid from the precipitate, the control of supersaturation is essential (Shaddel et al., 2019). Crystallization reactions at lower pH can lead to the formation of "micro-flocs" that aggregates together by adsorption and bridging, facilitating the subsequent liquid/precipitate separation (Shaddel et al., 2019; Ye et al., 2018), but, under the applied experimental conditions, precipitation was really fast, with a high nucleation rate, low crystals growth, and no aggregation.

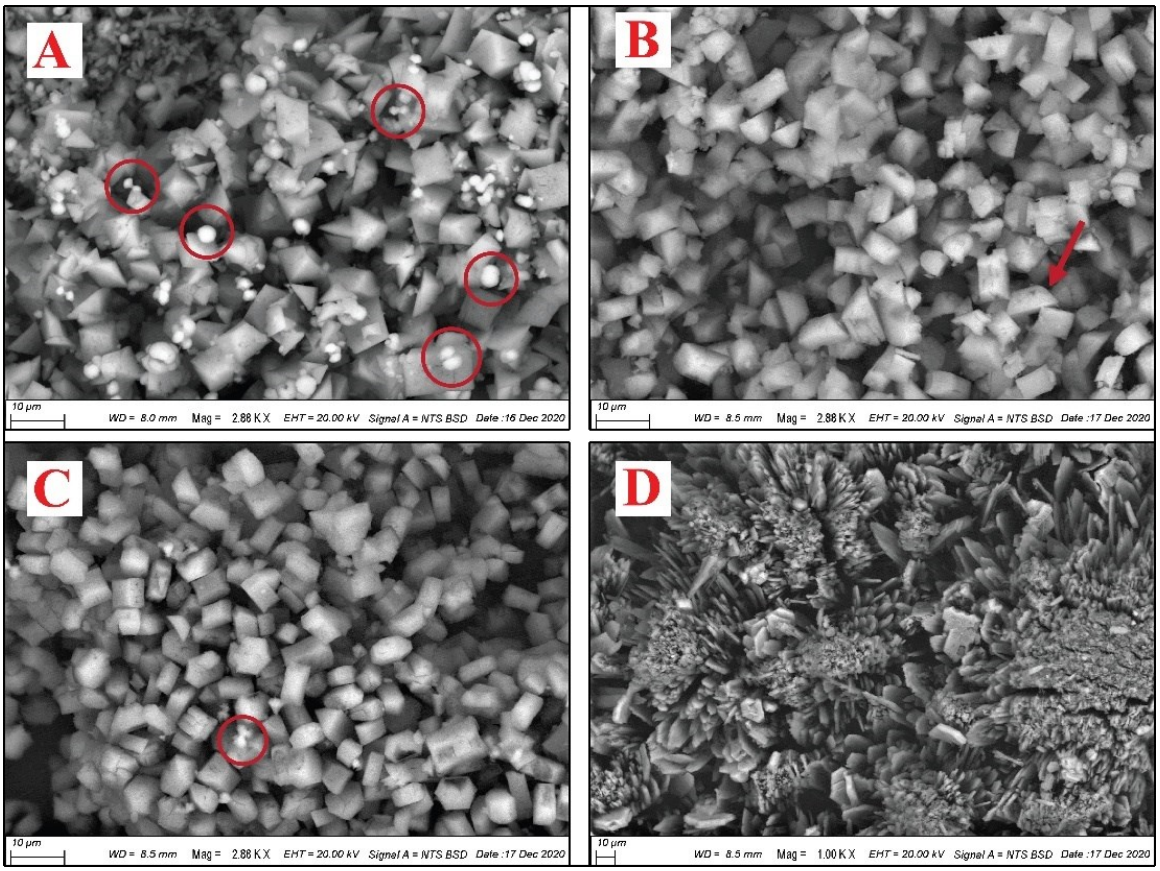

Figure 17. SEM images of precipitates. A: NZT-S_MR1; B: KZT-S_MR2; C: CNTR_MR2 and D: CNTR_MR2 secondary precipitates (these crystals developed after a few hours from struvite precipitation and separation). Red circles highlight the spherical and sheaf-of-wheat shaped calcite. The red arrow indicates a polyhedral struvite crystal (wedge shape) with unequally developed [001] and [00$\bar{1}$] faces.

The semiquantitative chemical composition of the precipitates, obtained by SEM-EDS mappings, are indicated in table 12.

Treatment	Molar Ratio	O	Mg	Al	Si	P	S	K	Ca	Sn
						[wt%]				
CNTR	**MR 1**	58.8	10.7	b.d.l.	0.15	14.2	0.10	3.11	0.96	b.d.l.
	MR 2	44.2	11.4	b.d.l.	0.49	15.0	0.25	5.38	0.68	b.d.l.
NZT-S	**MR 1**	56.9	9.40	0.10	0.19	12.2	0.08	3.17	6.28	b.d.l.
	MR 2	59.7	9.33	0.11	0.14	12.2	0.10	2.98	1.99	b.d.l.
KZT-S	**MR 1**	46.5	13.1	b.d.l.	0.32	17.3	0.15	6.71	1.14	b.d.l.
	MR 2	54.8	12.9	b.d.l.	0.09	16.8	0.20	5.88	b.d.l.	0.66

Table 12. EDS semiquantitative chemical composition of the precipitates. C and N data are not reported because their amount is illustrated in figure 16. b.d.l. means "below detection limit".

The Mg, P and K well correlated, as their amount followed the general trend: KZT-S > CNTR > NZT-S. NZT-S_MR1 precipitates showed higher amounts of Ca, indicating that the release of Ca^{2+} ions by the N_{ZT} led in part to the development of secondary Ca-phases. As suggested by their peculiar forms as spheric-shaped microaggregates, or sheaf-of-wheat morphologies (figure 17.A) (Acelas et al., 2015; Rautaray et al., 2004; Tracy et al., 1998), and by their semiquantitative chemical composition observed by SEM-EDS (13.7, 13.07 and 7.01% as C, Ca and Mg, respectively), these secondary precipitates were mainly constituted by Ca^{2+} and Mg^{2+} carbonates.

The increasing in Ca^{2+} load of the digestate after phase 1 (see section: 5.3.3) demonstrated that only a fraction of these cations, released by the cha-zeolitite, precipitated as insoluble crystals. The particular spherical morphology probably resulted from a rapid crystallization process (Ishikawa and Ichikuni, 1981) and/or, by the presence of limiting agents for calcite growth (Zhang et al., 2013).

In the CNTR_MR2, after a few hours from struvite precipitation and separation, isolated crystals grew up as dark and spheric-shaped millimetric agglomerates. Figure 17.D represents a particular of one of these aggregates. These phases were mainly composed of C, O and Mg-rich

lamellar crystals, as showed by SEM-EDS semiquantitative analysis (22.46, 61.8, 14.1, 1.32, 0.25 and 0.16 as C, O, Mg, P, K and Ca respectively). Their N content was low (0.2%), and they were highly reactive with HCl and poorly with H_2O_2.

Because of these characteristics, those phases were probably mainly constituted by secondary Mg-carbonates and possibly hydroxide ($Mg(OH)_2$). They were low in organic matter and without any struvite precipitates present.

These phases were a further indication of the low reagent use efficiency of the CNTR-MR2 treatment, where high amounts of Mg^{2+} ions were not involved in struvite precipitation, remaining in solution, and slowly precipitating as other unwanted phases.

Struvite purity of the NZT-S MR1 and KZT-S MR1 precipitates.

Phase characterizations were carried out only for the precipitates obtained by treatments that provided the use of the zeolitite (NZT-S and KZT-S), in MR1 condition. Struvite was the most prevailing phase, being it 89.94% and 99.60% in the NZT-S MR and KZT-S MR1 precipitates, respectively.

If these compositions represent only the "NH_4-struvite", it should be expected N contents at about 5.14% and 5.65% (NZT-S MR1 and KZT-S MR1, respectively), but the measured N were significantly lower, being 3.51±0.06 and 3.78±0.18%. This aspect, together with the presence of K mainly in the KZT-S precipitates, led to the hypothesis that the amounts of struvite calculated by XRD were affected by the presence of the isomorph phase K-struvite, which is generally difficult to distinguish from the "NH_4-one" (http://webmineral.com/data/Struvite-(K).shtml#.YdxbtP7MJPY, accessed the 22/12/2021). Indeed, the co-existence of these two phases in the K-NH_4 struvite system, may prevent accurate quantifications by XRD data (Meira et al., 2020) because the diffractograms of K-struvite and NH_4-struvite strongly overlap, differing only for certain intensity distributions between different peaks.

The presence of K-struvite is assessed in general, in conjunction with other chemical information. In this work, the SEM-EDS analysis and the N composition suggested the presence of K-struvite, along with the consideration that high amounts of K^+ were naturally present in the digestate and introduced by the K_{ZT} and the K_2HPO_4 reagent. To estimate the amounts of K-struvite and struvite, the following approach has been used.

It has been assumed that the TN measured in the precipitates (figure 16) corresponded to the NH_4-N of struvite. This is a plausible assumption, considering that: ì) The N in the digestate was about 82% composed of NH_4^+-N, and the remaining 13% was organic (see Tab. 2 in section 3.2.2); ìì) the precipitate was washed multiple times thus, negligible residual N was expected.

The relative amounts of K-struvite and struvite were then calculated from the XRD data and corrected for the N contents.

The NZT-S_MR1 and KZT-S_MR1 precipitates were thus approximatively composed of 62.56% and 67.43% NH_4-struvite, while K-struvite accounted for the 27.38% and 32.17, respectively.

A different approach may also be used, by considering the presence of K-struvite in the Rietveld refinement. In this way, the NH_4-struvite amounts were higher than the above-discussed N-based estimations, being 72.82% and 78.15% (NZT-S_MR1 and KZT-S_MR1, respectively). However, in this scenario, the N expected should be 4.16% and 4.46%, thus significantly higher than the measured values (3.57% and 3.85%). The first approach can therefore be considered with higher accuracy than the second.

XRD spectra (in the presence of K-struvite) are shown in Figure 18 from NZT-S_MR1 (18.A) and KZT-S_MR1 (18.B).

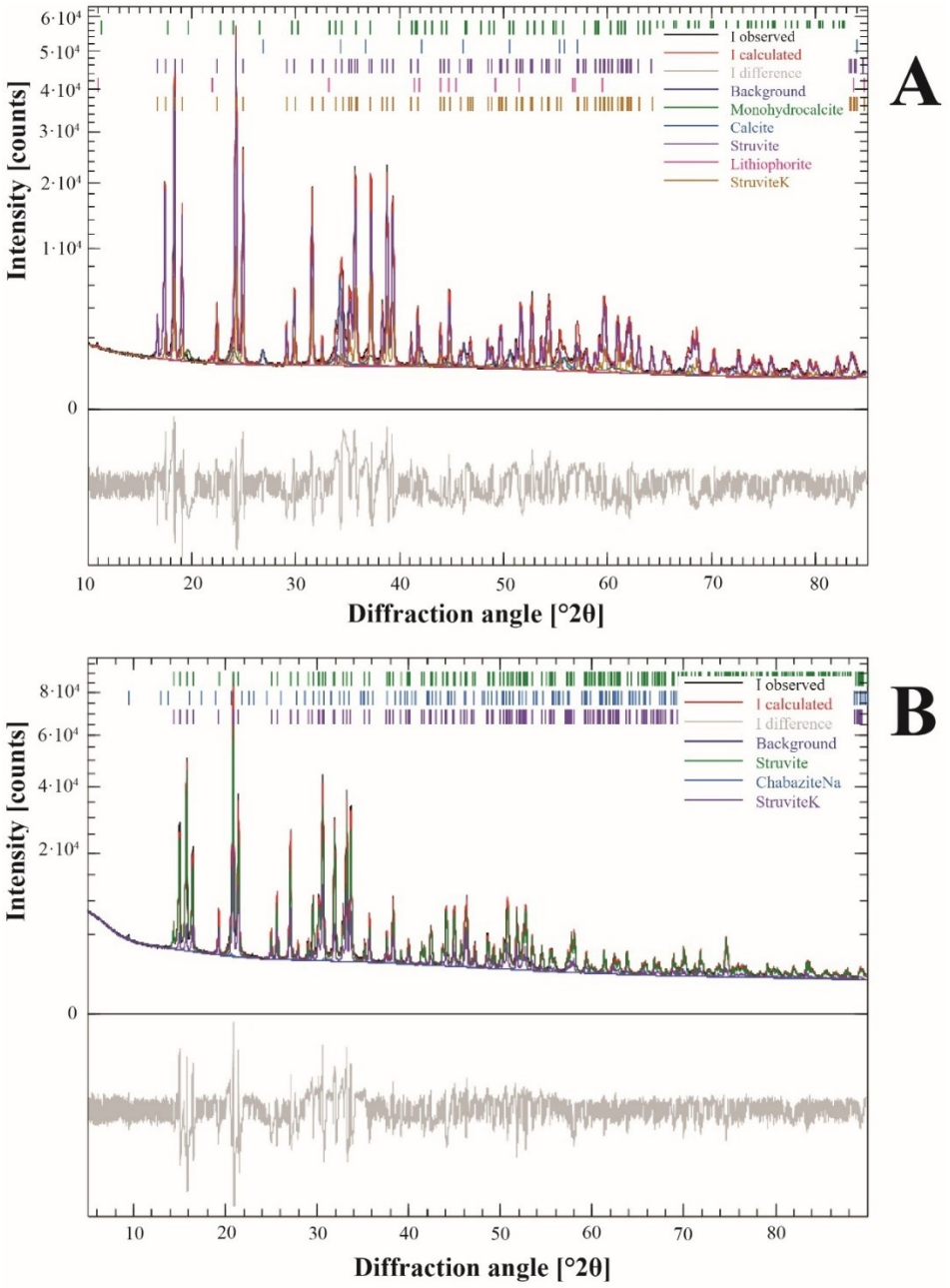

Figure 18. X-ray powder diffraction (XRD) spectra of the NZT-S MR1 (A) and KZT-S MR1 (B) precipitates.

Besides struvite and K-struvite, the NZT-S MR1 precipitate was composed also by $CaCO_3$ (7.5%), monohydrocalcite ($CaCO_3 \cdot H_2O$, 2.1%) and a small amount of lithiophorite ($(Al,Li)MnO_2(OH)_2$, 0.4%). In KZT-S MR1, a small fraction (0.4%) was composed of residual chabazite, remained from phase 1.

The sodium (Na), aluminum (Al), iron (Fe), as well as heavy metal contents of the NZT-S_MR1 precipitate are reported in table 13.

Na	Al	Fe	Cd	Cr	Hg	Ni	Pb	As	Cu
			[mg kg^{-1}]						
104	474	341	0.023	0.400	b.d.l.	0.652	2.450	0.882	0.347

Table 13. Na, Al, Fe (at the left), and heavy metals (at the right) of NZT-S_MR1 precipitate. "b.d.l." means "below detection limit".

The heavy metals in NZT-S_MR1 precipitate showed excellent results, as they were strongly lower than the European limitations, thus, at least from this point of view, the precipitate obtained by the NZT-S_MR1 treatment was suitable for fertilization (Annexes to Regulation EU 2019/1009, 2021).

6. CONCLUSION

In this work, a new integrated strategy for the treatment of nutrient-rich wastewaters and the recovery of N and P is described. The methodology involved the use of a chabazite-rich zeolitite for the removal of NH_4^+-N, and a subsequent phase that provided the precipitation of struvite crystals, for the recovery of the residual NH_4^+-N and PO_4^{3-}-P.

From the experiments performed, the following conclusions can be drawn:

1. As a preliminary study, experiment A aimed at the description of the cha-zeolitite adsorption properties from real zootechnical wastewater (pig manure), within the definition of the equilibrium isotherms, kinetic models, and thermodynamic parameters. This experiment allowed to better contextualize the 1st phase of the treatment process (adsorption phase), subsequently developed in experiment B.

   The cha-rich zeolitite revealed to be an efficient material for the recovery of NH_4^+-N. The outcomes of the experiment led to the choice of using the micronized material (N_{ZT}) for

experiment B, instead of the granular one (gN_{ZT}) because of its ì) higher adsorption capacities, ìì) better temperature stability in NH_4^+-N adsorption, and ìèì) higher velocities to reach equilibrium conditions. All these aspects are significant for the possible future scaling up of the system, while possible negative points may relate to the necessity of a grinding phase, for the micronization, and the possibly more difficult separation of the zeolitite from the liquid wastewater.

Anyway, even if it was not applied in experiment B, also the granular zeolitite proved to be an excellent material for the removal of NH_4^+-N from nutrient-rich wastewaters.

2. In the proposed wastewater treatment strategy, developed within experiment B, the removal of NH_4^+-N carried out by the cha-zeolitite improved the efficiency of the struvite precipitation by better balancing the molar ratios between the struvite constituents (Mg^{2+}, NH_4^+ and PO_4^{3-}), thus allowing to reduce the use of reagents by about 50%. This outcome is of great economical interest especially because of the high reagents cost which is one of the main limitations for the implementation of struvite technologies.

3. By considering all the parameters evaluated in experiment B, it is possible to express an opinion about which of the different treatments tested proved to be the most efficient way in terms of nutrient recovery, potentially lower costs, and environmental impacts.

Therefore, the use of cha-zeolitite (phase 1), in association with the precipitation of struvite in NH_4^+ excess conditions (phase 2), may be considered the most efficient strategy in terms of ì) nutrient recovery, ìì) reagents use efficiency, and ìèì) chemical alteration of the treated wastewater.

4. After the cha-zeolitite adsorption batch, the collected cha-zeolitites were enriched in N, making this material useful for plant nutrition, soil amendment, or as a growing medium.

5. The precipitate obtained by the treatment that may be considered as the best one (NZT-S_MR1) was composed of 89.9% of struvite (estimated as 62.56% NH_4-struvite, and 27.38% K-struvite, while KZT-S MR1 was 67.43% NH_4-struvite and 32.17% K-struvite. NZT-S MR1 precipitates was also constituted by Ca^{2+} and Mg^{2+} carbonates (about 9.6%). Its TN was 3.5%. The heavy metals highly fell within the EU limitations for phosphate precipitate fertilizers. From the experimental data, it is plausible, although not verified, that the concentration of C_{org} was also lower than the legal limit of 3%.

   Unfortunately, other important parameters for the evaluation of the potential marketability are missing, like the P content, which should be at least 16% as P_2O_5, and the presence of potentially dangerous microorganisms as *Salmonella* spp. and *Escherichia coli* or *Enterococcaceae*.

   Thus, although more characterization is needed, there are good expectations for the struvite precipitates to fall within the EU legal limits required.

Finally, it should be discussed also the enrichment in both K^+ and SO_4^{2-} of the treated wastewater, resulting from the use of reagents. Indeed, even if lower intensities were observed for NZT-S and KZT-S treatments (where the reagents were reduced by about one-half respect the CNTR), the accumulation of K^+ and SO_4^{2-} remained important, thus potentially posing limitations for the use of the treated wastewater in agriculture.

The use of natural zeolites has certainly increased the Mg^{2+}/NH_4^+ and PO_4^{3-}/NH_4^+ molar ratios, thus permitting to apply lower amounts of Mg^{2+} and PO_4^{3-}-based reagents. However, to further increase both the economic and environmental sustainability of the treatment process, other solutions may be implemented along with the use of natural zeolites, to further cut down the needs of reagents and surely make this system an attractive and feasible option.

Among these, the possibility to implement low expensive alternative sources for Mg^{2+} and PO_4^{3-}, as the bone meal (for PO_4^{3-}), magnesite (for Mg^{2+}), or seawater bittern (for Mg^{2+}), is an interesting perspective.

As a final consideration, it is important to point out that, even if in this work, the laboratory tests were carried out on animal wastewater and a derived one, the treatment developed can be extended to any other system that produces nutrient-rich wastewaters as, e.g., municipal wastewaters.

REFERENCES

Acelas, N.Y., Flórez, E., López, D., 2015. Phosphorus recovery through struvite precipitation from wastewater: effect of the competitive ions. Desalin. Water Treat. 54, 2468–2479. https://doi.org/10.1080/19443994.2014.902337

Ahmed, O.H., Braine Yap, C.H., Nik Muhamad, A.M., 2010. Minimizing ammonia loss from urea through mixing with zeolite and acid sulphate soil. Int. J. Phys. Sci. 5, 2198–2202.

Alshameri, A., Ibrahim, A., Assabri, A.M., Lei, X., Wang, H., Yan, C., 2014. The investigation into the ammonium removal performance of Yemeni natural zeolite: Modification, ion exchange mechanism, and thermodynamics. Powder Technol. 258, 20–31. https://doi.org/10.1016/j.powtec.2014.02.063

Aneja, V.P., Schlesinger, W.H., Erisman, J.W., 2008. Farming pollution. Nat. Geosci. 2008 17 1, 409–411. https://doi.org/10.1038/ngeo236

Aydın Temel, F., Kuleyin, A., 2016. Ammonium removal from landfill leachate using natural zeolite: kinetic, equilibrium, and thermodynamic studies. Desalin. Water Treat. 57, 23873–23892. https://doi.org/10.1080/19443994.2015.1136964

Barnett, G.M., 1994. Phosphorus forms in animal manure. Bioresour. Technol. 49, 139–147. https://doi.org/10.1016/0960-8524(94)90077-9

Bayuseno, A.P., Schmahl, W.W., 2019. Thermal decomposition of struvite in water: qualitative and quantitative mineralogy analysis. Environ. Technol. (United Kingdom). https://doi.org/10.1080/09593330.2019.1615558

Bhuiyan, M.I.H., Mavinic, D.S., Koch, F.A., 2008. Thermal decomposition of struvite and its phase transition. Chemosphere 70, 1347–1356. https://doi.org/10.1016/J.CHEMOSPHERE.2007.09.056

Bish, D.L., Howard, S.A., 1988. Quantitative phase analysis using the Rietveld method. J. Appl. Crystallogr. Crystallogr. 21, 86–91.

Bonmatí, A., Flotats, X., 2003. Air stripping of ammonia from pig slurry: characterisation and feasibility as a pre- or post-treatment to mesophilic anaerobic digestion. Waste Manag. 23, 261–272. https://doi.org/10.1016/S0956-053X(02)00144-7

Brown, K., Harrison, J., Bowers, K., 2018. Struvite Precipitation from Anaerobically Digested Dairy Manure. Water. Air. Soil Pollut. 229, 1–11. https://doi.org/10.1007/S11270-018-3855-5/TABLES/1

Capolupo, A., Pindozzi, S., Okello, C., Boccia, L., 2014. Indirect field technology for detecting areas object of illegal spills harmful to human health: application of drones, photogrammetry and hydrological models. Geospat. Health 8, S699–S707. https://doi.org/10.4081/GH.2014.298

Chabazite [WWW Document], n.d. URL http://www.iza-online.org/natural/Datasheets/Chabazite/Chabazite.html (accessed 9.25.20).

Chattopadhyay, A., 2017. SorptionAnalysis: Static Adsorption Experiment Plotting and Analysis.

Cheary, R.W., Coelho, A.A., Cline, J.P., 2004. Fundamental parameters line profile fitting in laboratory diffractometers. J. Res. Natl. Inst. Stand. Technol. 109, 1–25. https://doi.org/10.6028/JRES.109.002

Chemisorption and physisorption [WWW Document], n.d. URL https://old.iupac.org/reports/2001/colloid_2001/manual_of_s_and_t/node16.html (accessed 1.5.22).

Chen, H.-F., Lin, Y.-J., Chen, B.-H., Yoshiyuki, I., Liou, S., Huang, R.-T., 2018. A Further Investigation of NH4+ Removal Mechanisms by Using Natural and Synthetic Zeolites in Different Concentrations and Temperatures. Minerals 8, 499. https://doi.org/10.3390/min8110499

Chen, H.F., Lin, Y.J., Chen, B.H., Yoshiyuki, I., Liou, S.Y.H., Huang, R.T., 2018. A Further Investigation of NH4+ Removal Mechanisms by Using Natural and Synthetic Zeolites in Different Concentrations and Temperatures. Miner. 2018, Vol. 8, Page 499 8, 499. https://doi.org/10.3390/MIN8110499

Cheng, Q., Li, H., Xu, Y., Chen, S., Liao, Y., Deng, F., Li, J., 2017. Study on the adsorption of nitrogen and phosphorus from biogas slurry by NaCl-modified zeolite. PLoS One 12, e0176109. https://doi.org/10.1371/journal.pone.0176109

Cheung, C.W., Porter, J.F., Mckay, G., 2001. Sorption kinetic analysis for the removal of cadmium ions from effluents using bone char. Water Res. 35, 605–612. https://doi.org/10.1016/S0043-1354(00)00306-7

Colombani, N., Di Giuseppe, D., Faccini, B., Ferretti, G., Mastrocicco, M., Coltorti, M., 2016. Estimated Water Savings in an Agricultural Field Amended With Natural Zeolites. Environ. Process. 3, 617–628. https://doi.org/10.1007/s40710-016-0151-5

Coombs, D.S., 2001. Recommended nomenclature for zeolite minerals: Report of the subcommittee on zeolites of the international mineralogical association, commission on new minerals and mineral names. Bull. Mineral. Petrol. Geochemistry 20, 149–155.

Cortés-Martínez, R., Martínez-Miranda, V., Solache-Ríos, M., García-Sosa, I., 2004. Evaluation of natural and surfactant-modified zeolites in the removal of cadmium from aqaeous solutions. Sep. Sci. Technol. 39, 2711–2730. https://doi.org/10.1081/SS-200026766

Dada, A.O., Olalekan, A.P., Olatunya, A.M., Dada, O., 2012. Langmuir, Freundlich, Temkin and Dubinin–Radushkevich Isotherms Studies of Equilibrium Sorption of Zn 2+ Unto Phosphoric Acid Modified Rice Husk. IOSR J. Appl. Chem. 3, 38–45. https://doi.org/10.9790/5736-0313845

Degryse, F., Baird, R., da Silva, R.C., McLaughlin, M.J., 2017. Dissolution rate and agronomic effectiveness of struvite fertilizers – effect of soil pH, granulation and base excess. Plant Soil 410, 139–152. https://doi.org/10.1007/S11104-016-2990-2/FIGURES/6

Desmidt, E., Ghyselbrecht, K., Monballiu, A., Rabaey, K., Verstraete, W., Meesschaert, B.D., 2013. Factors influencing urease driven struvite precipitation. Sep. Purif. Technol. 110, 150–157. https://doi.org/10.1016/J.SEPPUR.2013.03.010

Dockhorn, T., 2009. About the economy of phosphorus recovery, in: International Conference on Nutrient Recovery from Wastewater Streams, Vancouver, Canada. IWA Publishing, London, pp. 145–158.

Doebelin, N., Kleeberg, R., 2015. Profex: A graphical user interface for the Rietveld refinement program BGMN. J. Appl. Crystallogr. 48, 1573–1580. https://doi.org/10.1107/S1600576715014685

Dursun, G., Çiçek, H., Dursun, A.Y., 2005. Adsorption of phenol from aqueous solution by using carbonised beet pulp. J. Hazard. Mater. 125, 175–182. https://doi.org/10.1016/j.jhazmat.2005.05.023

Dwairi, I.M., 1998. Evaluation of jordanian zeolite tuff as a controlled slow-release fertilizer for NH4+. Environ. Geol. 34, 1–4. https://doi.org/10.1007/s002540050251

Escudero, A., Blanco, F., Lacalle, A., Pinto, M., 2015. Struvite precipitation for ammonium removal from anaerobically treated effluents. J. Environ. Chem. Eng. 3, 413–419. https://doi.org/10.1016/J.JECE.2015.01.004

European Commission, 2021a. Regulation (EU) 2021/1768. Bruxelles.

European Commission, 2021b. COMMISSION DELEGATED REGULATION (EU) …/... amending Annexes II and IV to Regulation (EU) 2019/1009 of the European Parliament and of the Council for the purpose of adding precipitated phosphate salts and derivates as a component material category in EU fe [WWW Document]. 05/07/2021. URL https://eur-lex.europa.eu/legal-

content/EN/ALL/?uri=PI_COM:C(2021)4743 (accessed 8.9.21).

European Commission, 2009. Regulation (EC) 1069/2009 [WWW Document]. URL https://eur-lex.europa.eu/legal-content/en/ALL/?uri=CELEX%3A32009R1069

European Economic Community, 2008. Council Directive 91/676/EEC [WWW Document]. 11/12/2008. URL http://data.europa.eu/eli/dir/1991/676/2008-12-11

European Parliament and Council, 2021. FAQs related to Regulation (EU) 2019/1009. Bruxelles.

European Parliament and Council, 2019. Regulation (EU) 2019/1009 [WWW Document]. URL http://data.europa.eu/eli/reg/2019/1009/oj (accessed 8.9.21).

Faccini, B., Di Giuseppe, D., Ferretti, G., Coltorti, M., Colombani, N., Mastrocicco, M., 2018. Natural and NH4+-enriched zeolitite amendment effects on nitrate leaching from a reclaimed agricultural soil (Ferrara Province, Italy). Nutr. Cycl. Agroecosystems 110, 327–341. https://doi.org/10.1007/s10705-017-9904-4

Faccini, B., Di Giuseppe, D., Malferrari, D., Coltorti, M., Abbondanzi, F., Campisi, T., Laurora, A., Passaglia, E., 2015. Ammonium-exchanged zeolitite preparation for agricultural uses: From laboratory tests to large-scale application in ZeoLIFE project prototype. Period. di Mineral. 84, 303–321. https://doi.org/10.2451/2015PM0015

FAO, 2019. United Nations, World fertilizer trends and outlook to 2022. Rome.

FAO, 1997. FAOSTAT. Database [WWW Document]. URL http://www.fao.org/faostat/en/#data/RL/visualize (accessed 3.20.21).

Ferretti, G., Di Giuseppe, D., Faccini, B., Coltorti, M., 2018. Mitigation of sodium risk in a sandy agricultural soil by the use of natural zeolites. Environ. Monit. Assess. 190. https://doi.org/10.1007/s10661-018-7027-2

Ferretti, G., Di Giuseppe, D., Natali, C., Faccini, B., Bianchini, G., Coltorti, M., 2017a. C-N elemental and isotopic investigation in agricultural soils: Insights on the effects of zeolitite amendments. Chemie der Erde - Geochemistry 77, 45–52. https://doi.org/10.1016/j.chemer.2017.02.002

Ferretti, G., Keiblinger, K.M., Zimmermann, M., Di Giuseppe, D., Faccini, B., Colombani, N., Mentler, A., Zechmeister-Boltenstern, S., Coltorti, M., Mastrocicco, M., 2017b. High resolution short-term investigation of soil CO2, N2O, NOx and NH3 emissions after different chabazite zeolite amendments.

Appl. Soil Ecol. 119, 138–144. https://doi.org/10.1016/j.apsoil.2017.06.004

Ferretti, Galamini, Medoro, Coltorti, Di Giuseppe, Faccini, 2020. Impact of Sequential Treatments with Natural and Na-Exchanged Chabazite Zeolite-Rich Tuff on Pig-Slurry Chemical Composition. Water 12, 310. https://doi.org/10.3390/w12020310

Foo, K.Y., Hameed, B.H., 2010. Insights into the modeling of adsorption isotherm systems. Chem. Eng. J. https://doi.org/10.1016/j.cej.2009.09.013

Forrest, A.L., Fattah, K.P., Mavinic, D.S., Koch, F.A., 2008. Optimizing Struvite Production for Phosphate Recovery in WWTP. J. Environ. Eng. 134, 395–402. https://doi.org/10.1061/(ASCE)0733-9372(2008)134:5(395)

Frost, R.L., Weier, M.L., Erickson, K.L., 2004. Thermal decomposition of struvite. J. Therm. Anal. Calorim. 76, 1025–1033. https://doi.org/10.1023/B:JTAN.0000032287.08535.B3

Galli, E., Passaglia, E., 2011. Natural zeolites in environmental engineering, in: Harald Holzapfel (Ed.), Zeolites in Chemical Engineering. Verlag ProcessEng Engineering GmbH, pp. 392–416.

Ghosal, P.S., Gupta, A.K., 2017. Determination of thermodynamic parameters from Langmuir isotherm constant-revisited. J. Mol. Liq. 225, 137–146. https://doi.org/10.1016/j.molliq.2016.11.058

Giles, C.H., MacEwan, T.H., Nakhwa, S.N., Smith, D., 1960. 786. Studies in adsorption. Part XI. A system of classification of solution adsorption isotherms, and its use in diagnosis of adsorption mechanisms and in measurement of specific surface areas of solids. J. Chem. Soc. 3973–3993. https://doi.org/10.1039/jr9600003973

Gottardi, G., Galli, E., 1985. Natural Zeolites. Minerals and Rocks 18. https://doi.org/10.1007/978-3-642-46518-5

Gualtieri, A.F., 2000. Accuracy of XRPD QPA using the combined Rietveld-RIR method. J. Appl. Crystallogr. Crystallogr. 33, 267–278.

Gualtieri, A.F., Passaglia, E., 2006. Rietveld structure refinement of NH4-exchanged natural chabazite. Eur. J. Mineral. 18, 351–359. https://doi.org/10.1127/0935-1221/2006/0018-0351

Gunay, A., 2007. Application of nonlinear regression analysis for ammonium exchange by natural (Bigadiç) clinoptilolite. J. Hazard. Mater. 148, 708–713. https://doi.org/10.1016/j.jhazmat.2007.03.041

Gunay, A., Karadag, D., Tosun, I., Ozturk, M., 2008. Use of magnesit as a magnesium source for ammonium

removal from leachate. J. Hazard. Mater. 156, 619–623. https://doi.org/10.1016/J.JHAZMAT.2007.12.067

Guo, X., Zeng, L. (L)., Li, X., Park, H.S., 2008. Ammonium and potassium removal for anaerobically digested wastewater using natural clinoptilolite followed by membrane pretreatment. J. Hazard. Mater. 151, 125–133. https://doi.org/10.1016/j.jhazmat.2007.05.066

Halim, A.A., Aziz, H.A., Johari, M.A.M., Ariffin, K.S., 2010. Comparison study of ammonia and COD adsorption on zeolite, activated carbon and composite materials in landfill leachate treatment. Desalination 262, 31–35. https://doi.org/10.1016/j.desal.2010.05.036

Hao, X.-D., Wang, C.-C., Lan, L., van Loosdrecht, M.C.M., 2008. Struvite formation, analytical methods and effects of pH and Ca2 +. Water Sci. Technol. 58, 1687–1692. https://doi.org/10.2166/WST.2008.557

Harkins, W.D., Jura, G., 1944. The decrease (π) of free surface energy (γ) as a basis for the development of equations for adsorption isotherms; And the existence of two condensed phases in films on solids. J. Chem. Phys. https://doi.org/10.1063/1.1723913

Hata, S., Kobae, Y., Banba, M., 2010. Interactions between plants and arbuscular mycorrhizal fungi. Int. Rev. Cell Mol. Biol. 281, 1–48. https://doi.org/10.1016/S1937-6448(10)81001-9

Ho, Y.S., 2006. Review of second-order models for adsorption systems. J. Hazard. Mater. 136, 681–689. https://doi.org/10.1016/j.jhazmat.2005.12.043

Ho, Y.S., McKay, G., 2002. Application of Kinetic Models to the Sorption of Copper(II) on to Peat. Adsorpt. Sci. Technol. 20, 797–815. https://doi.org/10.1260/026361702321104282

Ho, Y.S., McKay, G., 1999. Pseudo-second order model for sorption processes. Process Biochem. 34, 451–465. https://doi.org/10.1016/S0032-9592(98)00112-5

Ho, Y.S., McKay, G., 1998. A Comparison of chemisorption kinetic models applied to pollutant removal on various sorbents. Process Saf. Environ. Prot. 76, 332–340. https://doi.org/10.1205/095758298529696

Ho, Y.S., Ng, J.C.Y., McKay, G., 2011. KINETICS OF POLLUTANT SORPTION BY BIOSORBENTS: REVIEW. http://dx.doi.org/10.1081/SPM-100100009 29, 189–232. https://doi.org/10.1081/SPM-100100009

Holford, I.C.R., 1997. Soil phosphorus: Its measurement, and its uptake by plants. Aust. J. Soil Res. 35, 227–

239. https://doi.org/10.1071/S96047

http://webmineral.com/data/Struvite-(K).shtml#.YdxbtP7MJPY [WWW Document], n.d.

http://webmineral.com/data/Struvite.shtml#.YdxXtP7MJPZ [WWW Document], n.d.

Huang, H., Chen, Y., Jiang, Y., Ding, L., 2014. Treatment of swine wastewater combined with MgO-saponification wastewater by struvite precipitation technology. Chem. Eng. J. 254, 418–425. https://doi.org/10.1016/J.CEJ.2014.05.054

Huang, H., Xiao, X., Yan, B., Yang, L., 2010. Ammonium removal from aqueous solutions by using natural Chinese (Chende) zeolite as adsorbent. J. Hazard. Mater. 175, 247–252. https://doi.org/10.1016/j.jhazmat.2009.09.156

Huang, H., Xu, C., Zhang, W., 2011. Removal of nutrients from piggery wastewater using struvite precipitation and pyrogenation technology. Bioresour. Technol. 102, 2523–2528. https://doi.org/10.1016/J.BIORTECH.2010.11.054

Ichihashi, O., Hirooka, K., 2012. Removal and recovery of phosphorus as struvite from swine wastewater using microbial fuel cell. Bioresour. Technol. 114, 303–307. https://doi.org/10.1016/J.BIORTECH.2012.02.124

International Zeolite Association, n.d. Chabazite [WWW Document]. URL http://www.iza-online.org/natural/Datasheets/Chabazite/Chabazite.html (accessed 1.13.22).

Ishikawa, M., Ichikuni, M., 1981. Coprecipitation of phosphate with calcite. Geochem. J. 15, 283–288. https://doi.org/10.2343/GEOCHEMJ.15.283

Iyer, K.P.D., Kunju, A.S., 1992. Extension of Harkins-Jura adsorption isotherm to solute adsorption. Colloids and Surfaces 63, 235–240. https://doi.org/10.1016/0166-6622(92)80244-V

Jha, V.K., Hayashi, S., 2009. Modification on natural clinoptilolite zeolite for its NH4+ retention capacity. J. Hazard. Mater. 169, 29–35. https://doi.org/10.1016/J.JHAZMAT.2009.03.052

Kabdaşlı, I., Tünay, O., 2018. Nutrient recovery by struvite precipitation, ion exchange and adsorption from source-separated human urine – a review. https://doi.org/10.1080/21622515.2018.1473504 7, 106–138. https://doi.org/10.1080/21622515.2018.1473504

Kataki, S., West, H., Clarke, M., Baruah, D.C., 2016. Phosphorus recovery as struvite: Recent concerns for use of seed, alternative Mg source, nitrogen conservation and fertilizer potential. Resour. Conserv.

Recycl. 107, 142–156. https://doi.org/10.1016/J.RESCONREC.2015.12.009

Kesraoui-Ouki, S., Cheeseman, C.R., Perry, R., 1994. Natural zeolite utilisation in pollution control: A review of applications to metals' effluents. J. Chem. Technol. Biotechnol. https://doi.org/10.1002/jctb.280590202

Khan, A.A., Singh, R.P., 1987. Adsorption thermodynamics of carbofuran on Sn (IV) arsenosilicate in H+, Na+ and Ca2+ forms. Colloids and Surfaces 24, 33–42. https://doi.org/10.1016/0166-6622(87)80259-7

Kim, D., Ryu, H.D., Kim, M.S., Kim, J., Lee, S.I., 2007. Enhancing struvite precipitation potential for ammonia nitrogen removal in municipal landfill leachate. J. Hazard. Mater. 146, 81–85. https://doi.org/10.1016/J.JHAZMAT.2006.11.054

Kozik, A., Hutnik, N., Piotrowski, K., Mazienczuk, A., Matynia, A., 2013. Precipitation and Crystallization of Struvite from Synthetic Wastewater under Stoichiometric Conditions. Adv. Chem. Eng. Sci. 03, 20–26. https://doi.org/10.4236/ACES.2013.34B004

Król, M., 2020. Natural vs. Synthetic Zeolites. Cryst. 2020, Vol. 10, Page 622 10, 622. https://doi.org/10.3390/CRYST10070622

Kumar, R., Pal, P., 2015. Assessing the feasibility of N and P recovery by struvite precipitation from nutrient-rich wastewater: a review. Environ. Sci. Pollut. Res. 22, 17453–17464. https://doi.org/10.1007/s11356-015-5450-2

Lagergren, S.Y., Sven, K., 1898. Zurtheorie der sogenannten adsorption gelösterstoffe. K. Sven. Vetenskapsakademiens. Handl. 24, 1–39.

Langmuir, I., 1918. The adsorption of gases on plane surfaces of glass, mica and platinum. J. Am. Chem. Soc. 40, 1361–1403. https://doi.org/10.1021/ja02242a004

Le Corre, K.S., Valsami-Jones, E., Hobbs, P., Parsons, S.A., 2009a. Phosphorus Recovery from Wastewater by Struvite Crystallization: A Review. http://dx.doi.org/10.1080/10643380701640573 39, 433–477. https://doi.org/10.1080/10643380701640573

Le Corre, K.S., Valsami-Jones, E., Hobbs, P., Parsons, S.A., 2009b. Phosphorus recovery from wastewater by struvite crystallization: A review. Crit. Rev. Environ. Sci. Technol. https://doi.org/10.1080/10643380701640573

LeVan, M.D., Carta, G., 2008. Adsorption and Ion Exchange, in: Green, D.W. (Ed.), Perry's Chemical

Engineers' Handbook. New York.

Leyva-Ramos, R., Monsivais-Rocha, J.E., Aragon-Piña, A., Berber-Mendoza, M.S., Guerrero-Coronado, R.M., Alonso-Davila, P., Mendoza-Barron, J., 2010. Removal of ammonium from aqueous solution by ion exchange on natural and modified chabazite. J. Environ. Manage. 91, 2662–2668. https://doi.org/10.1016/j.jenvman.2010.07.035

Li, M., Zhu, X., Zhu, F., Ren, G., Cao, G., Song, L., 2011. Application of modified zeolite for ammonium removal from drinking water. Desalination 271, 295–300. https://doi.org/10.1016/j.desal.2010.12.047

Lijima, A., 1980. GEOLOGY OF NATURAL ZEOLITES AND ZEOLITIC ROCKS. Print. Gt. Britain. Plenary Pap. Mineral. 52, 2–5.

Limousin, G., Gaudet, J.P., Charlet, L., Szenknect, S., Barthès, V., Krimissa, M., 2007. Sorption isotherms: A review on physical bases, modeling and measurement. Appl. Geochemistry. https://doi.org/10.1016/j.apgeochem.2006.09.010

Malferrari, D., Laurora, A., Brigatti, M.F., Coltorti, M., Di Giuseppe, D., Faccini, B., Passaglia, E., Vezzalini, M.G., 2013a. Open-field experimentation of an innovative and integrated zeolitite cycle: Project definition and material characterization. Rend. Lincei 24, 141–150. https://doi.org/10.1007/s12210-013-0235-3

Malferrari, D., Laurora, A., Franca Brigatti, M., Coltorti, M., Di Giuseppe, D., Faccini, B., Passaglia, E., Giovanna Vezzalini, M., 2013b. Open-field experimentation of an innovative and integrated zeolitite cycle: project definition and material characterization. Rend. Lincei 24, 141–150. https://doi.org/10.1007/s12210-013-0235-3

Mall, I.D., Srivastava, V.C., Agarwal, N.K., 2006. Removal of Orange-G and Methyl Violet dyes by adsorption onto bagasse fly ash - Kinetic study and equilibrium isotherm analyses. Dye. Pigment. 69, 210–223. https://doi.org/10.1016/j.dyepig.2005.03.013

Martí, N., Pastor, L., Bouzas, A., Ferrer, J., Seco, A., 2010. Phosphorus recovery by struvite crystallization in WWTPs: Influence of the sludge treatment line operation. Water Res. 44, 2371–2379. https://doi.org/10.1016/J.WATRES.2009.12.043

Martins, A.C., Pezoti, O., Cazetta, A.L., Bedin, K.C., Yamazaki, D.A.S., Bandoch, G.F.G., Asefa, T., Visentainer, J. V., Almeida, V.C., 2015. Removal of tetracycline by NaOH-activated carbon produced

from macadamia nut shells: Kinetic and equilibrium studies. Chem. Eng. J. 260, 291–299. https://doi.org/10.1016/J.CEJ.2014.09.017

Mazzi, F., Galli, E., 1983. The tetrahedral framework of chabazite. N. Jb. Miner. Mh. 461–480.

Meira, R.C. de S., Paz, S.P.A. da, Corrêa, J.A.M., 2020. XRD-Rietveld analysis as a tool for monitoring struvite analog precipitation from wastewater: P, Mg, N and K recovery for fertilizer production. J. Mater. Res. Technol. 9, 15202–15213. https://doi.org/10.1016/J.JMRT.2020.10.082

Ming, D.W., Allen, E.R., 2001. Use of natural zeolites in agronomy, horticulture, and environmental soil remediation. Rev. Mineral. Geochemistry 45, 618–654. https://doi.org/10.2138/rmg.2001.45.18

Mohan, G.R., Gadekar, S., Pullammanappallil, P., 2011. Development of a Process Model for Recovery of Nutrients from Wastewater by Precipitation as Struvite.

Moshoeshoe, M., Silas Nadiye-Tabbiruka, M., Obuseng, V., 2017. A Review of the Chemistry, Structure, Properties and Applications of Zeolites. Am. J. Mater. Sci. 2017, 196–221. https://doi.org/10.5923/j.materials.20170705.12

Moussavi, G., Talebi, S., Farrokhi, M., Sabouti, R.M., 2011. The investigation of mechanism, kinetic and isotherm of ammonia and humic acid co-adsorption onto natural zeolite. Chem. Eng. J. 171, 1159–1169. https://doi.org/10.1016/j.cej.2011.05.016

Mumpton, F.A., 1999. La roca magica: Uses of natural zeolites in agriculture and industry. Proc. Natl. Acad. Sci. U. S. A. 96, 3463–3470. https://doi.org/10.1073/pnas.96.7.3463

Muster, T.H., Douglas, G.B., Sherman, N., Seeber, A., Wright, N., Güzükara, Y., 2013. Towards effective phosphorus recycling from wastewater: Quantity and quality. Chemosphere 91, 676–684. https://doi.org/10.1016/J.CHEMOSPHERE.2013.01.057

Nelson, N.O., Mikkelsen, R.L., Hesterberg, D.L., 2003. Struvite precipitation in anaerobic swine lagoon liquid: effect of pH and Mg:P ratio and determination of rate constant. Bioresour. Technol. 89, 229–236. https://doi.org/10.1016/S0960-8524(03)00076-2

Nguyen, M.L., Tanner, C.C., 2010. Ammonium removal from wastewaters using natural New Zealand zeolites. New Zeal. J. Agric. Res. 41, 427–446. https://doi.org/10.1080/00288233.1998.9513328

Nolan, J., Weber, K.A., 2015. Natural Uranium Contamination in Major U.S. Aquifers Linked to Nitrate. Environ. Sci. Technol. Lett. 2, 215–220. https://doi.org/10.1021/acs.estlett.5b00174

Omar, L., Ahmed, O.H., Majid, N.M.A., 2015. Improving ammonium and nitrate release from urea using clinoptilolite zeolite and compost produced from agricultural wastes. Sci. World J. 2015. https://doi.org/10.1155/2015/574201

Ongley, E.D., 1996. Fertilizers as water pollutants, in: Control of Water Pollution from Agriculture - FAO Irrigation and Drainage Paper 55. FAO, Rome, p. 101.

Passaglia, E., 2008. Zeoliti naturali, zeolititi e loro applicazioni. Arvan.

Petzing, J., Chester, B., 1979. Authigenic marine zeolites and their relationship to global volcanism. Mar. Geol. 29, 253–271. https://doi.org/10.1016/0025-3227(79)90112-9

Prywer, J., Sieroń, L., Czylkowska, A., 2019. Struvite grown in gel, its crystal structure at 90 k and thermoanalytical study. Crystals 9. https://doi.org/10.3390/CRYST9020089

Qiu, H., Lv, L., Pan, B.C., Zhang, Q.J., Zhang, W.M., Zhang, Q.X., 2009. Critical review in adsorption kinetic models. J. Zhejiang Univ. Sci. A. https://doi.org/10.1631/jzus.A0820524

Quintana, M., Sánchez, E., Colmenarejo, M.F., Barrera, J., García, G., Borja, R., 2005. Kinetics of phosphorus removal and struvite formation by the utilization of by-product of magnesium oxide production. Chem. Eng. J. 111, 45–52. https://doi.org/10.1016/J.CEJ.2005.05.005

R Core Team, 2019. R Studio.

Raghav, S., Kumar, D., 2018. Adsorption Equilibrium, Kinetics, and Thermodynamic Studies of Fluoride Adsorbed by Tetrametallic Oxide Adsorbent. J. Chem. Eng. Data 63, 1682–1697. https://doi.org/10.1021/ACS.JCED.8B00024/SUPPL_FILE/JE8B00024_SI_001.PDF

Rahman, M.M., Liu, Y.H., Kwag, J.H., Ra, C.S., 2011. Recovery of struvite from animal wastewater and its nutrient leaching loss in soil. J. Hazard. Mater. 186, 2026–2030. https://doi.org/10.1016/J.JHAZMAT.2010.12.103

Rautaray, D., Sinha, K., Shankar, S.S., Adyanthaya, S.D., Sastry, M., 2004. Aqueous Foams as Templates for the Synthesis of Calcite Crystal Assemblies of Spherical Morphology. Chem. Mater. 16, 1356–1361. https://doi.org/10.1021/CM035182L/SUPPL_FILE/CM035182LSI20040213_123429.PDF

Rawajfih, Z., Mohammad, H. Al, Nsour, N., Ibrahim, K., 2010. Study of equilibrium and thermodynamic adsorption of α-picoline, β-picoline, and γ-picoline by Jordanian zeolites: Phillipsite and faujasite. Microporous Mesoporous Mater. 132, 401–408. https://doi.org/10.1016/j.micromeso.2010.03.019

Reháková, M., Čuvanová, S., Dzivák, M., Rimár, J., Gaval'Ová, Z., 2004. Agricultural and agrochemical uses of natural zeolite of the clinoptilolite type. Curr. Opin. Solid State Mater. Sci. 8, 397–404. https://doi.org/10.1016/j.cossms.2005.04.004

Rietveld, H.M., 1967. Line profiles of neutron powder-diffraction peaks for structure refinement. Acta Crystallogr. 22, 151–152.

Robles-Aguilar, A.A., Grunert, O., Hernandez-Sanabria, E., Mysara, M., Meers, E., Boon, N., Jablonowski, N.D., 2020. Effect of Applying Struvite and Organic N as Recovered Fertilizers on the Rhizosphere Dynamics and Cultivation of Lupine (Lupinus angustifolius). Front. Plant Sci. 11, 1752. https://doi.org/10.3389/FPLS.2020.572741/BIBTEX

Roser, M., Ortiz-Ospina, E., 2019. Meat production by livestock type, World, 1961 to 2018 [WWW Document]. OurWorldInData.org. URL https://ourworldindata.org/grapher/global-meat-production-by-livestock-type (accessed 6.20.21).

Rudzinski, W., Panczyk, T., 2000. Kinetics of isothermal adsorption on energetically heterogeneous solid surfaces: A new theoretical description based on the statistical rate theory of interfacial transport. J. Phys. Chem. B 104, 9149–9162. https://doi.org/10.1021/jp000045m

Sağ, Y., Aktay, Y., 2002. Kinetic studies on sorption of Cr(VI) and Cu(II) ions by chitin, chitosan and Rhizopus arrhizus. Biochem. Eng. J. 12, 143–153. https://doi.org/10.1016/S1369-703X(02)00068-2

Saha, P., Chowdhury, S., 2011. Insight Into Adsorption Thermodynamics. Thermodynamics. https://doi.org/10.5772/13474

Saltali, K., Sari, A., Aydin, M., 2007. Removal of ammonium ion from aqueous solution by natural Turkish (Yi{dotless}ldi{dotless}zeli) zeolite for environmental quality. J. Hazard. Mater. 141, 258–263. https://doi.org/10.1016/j.jhazmat.2006.06.124

Saroyda, J.R. V., Cruz, R.Y.S., Antonio, R.J.C., Flestado, C.L.P., Magalong, J.R.S., Zagala, K.Z.P., Barbacena, C.L., Bumatay, J.M., Bautista, L.F., Deocaris, C.C., 2001. PUPAIM.

Science Communication Unit, U. of the W. of E., 2013. Science for Environment Policy Indepth Report: Sustainable Phosphorus Use. Bristol.

Sena, M., Hicks, A., 2018. Life cycle assessment review of struvite precipitation in wastewater treatment. Resour. Conserv. Recycl. https://doi.org/10.1016/j.resconrec.2018.08.009

Shaddel, S., Ucar, S., Andreassen, J.-P., Østerhus, S.W., 2019. Engineering of struvite crystals by regulating supersaturation – Correlation with phosphorus recovery, crystal morphology and process efficiency. J. Environ. Chem. Eng. 7, 102918. https://doi.org/10.1016/j.jece.2019.102918

Shanavas, S., Salahuddin Kunju, A., Varghese, H.T., Yohannan Panicker, C., 2011. Comparison of Langmuir and Harkins-Jura Adsorption Isotherms for the Determination of Surface Area of Solids : Oriental Journal of Chemistry. Orient. J. Chem. 27, 245–252.

Siciliano, A., De Rosa, S., 2014. Recovery of ammonia in digestates of calf manure through a struvite precipitation process using unconventional reagents. Environ. Technol. 35, 841–850. https://doi.org/10.1080/09593330.2013.853088

Siciliano, A., Limonti, C., Curcio, G.M., Molinari, R., 2020. Advances in Struvite Precipitation Technologies for Nutrients Removal and Recovery from Aqueous Waste and Wastewater. Sustainability 12, 7538. https://doi.org/10.3390/su12187538

Simonin, J.P., 2016. On the comparison of pseudo-first order and pseudo-second order rate laws in the modeling of adsorption kinetics. Chem. Eng. J. 300, 254–263. https://doi.org/10.1016/j.cej.2016.04.079

Simonin, J.P., Bouté, J., 2016. Intraparticle diffusion-adsorption model to describe liquid/solid adsorption kinetics. Rev. Mex. Ing. Quim. 15, 161–173.

Söderström, B., Hedlund, K., Jackson, L.E., Kätterer, T., Lugato, E., Thomsen, I.K., Bracht Jørgensen, H., 2014. What are the effects of agricultural management on soil organic carbon (SOC) stocks? Environ. Evid. 3, 2. https://doi.org/10.1186/2047-2382-3-2

Sparks, D.L., 2002. Environmental Soil Chemistry - 2nd Edition. Academic Press.

Stefov, V., Šoptrajanov, B., Spirovski, F., Kuzmanovski, I., Lutz, H.D., Engelen, B., 2004. Infrared and Raman spectra of magnesium ammonium phosphate hexahydrate (struvite) and its isomorphous analogues. I. Spectra of protiated and partially deuterated magnesium potassium phosphate hexahydrate. J. Mol. Struct. 689, 1–10. https://doi.org/10.1016/J.MOLSTRUC.2003.08.019

Stratful, I., Scrimshaw, M.D., Lester, J.N., 2004. Removal of Struvite to Prevent Problems Associated with its Accumulation in Wastewater Treatment Works. Water Environ. Res. 76, 437–443. https://doi.org/10.2175/106143004X151491

Stratful, I., Scrimshaw, M.D., Lester, J.N., 2001. Conditions influencing the precipitation of magnesium

ammonium phosphate. Water Res. 35, 4191–4199. https://doi.org/10.1016/S0043-1354(01)00143-9

Subramanyam, B., Das, A., 2014. Linearised and non-linearised isotherm models optimization analysis by error functions and statistical means. J. Environ. Heal. Sci. Eng. 12. https://doi.org/10.1186/2052-336X-12-92

Talboys, P.J., Heppell, J., Roose, T., Healey, J.R., Jones, D.L., Withers, P.J.A., 2016. Struvite: a slow-release fertiliser for sustainable phosphorus management? Plant Soil 401, 109–123. https://doi.org/10.1007/S11104-015-2747-3

Tansel, B., Lunn, G., Monje, O., 2018. Struvite formation and decomposition characteristics for ammonia and phosphorus recovery: A review of magnesium-ammonia-phosphate interactions. Chemosphere 194, 504–514. https://doi.org/10.1016/J.CHEMOSPHERE.2017.12.004

Temkin, M.J., Pyzhev, V., 1940. Kinetics of Ammonia Synthesis on Promoted Iron Catalysts. Acta Phys. Chim. USSR 12, 327–356.

Tracy, S.L., Williams, D.A., Jennings, H.M., 1998. The growth of calcite spherulites from solution: II. Kinetics of formation. J. Cryst. Growth 193, 382–388. https://doi.org/10.1016/S0022-0248(98)00521-1

Tuszynska, A., Czerwionka, K., Obarska-Pempkowiak, H., 2021. Phosphorus concentration and availability in raw organic waste and post fermentation products. J. Environ. Manage. 278, 111468. https://doi.org/10.1016/j.jenvman.2020.111468

Vilcek, J., Torma, S., Adamisin, P., Hronec, O., 2013. Nitrogen sorption and its release in the soil after zeolite application. Bulg. J. Agric. Sci. 19, 228–234.

Wang, J., Guo, X., 2020. Adsorption isotherm models: Classification, physical meaning, application and solving method. Chemosphere 258, 127279. https://doi.org/10.1016/J.CHEMOSPHERE.2020.127279

Wang, J., Ye, X., Zhang, Z., Ye, Z.L., Chen, S., 2018. Selection of cost-effective magnesium sources for fluidized struvite crystallization. J. Environ. Sci. 70, 144–153. https://doi.org/10.1016/J.JES.2017.11.029

Wasielewski, S., Rott, E., Minke, R., Steinmetz, H., 2018. Evaluation of Different Clinoptilolite Zeolites as Adsorbent for Ammonium Removal from Highly Concentrated Synthetic Wastewater. Water 10, 584. https://doi.org/10.3390/w10050584

Water, U.N., n.d. Water Quality and Wastewater [WWW Document]. URL https://www.unwater.org/water-

facts/quality-and-wastewater/#:~:text=Globally%2C 80%25 of wastewater flows,%2C dysentery%2C typhoid and polio. (accessed 1.15.22).

Weber, W.., Morris, C.J., 1962. Advances in Water Pollution Research, in: Proceeding of 1st International Conference on Water Pollution Research, Vol. 2. p. 231.

Widiastuti, N., Wu, H., Ang, H.M., Zhang, D., 2011. Removal of ammonium from greywater using natural zeolite. Desalination 277, 15–23. https://doi.org/10.1016/j.desal.2011.03.030

World Health Organization, 2006. Guidelines for the safe use of wastewater, excreta and greywater in agriculture and aquaculture. World Health Organization.

Worldometers.info, n.d. Worldometer [WWW Document]. 2022,. URL https://srv1.worldometers.info/ (accessed 3.31.21).

Wu, F.C., Tseng, R.L., Juang, R.S., 2009. Characteristics of Elovich equation used for the analysis of adsorption kinetics in dye-chitosan systems. Chem. Eng. J. 150, 366–373. https://doi.org/10.1016/j.cej.2009.01.014

Xavier, L.D., Cammarota, M.C., Yokoyama, L., Volschan, I., 2014. Study of the recovery of phosphorus from struvite precipitation in supernatant line from anaerobic digesters of sludge. Water Sci. Technol. 69, 1546–1551. https://doi.org/10.2166/WST.2014.033

Xiang, L., Wang, X.D., Chen, X.H., Mo, C.H., Li, Y.W., Li, H., Cai, Q.Y., Zhou, D.M., Wong, M.H., Li, Q.X., 2019. Sorption Mechanism, Kinetics, and Isotherms of Di- n-butyl Phthalate to Different Soil Particle-Size Fractions. J. Agric. Food Chem. 67, 4734–4745. https://doi.org/10.1021/acs.jafc.8b06357

Yang, H., Sun, H.J., 2004. Crystal structure of a new phosphate compound, Mg2KNa(PO 4)2·14H2O. J. Solid State Chem. 177, 2991–2997. https://doi.org/10.1016/J.JSSC.2004.05.008

Yang, H., Sun, H.J., Downs, R.T., 2011. Hazenite, KNaMg2(PO4)2·14H2O, a new biologically related phosphate mineral, from Mono Lake, California, U.S.A. Am. Mineral. 96, 675–681. https://doi.org/10.2138/AM.2011.3668

Ye, Z.L., Deng, Y., Ye, X., Lou, Y., Chen, S., 2018. Application of image processing on struvite recovery from swine wastewater by using the fluidized bed. Water Sci. Technol. 77, 159–166. https://doi.org/10.2166/WST.2017.533

Zhang, C., Zhu, X., Zhu, J., Huang, F., Shen, Y., Xie, A., 2013. Mechanism of crystallization of CaCO3 in

system H2O-CaCl2-Na2CO3-1,2-Bis(4-aminophenoxy)ethane-N,N,N′,N′-tetraacetic acid-cetyltrimethylammonium bromide. Russ. J. Phys. Chem. A 2013 877 87, 1222–1227. https://doi.org/10.1134/S003602441307039X

Zhang, T., Fang, C.I., Li, P., Jiang, R., 2014. Application of struvite process for nutrient recovery from anaerobic digesters of livestock wastewater. Environ. Prot. Eng. 40, 29--42. https://doi.org/10.5277/EPE140303

ZhangHan, GongWeijia, LuoXinsheng, XieBinghan, LiGuibai, LiangHeng, 2019. Obtaining High-Purity Struvite from Anaerobically Digested Wastewater: Effects of pH, Mg/P, and Ca2+ Interactions. https://home.liebertpub.com/ees 36, 102–113. https://doi.org/10.1089/EES.2018.0065